VYSOKÉ UČENÍ TECHNICKÉ V BRNĚ
BRNO UNIVERSITY OF TECHNOLOGY

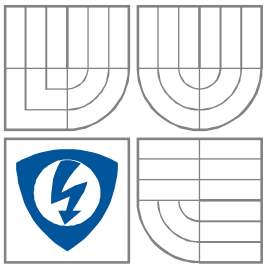

FAKULTA ELEKTROTECHNIKY A KOMUNIKAČNÍCH TECHNOLOGIÍ
ÚSTAV RADIOELEKTRONIKY

FACULTY OF ELECTRICAL ENGINEERING AND COMMUNICATION
DEPARTMENT OF RADIO ELECTRONICS

MOBILNÍ PLATFORMA PRO TESTOVÁNÍ AUTOMOBILOVÝCH SYSTÉMŮ PRO BLUETOOTH HANDS-FREE KOMUNIKACI

Mobile platform for testing automotive Bluetooth Hands-Free Communications systems

DIPLOMOVÁ PRÁCE
MASTER'S THESIS

AUTOR PRÁCE — Bc. Václav Mecerod
AUTHOR

VEDOUCÍ PRÁCE — doc. Ing. Tomáš Kratochvíl, Ph.D.
SUPERVISOR

BRNO, 2013

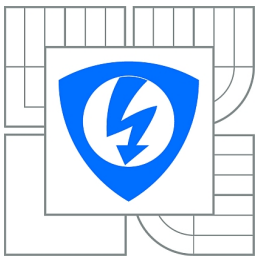

VYSOKÉ UČENÍ TECHNICKÉ V BRNĚ

Fakulta elektrotechniky a komunikačních technologií

Ústav radioelektroniky

Diplomová práce

magisterský navazující studijní obor
Elektronika a sdělovací technika

Student:	Bc. Václav Mecerod	***ID:***	125540
Ročník:	2	***Akademický rok:***	2013/2014

NÁZEV TÉMATU:

Mobilní platforma pro testování automobilových systémů pro Bluetooth Hands-Free komunikaci

POKYNY PRO VYPRACOVÁNÍ:

V teoretické části práce detailně prostudujte implementaci hlasu a telefonie v současné generaci automobilových infotainment systémů a základy teorie potlačení akustického echa v Hands-Free systémech. Navrhněte kompaktní a přenosný systém pro testování bezdrátových modulů v automobilech. Systém by měl obsahovat koncový zesilovač ve třídě D, dvojkanálový mikrofonní vstup s plně nastavitelnými parametry a duplexní multikanálový D/A převodník s I2S rozhraním a nastavitelným směrováním audio signálů.

V experimentální části práce realizujte systém formou prototypu, který bude integrován do přenosného boxu. Systém by měl být jednoduše připojitelný do existujícího audio systému automobilu. Ověřte funkčnost a audio parametry realizace. Vytvořte kompletní konstrukční podklady k realizaci návrhu (schéma zapojení, návrh desky plošného spoje, rozložení a soupiska součástek atd.).

DOPORUČENÁ LITERATURA:

[1] TALBOTH-SMITH, M. Audio Engineer's Reference Book, 2nd edition. New York: Focal press, 1999.

Termín zadání:	10.2.2014	***Termín odevzdání:***	23.5.2014

Vedoucí práce: doc. Ing. Tomáš Kratochvíl, Ph.D.
Konzultanti diplomové práce:

doc. Ing. Tomáš Kratochvíl, Ph.D.
Předseda oborové rady

UPOZORNĚNÍ:

ABSTRAKT

Tato diplomová práce se zabývá problematikou implementace Hands-Free komunikačních systémů v automobilovém průmyslu. První kapitola je zaměřena na teoretické aspekty zpracování řeči v embedded aplikacích, jako je potlačení šumu, potlačení akustické zpětné vazby a další faktory ovlivňující kvalitu Hands-Free systémů. Druhá kapitola obsahuje návrh kompaktního flexibilního mobilního testovacího zařízení pro bezdrátové komunikační Hands-Free moduly.

KLÍČOVÁ SLOVA

Hands-Free, zpracování řeči, potlačení akustické zpětné vazby, potlačení šumu, mikrofon, filtr, zesilovač ve třídě D, Raspberry Pi.

ABSTRACT

This master's thesis deals with the main issues of the Hands-Free communication systems implementation in the automotive industry. The first chapter focuses on the theoretical aspects of speech processing in embedded applications, such as noise suppressing, acoustic echo cancelation and Hands-Free performance in general. The second chapter includes the design of compact flexible mobile testing tools for wireless communication Hands-Free modules.

KEYWORDS

Hands-Free, speech processing, acoustic echo cancellation, noise suppression, microphone, filter, class D amplifier, Raspberry Pi.

MECEROD, V. *Mobilní platforma pro testování automobilových systémů pro bluetooth Hands-Free komunikaci*. Brno: Vysoké učení technické v Brně, Fakulta elektrotechniky a komunikačních technologií. Ústav radioelektroniky, 2013. 49 s., 80 s. příloh. Diplomová práce. Vedoucí práce: doc. Ing. Tomáš Kratochvíl, Ph.D.

PROHLÁŠENÍ

Prohlašuji, že svůj semestrální projekt na téma *Mobilní platforma pro testování automobilových systémů pro bluetooth Hands-Free komunikaci* jsem vypracoval samostatně pod vedením vedoucího diplomové práce a s použitím odborné literatury a dalších informačních zdrojů, které jsou všechny citovány v práci a uvedeny v seznamu literatury na konci práce.

Jako autoru vedené diplomové práce dále prohlašuji, že v souvislosti s vytvořením této diplomové práce jsem neporušil autorská práva třetích osob, zejména jsem nezasáhl nedovoleným způsobem do cizích autorských práv osobnostních a/nebo majetkových a jsem si plně vědom následků porušení ustanovení § 11 a následujících zákona č. 121/2000 Sb., o právu autorském, o právech souvisejících s právem autorským a o změně některých zákonů (autorský zákon), ve znění pozdějších předpisů, včetně možných trestněprávních důsledků vyplývajících z ustanovení části druhé, hlavy VI. díl 4 Trestního zákoníku č. 40/2009 Sb.

V Brně dne ....

(podpis autora)

PODĚKOVÁNÍ

Děkuji vedoucímu diplomové práce doc. Ing. Tomáši Kratochvílovi, Ph.D. a odbornému vedoucímu práce Ing. Josefovi Nevrlému. Za účinnou metodickou, pedagogickou a odbornou pomoc a další cenné rady při zpracování mé diplomové práce.

V Brně dne ....

(podpis autora)

SIX research centre
sensor, information and communication systems

Faculty of Electrical Engineering
and Communication

Brno University of Technology
Technicka 12, CZ-61600 Brno, Czechia

http://www.six.feec.vutbr.cz

Experimentální část této diplomové práce byla realizována na výzkumné infrastruktuře
vybudované v rámci projektu CZ.1.05/2.1.00/03.0072
Centrum senzorických, informačních a komunikačních systémů (SIX)
operačního programu Výzkum a vývoj pro inovace.

MINISTERSTVO ŠKOLSTVÍ, MLÁDEŽE A TĚLOVÝCHOVY

EVROPSKÁ UNIE
EVROPSKÝ FOND PRO REGIONÁLNÍ ROZVOJ
INVESTICE DO VAŠÍ BUDOUCNOSTI

2007-13
OP Výzkum a vývoj pro inovace

CONTENTS

LIST OF FIGURES

LIST OF TABLES

INTRODUCTION

The aim of this master's thesis is to design a flexible testing system (tool) for the automotive Hands-Free Echo Cancellation and the Noise Reduction systems (ECNR). That system could be used for:

- ECNR algorithm testing and the benchmark for deployment in the Hands-Free system
- testing ECNR system implementation during its development
- presentation of ENCR systems to customers
- Hands-Free system performance in comparison to a reference platform

For this reason, there are some complex requirements that exist for such testing tools, such as high quality analog audio chain, flexibility of the analog and digital interfaces, and system compactness and mobility.

High quality audio chain (in terms of linearity, low additive noise, etc.) is necessary for correct implementation of ECNR systems, especially for its usage as a reference platform. System must enable connection of various analog components (microphones) and digital modules (DSP, Bluetooth modules/kits), depending on different customer's requirements. Compact, easily packable and portable case of the tool is required too, because this equipment will be primarily used at the customer's place.

The first chapter discusses general theoretical aspects of speech processing in embedded applications, such as noise suppression, acoustic echo cancelation and overall Hands-Free performance.

The second chapter includes design documentation of compact flexible mobile testing tool for wireless communication modules with embedded Hands-Free function. It consists of the subsections dealing with microphone input, duplex multichannel converter, class D amplifier, control board, power sources, and user interface.

The appendix includes the measured results of the prototype boards and photo documentation.

1 BACKGROUND THEORY

This chapter contains a general, theoretical introduction to the speech processing in Hands-Free systems. Main issues and requirements of the audio communication chain are discussed and explained.

1.1 Automotive Hands-Free system

The basic idea of a Hands-Free (HF) system should contain a cell phone, an open microphone and a loudspeaker. At first sight it might work correctly. We have the equipment for a voice pickup, sound reproduction and a cellular network connection. However, many problems will arise while operating this simple system in a car, such as the additive noise, line and acoustic echo, acoustic feedback etc. As a result, we get unintelligible and annoying output, which makes normal phone conversation difficult or impossible.

Therefore we need to improve this basic idea by adding another device, which would remove these undesirable effects. Such device will perform and Echo-Cancellation, Noise-Reduction (ECNR) processing (see Fig. 1). In reality, ECNR processing can take form of a separate hardware, software layer running on the infotainment system's processor, or be a part of universal communication module such as a Bluetooth™ module.[1]

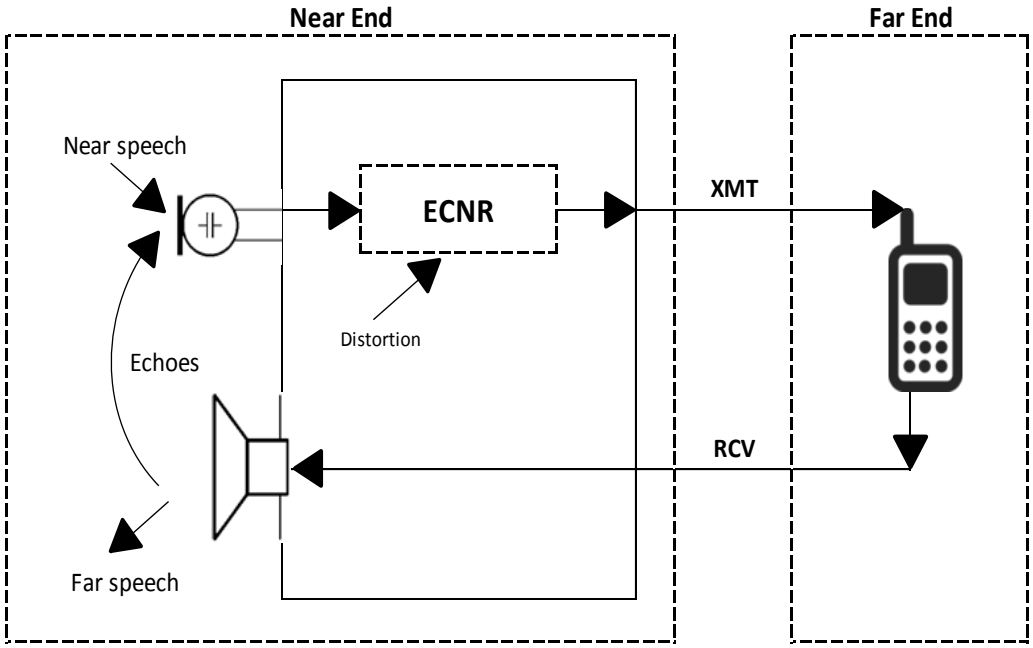

Fig. 1: Illustration of the Hands-Free system with nonlinear processing

According to [1] there are at least five factors that determine the success of hands-free development: Hans-Free Performance, Supplier Excellence, Tool Excellence, Feasibility, and Documentation.

1.2 Hands-Free Performance

This is the most important aspect of the solution, as it ultimately determines end-user satisfaction. In order to achieve performance which is acceptable in market it is necessary to keep international standards. Also it is necessary to know and make tests associated with these standards. This includes both subjective and objective methods of testing.

In a Hands-Free call, the downlink speech signal is played out over a loudspeaker and picked up again by a microphone. Thus the people on the far-side hear their own voice with a short time delay again. This is known as the acoustic echo. The Acoustic Echo Cancellation (AEC) prevents the remote end from hearing this unpleasant effect. This enables a usage of double-talk. Double-talk describes a situation when the both talkers talk at the same time. So both the downlink and uplink channels are in use. AEC, which is doing its job properly, cannot let any echo leak through under any condition, such as common shortcomings in a mobile cellular network, variable noise level, large gain variation across phones or high acoustic coupling. It must be able to cancel the echo during some acoustic path variations when the space containing Hands-Free device is changed by call participants movements, especially near loudspeakers and microphones.[1]

Furthermore, noise reduction and the speech reconstruction are also important features. In a vehicle, there are a lot of acoustic noise sources such as heating, ventilation, and air conditioning system (HVAC), open windows, engine, road surface, tires, aerodynamic noise and suchlike. Most of the engine and road noise is at low frequency, but cannot be simply cut out by an ordinary filter without any significant change in the talker's voice, because human voice in the frequency domain includes frequency components reaching the border of 10 Hz. As a result, the filtered voice may sound thinner. Directional microphones are more susceptible to wind from HAV, windows, sun roofs, and any other turbulent air flow. The acoustic effect of a wind to a microphone varies with the force of the wind, the sensitivity and look direction of the microphone. The frequency range of the acoustic effect is from (100-200) Hz to (400-800) Hz in normal conditions, or up to (2-4) kHz in extreme conditions when wind causes clipping. Nowadays, the target value is more than 16 dB of noise level attenuation and manufacturers must deal with these challenging requirements. It is not possible without active speech filtering, voice reconstruction, and dynamic noise removal.[1] [2]

A noise removal may cause reduced intelligibility of a call if it manages to remove information masked by noise. However, consonants, which are critical for intelligibility, have higher frequency. In that case, these consonants are not masked by typical vehicle's noise.[1]

1.2.1 Multiple microphones

If more passengers want to participate in a Hands-Free call, two or more microphones can be used to accommodate such use-case. Microphones are placed as close to the passengers as possible. By evaluating voice activity detection, an adaptive algorithm is able to switch microphones dynamically to reduce background noise or to block inputs from microphones near to the non-speaking passengers. It is important that the mixed voices sound naturally and the transitions between individual microphones are smooth.[1]

Other technique utilizing multiple microphones is microphone array. A microphone array consists of any number of omnidirectional microphones and these are operating in tandem. Microphones are placed close to each other with distance of two to five cm. Using signal processing on the individual inputs, it is possible to modify the resulting directional characteristic of the complete array. This is known as beam forming. More advanced techniques allow beam shape or direction to be changed dynamically (beam steering). Quality of such solutions depends on the type and the look direction of each microphone, and on the inter microphone spacing.

1.2.2 Automatic Gain Control

An automatic gain control keeps consistent voice level for each person speaking. This system should not respond to any non-speech noises, such as wind buffeting from ventilation, GSM buzz, movements inside the car etc. AGC should recognise the quieter voice of a person speaking from a long distance and amplify his voice without the far-side having to ask him to speak up. Conversely, if a person with a loud voice talks near a microphone, AGC should be able to attenuate the captured voice, using a look-ahead (soft) limiter to handle the sudden rise of the voice. Anywhere along the chain (from the near side to the remote side) great level variations occur, often up to 30 dB. It is important to achieve a stable voice level without sudden, annoying, or otherwise noticeable increases or decreases in received noise. Furthermore, the voice should not be clipped or audibly distorted.[1], [2]

On the receive side, it may be appropriate to control gain with regards to the ambient noise. Again, the gain should be adjusted smoothly in response to noise increases and decreases. If the change is too slow, the driver may feel the need to use the manual volume control (effect known as gain chasing). On the other hand, if the action time is too quick, a sudden increase or decrease may seem unnatural or startling.[1]

Phone line level varies with the type of used phone and network. Mobile operators may also differ in the signal levels. For this reason, a receive-side AGC is also necessary to achieve comfortable user experience.

1.2.3 Frequency response

Significant variations in a sending and receiving frequency response may be caused by the acoustic path. Every block in the path of a voice signal has its own frequency response. The most problematic blocks are typically mechanical-electrical converters including microphones and speakers (example of microphone's frequency response on Fig. 2).

Acoustic of a vehicle cabin has also unbalanced frequency response. Thus we should have some equalization (EQ) block in a Hands-Free system. It may be formed by a series of band pass filters, or by a parametric equalizer that allows to changing specification such as node center, width of the pass band and gain values. Some systems may even support changing the EQ settings dynamically depending on circumstances. For example, one EQ curve could be used in quiet noise conditions and other in high noise conditions. In such system, the curves are being dynamically blended from one to another, in reaction to the noise level or signal to noise ratio (SNR).

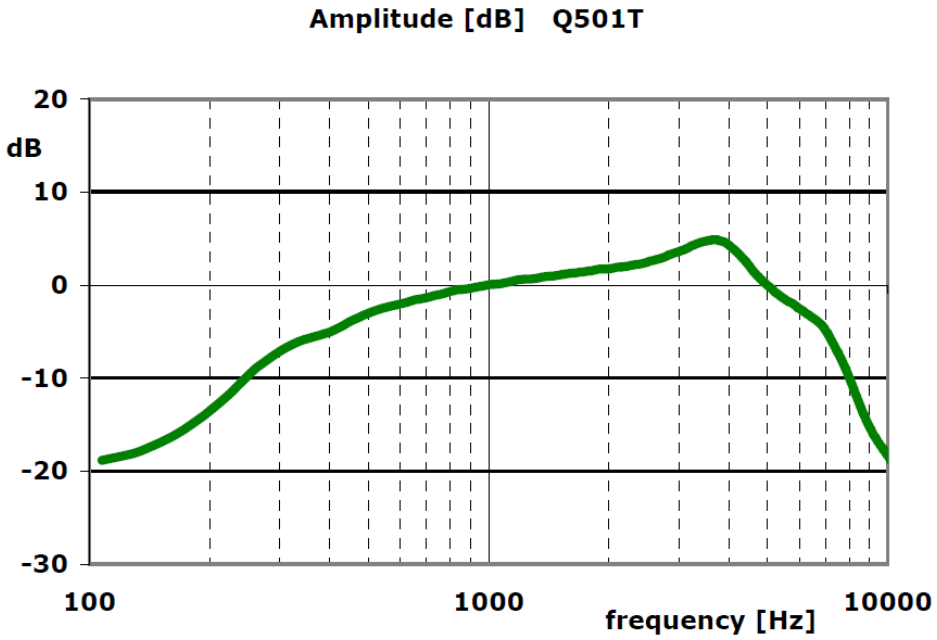

Fig. 2: Frequency response of microphone AKG Q501T [3]

Hands-Free system should support modern standards for wireless communication of high speed data, such as LTE and VoIP. Systems working under these standards are capable of running at a sample rate 16 kHz, 24 kHz or 32 kHz for VoIP call. Depending on that the bandwidth of transmitted voice is about 7 kHz for wideband, or super-wideband with frequencies up to 15 kHz.[1]

1.2.4 Full-Duplex systems

According to [4], in a full-duplex system both coding and decoding are performed simultaneously (as shown in Fig. 3). Typically, speech captured by local microphone is sampled and processed and transmitted by the system while encoded speech data received over the communication channel are processed and converted to analog output for playback over local speaker.

Double-talk is the determining facility of the Hands-Free system. It is a state of the system when both far-in and near-in speeches are present simultaneously. Hands-Free systems have additional half-duplex modes (receive and transmit mode) and idle mode, where no speech is present. In half-duplex modes only one side is talking in one moment and noise from other side is suppressed. A state machine is responsible for switching of these four states. The quality of a state machine has the most drastic effect on the audio quality of the system, and is what will make the most difference in the perceived quality between one system and another.[2] One of the most difficult tests of state machine is a dynamic conversation, because it switches state between the full-duplex and half-duplex. If a state machine is poorly implemented, there could be noticeable changes in the volume level, changes in background noise level, or even audible clicks as the states are changed. These would be especially noticeable during the beginning and end of pauses in conversation, or even between words. The listening subjective test is the only way to evaluate state machine performance.[2]

Another example of half-duplex systems is a speakerphone. Most cell phones offer this feature. A microphone and a loud speaker of the mobile phone are used to include several people in a conversation. But many implementations of this feature suffer from certain limitations. Only one person can talk at once. The active side is determined by comparing signal levels (or loudness) on both sides. Occasionally, it can lead to some complications, because until the louder participant is talking, the other side is muted. There is no possibility to contribute to a telephone call and it may inhibit the natural flow of the conversation.

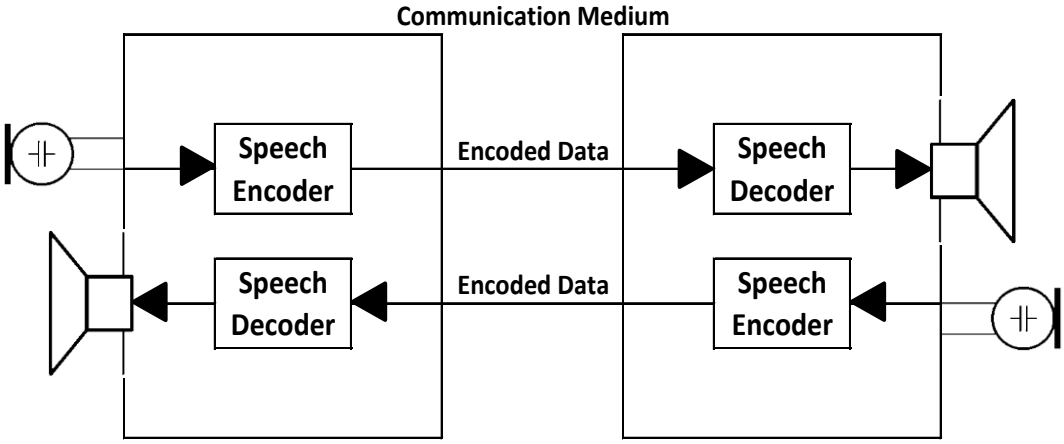

Fig. 3: Typical full-duplex speech compression application

1.2.5 Acoustic Echo Cancellation

Every Hands-Free system is influenced by its acoustic environment. The picture (Fig. 4) shows schematically a room with one sound source - the loudspeaker of Hands-Free system. We can see that sound waves from this speaker impinge on the microphone in several different ways. The shortest one is a direct path from the speaker to the microphone. Other paths are reflections of the sound from the walls, ceiling, floor, furniture and other objects in the room. As a result, person on the far end hears his own voice multiple times with time delays. This phenomenon is called acoustic echo. The acoustic echo is most noticeable and annoying when the delay is present in the transmission path. Furthermore, howling can occur if the microphone is positioned too close to the speaker [2]. If the attenuation between the microphone and the speaker reaches approximately 60 dB, the echo will be negligible. Usually, this condition occurs only with the telephone handset. Time, during which the sound is heard again in the area of the sound source, is directly dependent on the distance, which the sound has to arrive, and inversely proportional to the speed at which the wave moves. Speed of the sound is affected by the temperature and humidity of air.[5] Equation number 1 describes mathematically the speed of the sound in the air:

$$v(t) = (331{,}82 + 0{,}61 \cdot T) \quad \text{[m/s, °C].} \qquad (1)$$

Examples of environments with different properties could be a car cabin and a conference room. The car cabin is a relatively small rugged area with lots of soft and sound absorbing materials that reduce the reverberation time. It also includes hard materials such as glass windows. On the other hand, the conference room is usually a large room with bare walls, without any furniture. Environments such as these can cause much more acoustic reflections which are captured by the microphone, making it even more challenging to remove this echo. The room together with the speaker and the microphone form the electro-acoustic system "LEM-System" (Loudspeaker-Enclosure-Microphone-System). The acoustic space for operation of the Hands-Free systems can be described by a time-variant impulse response. Convolution of the reproduced speech and the impulse response is the signal which is supressed by the Acoustic Echo Cancellation unit. [6]

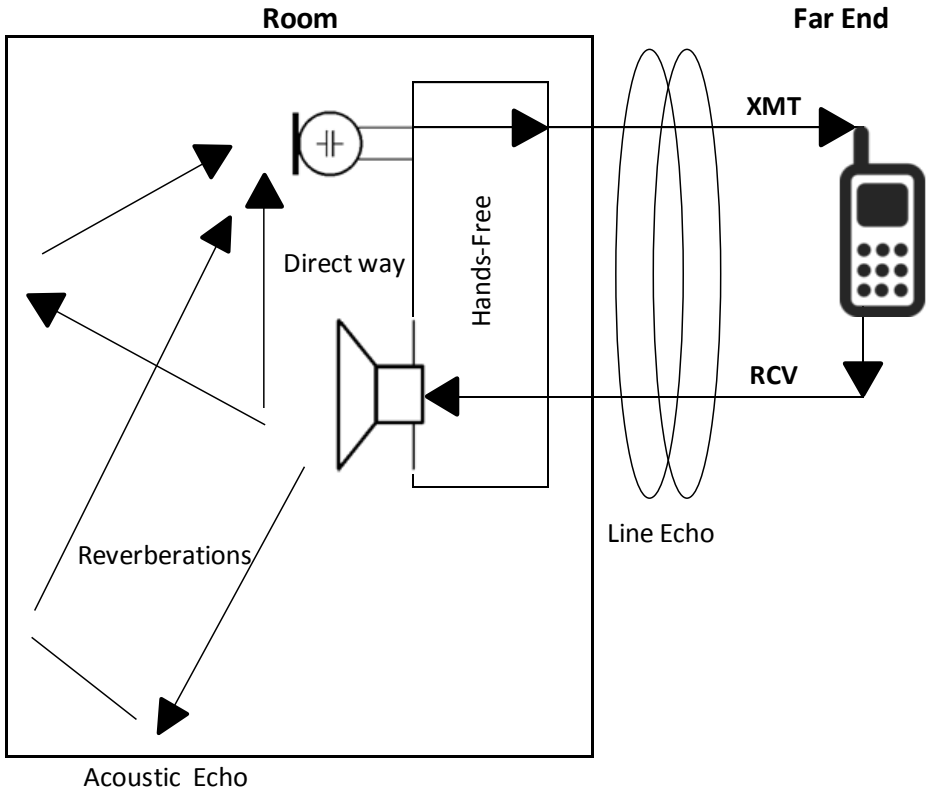

Fig. 4: Example of creation the acoustic and line echoes

Line Echo Cancellation (LEC) is another closely related problem. If we compare both the line and the acoustic echo cancellation, we see that they are often based on the same technology. However, the acoustic echo cancellation is more difficult problem. With the line echo cancellation there are generally only one or two reflections from telephone hybrids or impedance mismatches on the telephone line. These echoes are usually delayed by less than 32ms, and do not change very frequently. With the acoustic echo cancellation, the echo path is very complex. It consists of hundreds reflections. The figure (Fig. 5) shows the basic structure of the acoustic echo. We can see:

- Pre-delay –time between the direct sound and the first reflection,
- early reflections – first reflections of the low frequency and relatively high level,
- dense reflections - complete the character of the sound.

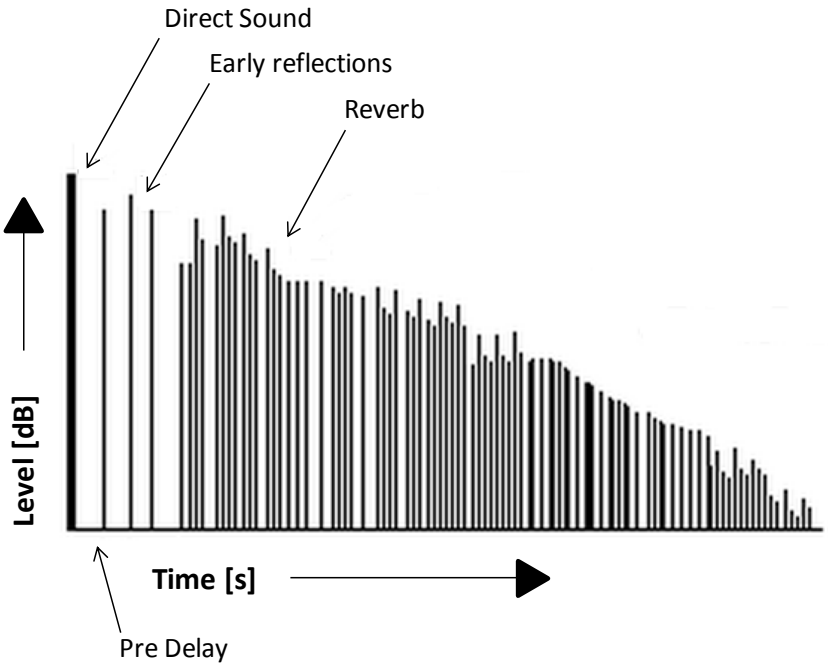

Fig. 5: Example of the basic structure of the acoustic echo [6]

Reflective components of the acoustic echo could last (100 – 200) ms, and can vary continuously during the conversation as people move around the room.[2] Both AEC and LEC are associated with specific International Telecommunications Union (ITU) recommendations. It is G.167 for the acoustic echo cancellation and G.168 for the line echo cancellation. This recommendation is applicable to design of AECs for audio terminals with digital or analog line interfaces and is intended for use in the following areas of telecommunications:

- teleconferencing;
- louds peaking (hands-free) telephones;
- videophone terminals;
- mobile and personal applications.

The recommendation specifies performance characteristics and values with which AECs must comply, and methods to verify these performances. The performances depend on the considered applications. Particular processing techniques are indicated as guidance for possible implementations, but they are not compulsory. Further, it describes in detail the general definition (such as audio terminal, interfaces etc.), definitions related to the acoustic echo controllers, the transmission specifications, the acoustic echo control specifications (within Measurement conditions, signals etc.), and specifications for interworking with the network.[7]

Like G.167 for AECs, there are some recommendation P.1100 that exist for a narrow-band Hands-Free communication in motor vehicles or P.1110 for a wide-band Hands-Free communication in motor vehicles, or VDA Specification for Car Hands-Free Terminals.[8]

An adaptive filter is used to remove the echo, because the LEM system is time

variable. Adaptive Filter (Fig. 6), as the name suggests, is a digital filter whose coefficients are not constant. Rather, the coefficient values are periodically (and frequently) updated based on changes in environmental parameters and the characteristics of the input data.[4] It is generally used for reconstruction of the distorted signal, elimination variable interferences and for other cases where it is not possible to design a fixed filter beforehand. The adaptation algorithm mainly refers to the process and criteria used in updating the coefficients, whereas the filter itself may utilize any of the FIR or IIR filter topologies. Filter with finite impulse response (FIR) is commonly used for its absolute stability, simplicity and popularity. There are several adaption algorithms, each with different speed adaptation, accuracy and stability of adaptation algorithm, such as Least Mean Squares (LMS) and Recursive Least Squares (RLS). The RLS technique, while actually being one of the most effective and robust adaptation methods, is computationally prohibitive for deployment in embedded systems. Common feature of all adaptation algorithms is an effort to minimize the energy difference (2) between the reference signal ($d[n]$) and the output of the adaptive filter ($y[n]$):

$$e[n] = d[n] - y[n]. \tag{2}$$

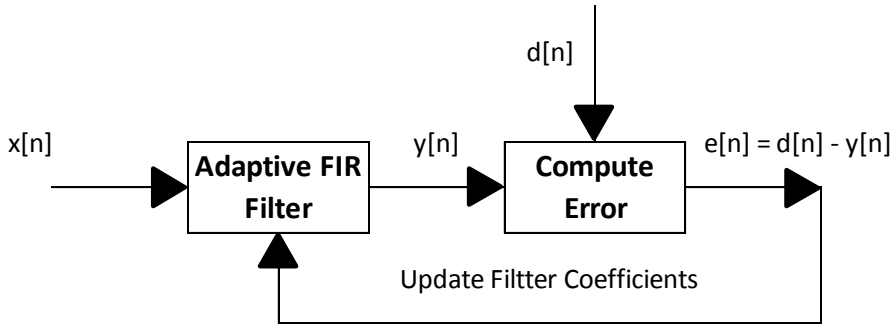

Fig. 6: Basic LMS adaptive FIR filter algorithm

In the context of AEC, the input $x[n]$ is the received far-end speech signal, the input $d[n]$ is the reference or desired signal of the near-end (echo-corrupted) speech signal, and the error output $e[n]$ are the resultant echo-cancelled speech signal.

According to [4] the output signal $y[n]$ of the adaptive filter is given by the convolution of the input signal $x[n]$ and the current filter impulse response $h_n[m]$:

$$y[n] = \sum_{m=0}^{M-1} h_n[m] - x[n-m]. \tag{3}$$

New FIR filter coefficients can be calculated according to the equation 4.

$$h_{n+1}[m] = h_n[m] + \mu \cdot e[n] \cdot x[n-m] \tag{4}$$

To avoid problems of numerical stability during updating filter coefficients, most practical AEC implementations use a Normalized LMS Filter. In Normalized LMS, the adaptation Constant is normalized by the average received far-end energy for the current frame. Since this division can cause divide-by-zero errors, a small

constant is added to the denominator, as shown in (5):

$$\mu_{norm} = \frac{1}{\delta + E_x[n]}. \qquad (5)$$

The order of the LMS FIR Filter is directly proportional to the Echo Tail Length. Hence, the choice of a filter size is often a trade-off between the available memory and computational speed of the processor and the maximum echo delays the algorithm can eliminate. The Echo Tail Length requirement for any particular application is determined by its acoustic environment as well as the loudness of the speaker output.[4]

1.2.6 Noise Suppression

If we capture speech by the microphone in a real environment (for example in a car cabin), the desired signal is degraded by additive noise of various frequencies. In this case, listeners of the recorded speech may have a negative listening experience and problems understanding content of the speech.

The simplest case of noise is from a narrowband source. Such type of noise is easy to eliminate using a highly selective band-stop filter known as a Notch Filter. However, such situations are not so common. Noise characteristics are often not known, the noise energy is distributed over a wide band spectrum and can be dynamically changing over time. Therefore, it is necessary to employ sophisticated algorithms that can dynamically track the profile of the captured noise and suppress it. The most intuitive approach for cancelling the effect of noise in speech signals may be to separately capture the noise from its source and simply subtract this noise from the noise-corrupted speech signal. This is, of course, possible only if we have access to the noise by itself.[4]

In cases where a noise source is very close to the primary microphone (like in the car) simplistic Frequency Domain techniques may be employed. This means that an FFT can be computed for the both noise corrupted speech signal as well as for noise reference signal. Frequency components of noise are subtracted from the speech + noise signal in next step. After that, we would get relatively noise-free speech signal using inverse FFT. [4]

A less used algorithm (in automotive) is Adaptive noise cancelation. The core of algorithm is the Adaptive LMS FIR Filter, similar to what has already been discussed for AEC systems (see Fig. 6). Filter coefficients are adapted for every new input sample *x[n]* the way of minimizes the Mean Squared Error (MSE) between desired signal and filter output. In the context of Adaptive Noise Cancellation, the input $x[n]$ is the source noise samples captured by Reference microphone, the input $d[n]$ is the noise-corrupted speech signal samples captured by the Primary microphone, and the output $e[n]$ is the resultant noise–cancelled speech signal. The Adaptive FIR filter models effective acoustic path between the Reference microphone (source of noise) and the Primary microphone (source of speech). The filter coefficients converge to their optimal values after several iterations of the algorithm. Therefore, it is suitable to consider an initial value and speed of convergence.[4]

A precise knowledge of customer requirements is necessary in order to successfully

develop a high quality HF solution or to select the best market solution. These requirements are, of course, evolving. In older vehicles, it was sufficient if just a driver was able to talk at low driving speed. Today, it is expected that anyone in the vehicle could participate in a Hands-Free phone call, in any vehicle, any noise conditions, and at any speed. Requirements necessary for deployment of the HF system, such as easy parameter-tuning and good tuning tool set, are becoming increasingly important as well.. Furthermore, as expectations of the end-user increase, cell phones evolve from narrow band devices to VoLTE and 4G wideband, super-wideband, and VoIP devices. Current HF systems should be already prepared to accommodate these new technologies.

2 DESIGN OF THE TESTING TOOL

Good, intuitive and well documented tuning and testing tool is a significant advantage for creating a high quality hands-free solution and also provides a good basis for integration of such solution into the complete infotainment system. It should offer comprehensive graphical user interface for controlling the behaviour of audio signal path and all adjacent parts of HF system.

We can see the basic block diagram of a testing tool on the picture (Fig. 7). Main purpose of this tool is to provide a highly customizable audio path and allow connection of various audio sources. It consists of a several function blocks.

Microphone inputs allow connection of microphones and include preamplifier. It could set gain and control the excitation of audio channel. There are also other audio inputs. These are line level inputs and are directly connected to the signal routing block.

Signal routing takes care of delivering analog audio signal to the selected codec or alternate output. Codecs convert analog audio signal to digital audio signal and send it device under test (DUT) over the I2S bus. Conversely, codecs convert signal received from I2S bus back to analog. The whole testing tool has two main outputs. The first one has line level of output, and other one has volume control and power amplifier. Amplifier can be connected to the speaker in the existing car audio system.

All features are controlled by control unit consisting of Raspberry Pi module and user interface accessible through Ethernet connection.

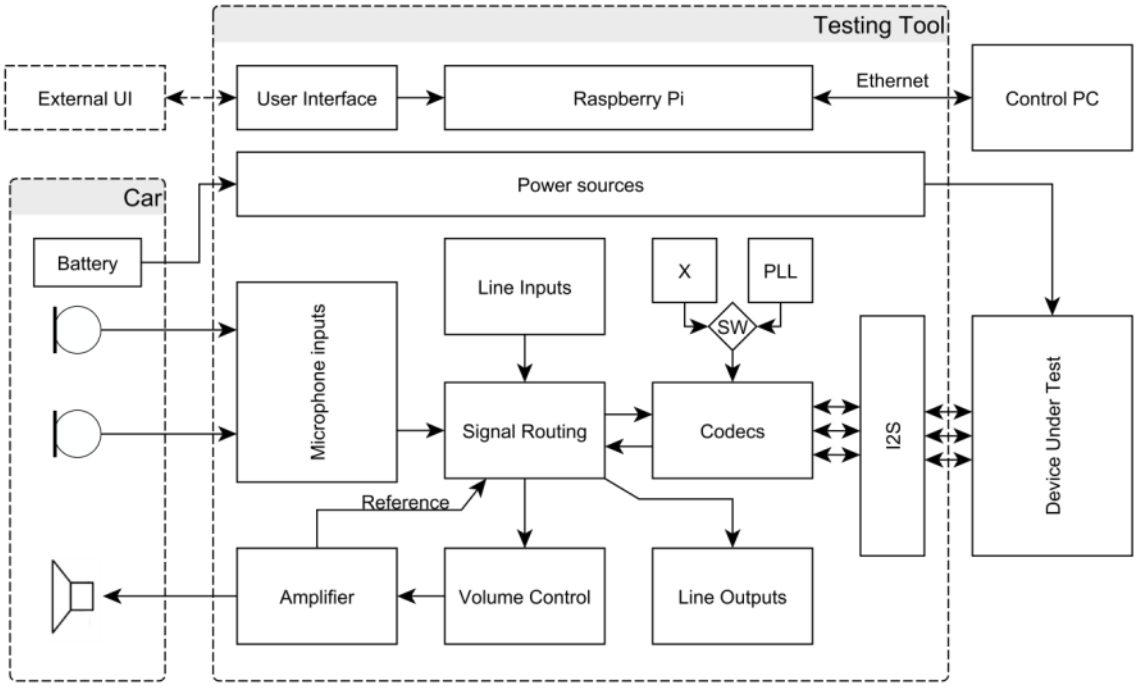

Fig. 7: Block diagram of testing tool

2.1 Microphone input

The usually used microphone for HF systems and its frequency response are mentioned in the background theory. It is a single electret condenser microphone. It means AKG Q501T is representative of the capacitor microphone. It consists of electret (dielectric material contains polar molecules), conductive membrane and FET preamplifier. The whole device is enclosed into small capsule which serves as an electromagnetic shield. Due to the movement of the membrane the capacity is changing and the voltage between the capacitor plates is changed also. Voltage differences are small and they must be processed by preamplifier with high input impedance (typically FET transistor). Electret microphones require biasing of built-in amplifier with constant voltage and recommended current.[8]

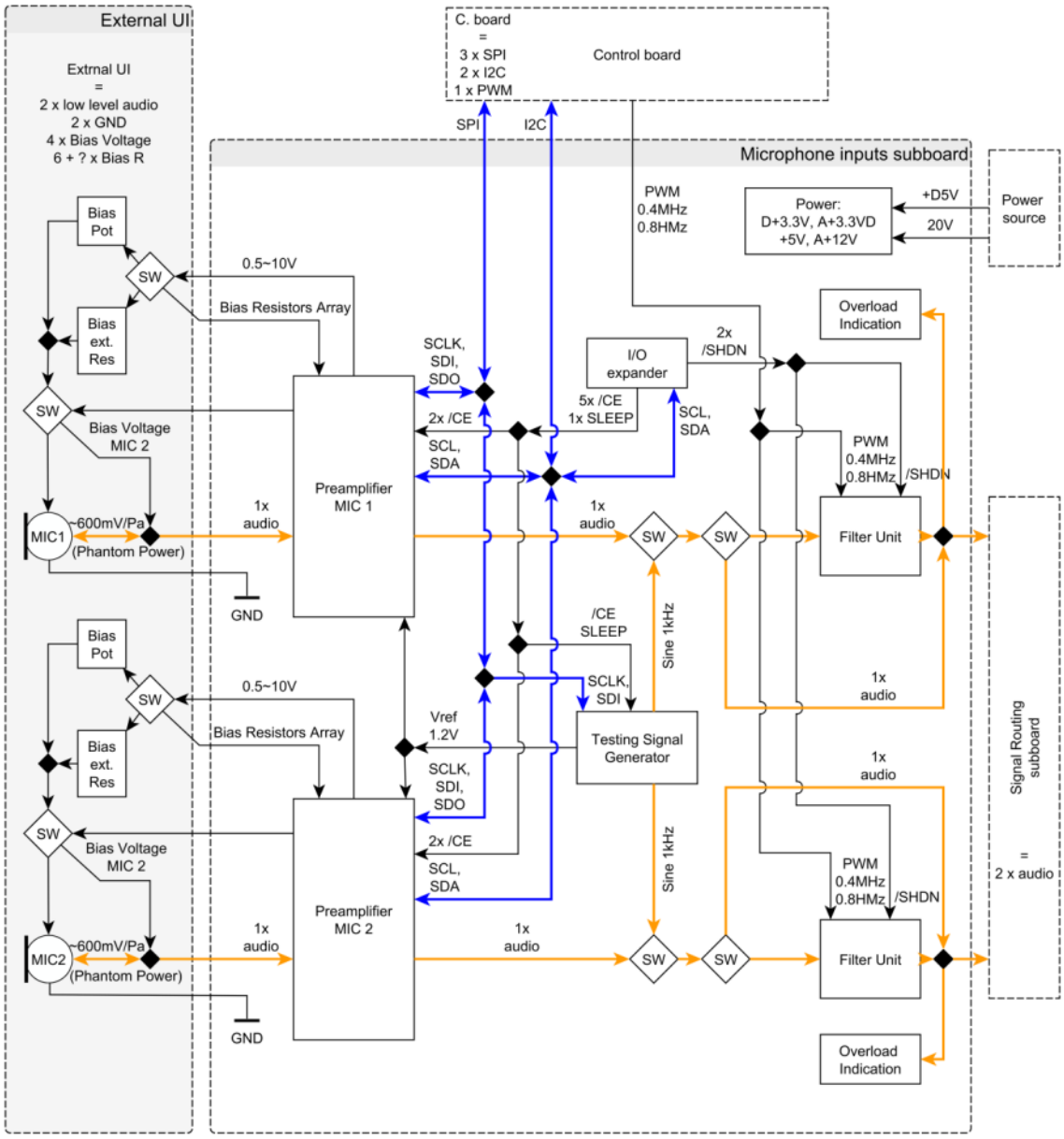

Fig. 8: Block diagram of the whole microphone input

Although AKG's Q501T may be considered as typical automotive microphone, many other types are being used, especially in low-end, cheaper systems. The Test tool must therefore be designed in such way, that it is able to accommodate wide range of microphone types, with various bias-voltages, input adapters etc.

Fig. 8 shows block diagram of the microphone input sub-board. It consists of two microphone channels. Each channel contains a preamplifier, filter unit and overload detection. Generator of the testing signal is common for the sub-board and can be connected into the audio path. Microphone sub-board has two audio analog outputs connected to the signal routing sub-board. External user interface illustrates connection of the microphones and bias resistor selection. The bias voltage, sensing of the bias resistor, gain of the preamplifier, testing signal generator, I/O expander and tuneable band pass filter are driven by control board.

2.1.1 Preamplifier

Microphone signal is often weak and very sensitive to interferences. The resulting requirements for microphone input are therefore large gain range, low noise level and low harmonic distortion of the microphone preamplifier. In order to support various microphone types, it is necessary to ensure different connection and biasing options. Two wire connection of the microphone with phantom power, or three wire connection with separate bias pin. Block representation of the microphone bias and signal gain is on the Fig. 9.

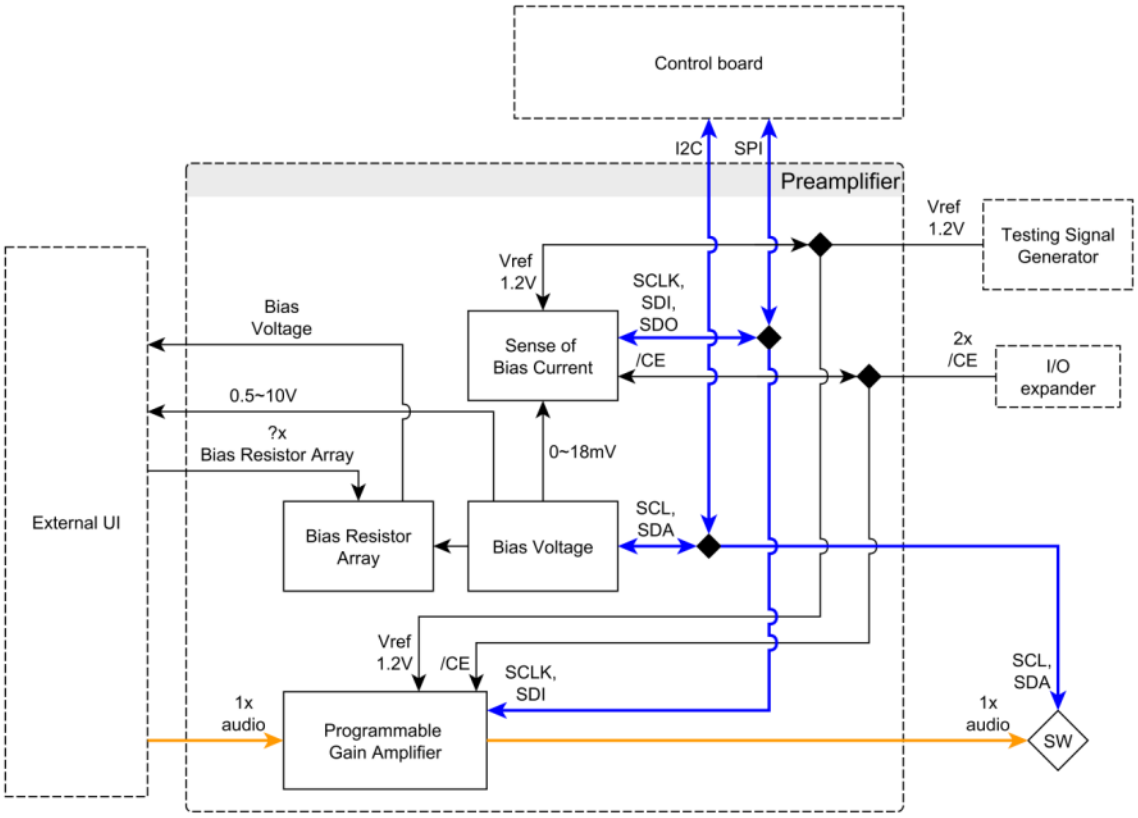

Fig. 9: Block diagram of the microphone preamplifier

2.1.1.1 Bias Unit

As an example of typical connection and biasing of microphone, schematic from VDA specifications [10] on the picture (Fig. 10) is included. It contains capsule with the preamplifier, voltage supply for biasing, resistor for the recommended current and capacitor for separation of useful microphone signal from bias dc voltage. This all together defines microphone sensitivity. Fig. 12 shows part of the preamplifier schematic, which is responsible for microphone biasing – Bias unit.

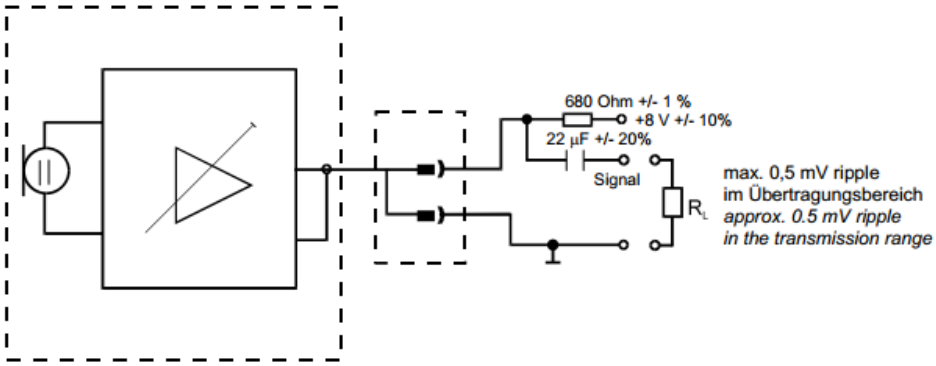

Fig. 10: Microphone connection example by VDA specifications [10]

There are two main types of electret microphones. One uses the connection as shown on the picture Fig. 10. It means, that the microphone has two electrical contacts. The bias voltage and audio signal are together lead at one contact and second is used for GND. This type of connection is known as the phantom power. The second type of electret microphone has three electrical contacts. One contact is common GND. The second contact provides the signal transport and the third allows connection of the bias voltage. To provide a universal interface, the testing tool includes a here is a mechanical switch, which provides suitable connection of the bias voltage to the microphone.

The central part of the bias unit is 10-bit, low power buffered voltage output digital to analog convertor from Texas Instruments. The DAC6573 utilizes an I2C communication supporting high-speed interface mode with address support of up to sixteen ICs. Address of DAC consists of nine bits. First five bits (MSB) are factory preset to 10011. Next two bits of the address byte are the device select bits (correspondent with A0 and A1 pins on Fig. 12). These inputs can be connected to V_{DD} or GND. Last two address bits (correspondent with A2 and A3 pins) are also the device select bits but they are MSB in a control byte. For both required microphones is needed only one DAC6573. Because of this reason all pins (A0 to A3) are connected to GND.[11]

DAC6573 requires an external reference voltage to set output level. Pin $V_{REF}H$ sets positive reference input which can be in range from GND to V_{DD}. Negative reference voltage input is set by $V_{REF}L$ pin and it should be in range from GND to $V_{DD}/2$. The output buffer is capable of generating rail-to-rail voltages on its output, which gives an output range of 0 V to V_{DD}. In this application both digital and analog voltage are $V = 3.3$ V. But this range is not enough for the requirements of microphones. From this reason IC5 is connected as non-inverting amplifier with constant gain

G = 3.2. Therefore real output range is of 0 V to 10.5 V with voltage step about 10.3 mV. Range of the resulting bias voltage depending on the DAC value is in the Fig. 11 measured on a prototype board with set bias resistor R = 330 Ω. There is a noticeable difference between the channels of convertor. This difference may be caused by differential error of DAC which makes 0.5 LSB according to the manufacturer's documentation. With the positive voltage reference $V_{REF}H$ = 1.2 V error 0.5 LSB represents voltage about 0.6 mV. Or more likely difference may be caused by 5 % resistance tolerance of used components on the prototype testing board.[11]

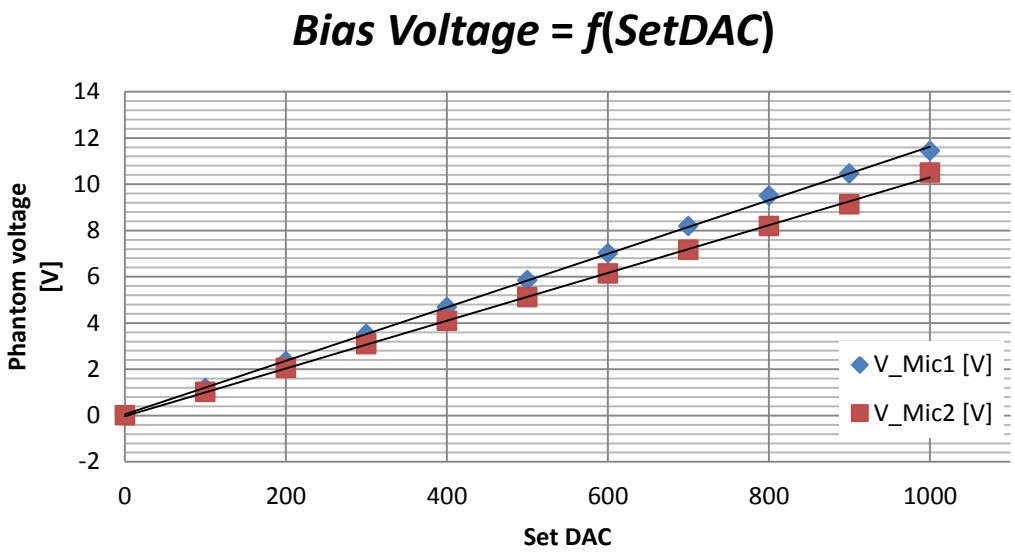

Fig. 11: Voltage characteristic of bias unit (330 Ω)

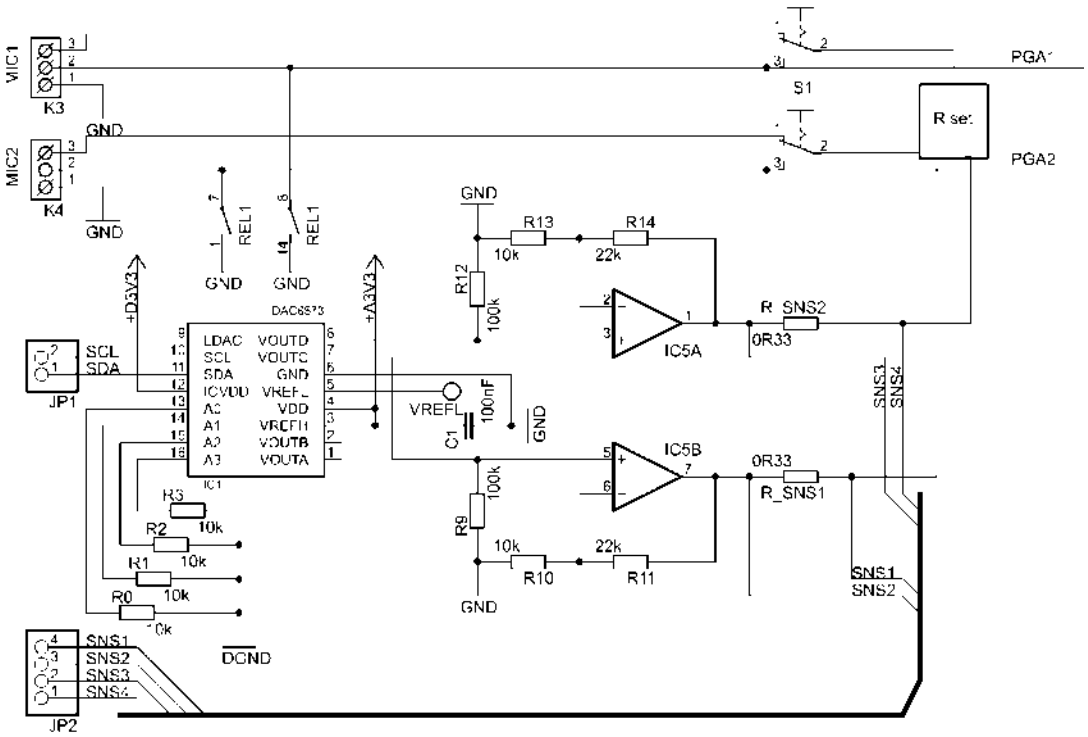

Fig. 12: Part of preamplifier schematic - Bias unit

The "R set" block (Fig. 12) is used for setting the bias resistor and it consists of three options among which it can be switched. The first option is array of typically used resistor values (using high-precision parts). The second one is potentiometer for setting arbitrary microphone biasing resistance. The third option allows connecting an external through-hole resistor. It is located on the external user interface and allows using any required bias resistor value with. For accurate setting of the potentiometer, there are precise sensing resistors of value R_{SNS} = 0.33 Ω connected in series with R set block. Voltage drop is measured through the sensing resistors by the AD converter and the calculated value of the potentiometer is shown in the user interface to allow user-feedback. Example of bias resistor calculation is shown in the Fig. 13.

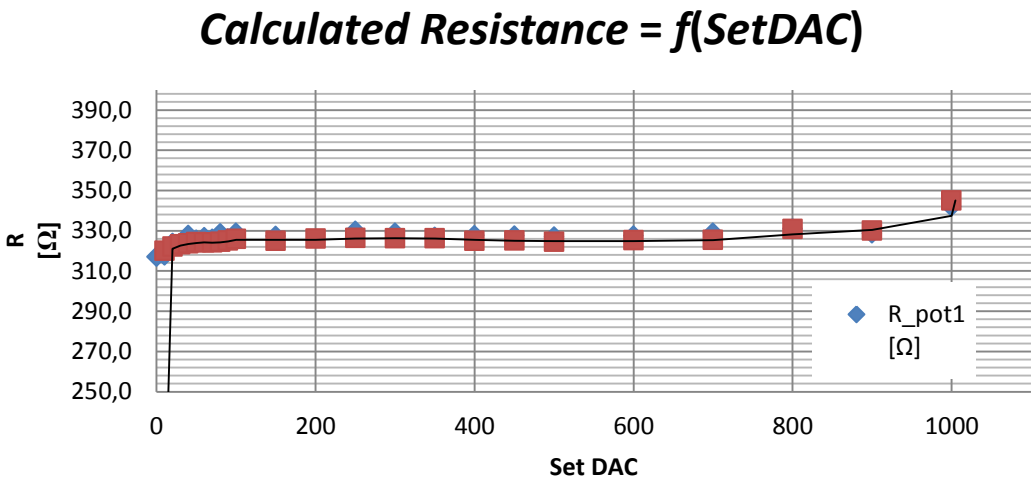

Fig. 13: Example of bias resistor calculation (330 Ω)

Measurement of the bias voltage shows sufficiently accurate results in the middle of the DAC output levels.

2.1.1.2 Programmable gain amplifier

To achieve a suitable output level from the microphone sub-board, the programmable gain amplifier PGA112 from Texas Instruments manufacturer is used. The PGA112 is single-ended, single-supply IC with input multiplexer. The PGA uses a standard serial peripheral interface (SPI) with both supported SPI modes 0,0 and 1,1. It provides good audio parameters such as low noise, low gain error or zero thermal drift of output level and allows binary gain selection (1, 2, 4, 8, 16, 32, 64, 128). Fig. 14 represents related part of the preamplifier schematic. Each microphone channel has its own PGA112 which uses CH0/CAL input of the integrated multiplexer. This input includes the four internal calibration channels for ADC gain and offset errors calibration. The PGA op amp is a rail-to-rail input and output single supply op amp. In this reason usage of the reference voltage in the middle of AV_{DD} is necessary to process input audio signal.[12]

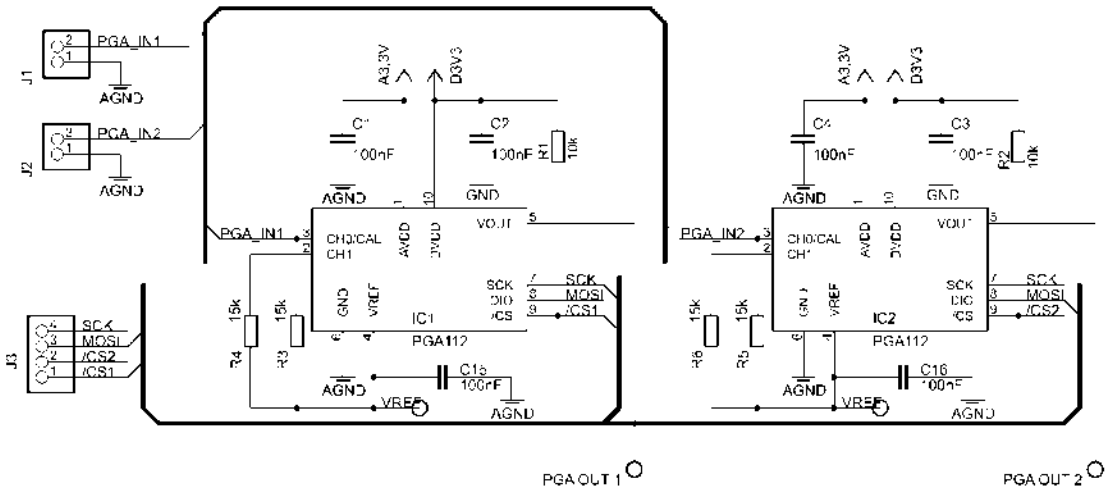

Fig. 14: Part of preamplifier schematic – Programmable gain amplifier

Prototype board for interface testing, audio performance measurements and verification was prepared. SPI was tested in 0,0 mode with read/write commands. The PGA has only one pin for both serial input and output operations. Direction of communication (MOSI, MISO) is determined by the previous SPI command. Measurements of the audio performance were conducted using audio analyser Kenwood VA-2230A. Fig. 15 and Fig. 18 are results of the measurements. The frequency response (Fig. 15) is relatively flat and smooth. In the frequency range f_1 = 25 Hz to f_2 = 25 kHz easily meets -3 dB condition. In the required maximum frequency range (f_1 = 80 Hz to f_2 = 8 kHz corresponding to wideband speech) ripple of the frequency response is only about ΔKu = 0.4 dB when gain was set G = 1.

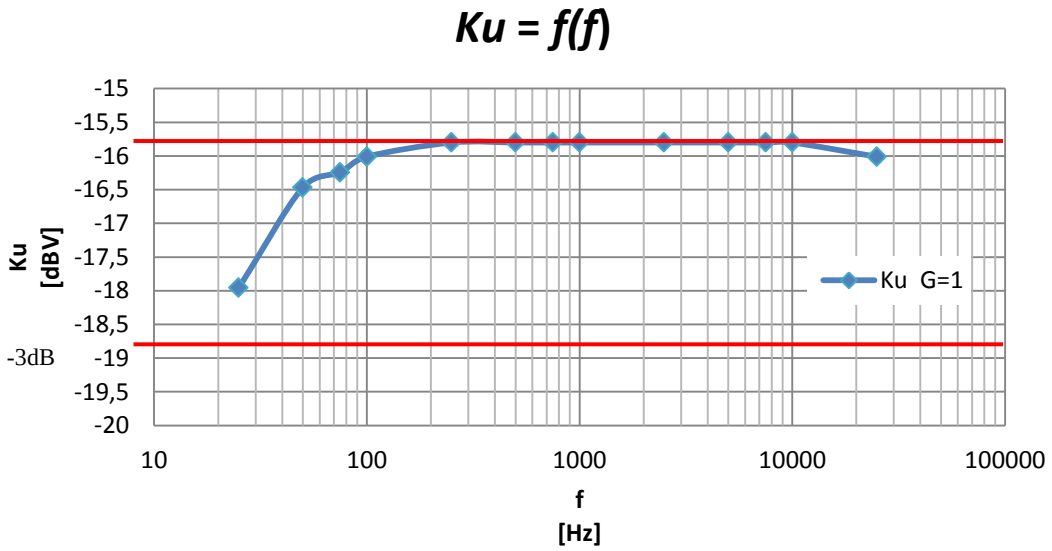

Fig. 15: Frequency response of the PGA112

The manufacturer states good noise performance. The measurement of the signal

to noise ratio (*S/N*) depending on the gain (Fig. 16), was done with low input signal (V_{in} = 100 mV_{PP}) to achieve the best approximation of real situation.

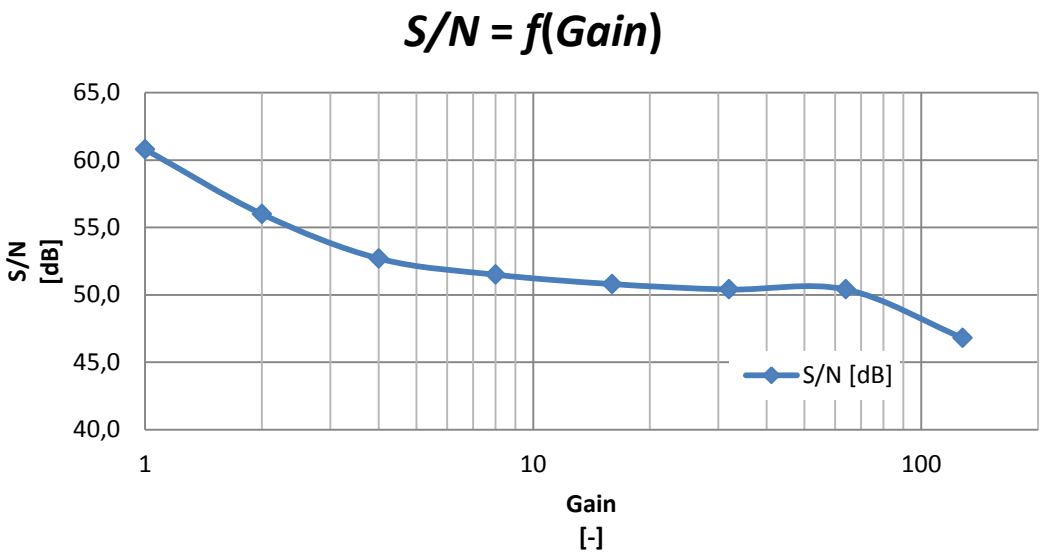

Fig. 16: Signal to noise ratio depending on the gain

The measured value *S/N* =60.8 dB for gain *G* = 1 and input signal V_{in} = 100 mV_{PP} is acceptable. With gain increasing *S/N* ratio decreases, S/N ratio has value under 50 dB for gain *G*=128.

Total harmonic distortion (*THD*) and *THD* plus noise (*THD+N*) was measured depending on the gain (Fig. 17) and on the frequency (Fig. 18). There is a quite low *THD* < 0.052 % correspondent to low gain values *G* = (1, 2, 4, 8) shown on the graph (Fig. 17). Higher values of the *THD+N* may be caused due to low input signal V_{in} = 100 mV_{PP}. The excitation signal has frequency *f* = 1 kHz. The manufacturer gives values 0.005 % under following test conditions: *G* = 10, *f* = 1 kHz, V_{OUT} = 4 V_{PP} at 2.5 V_{DC}, and load R_L = 10 kΩ, C_L = 100 pF.

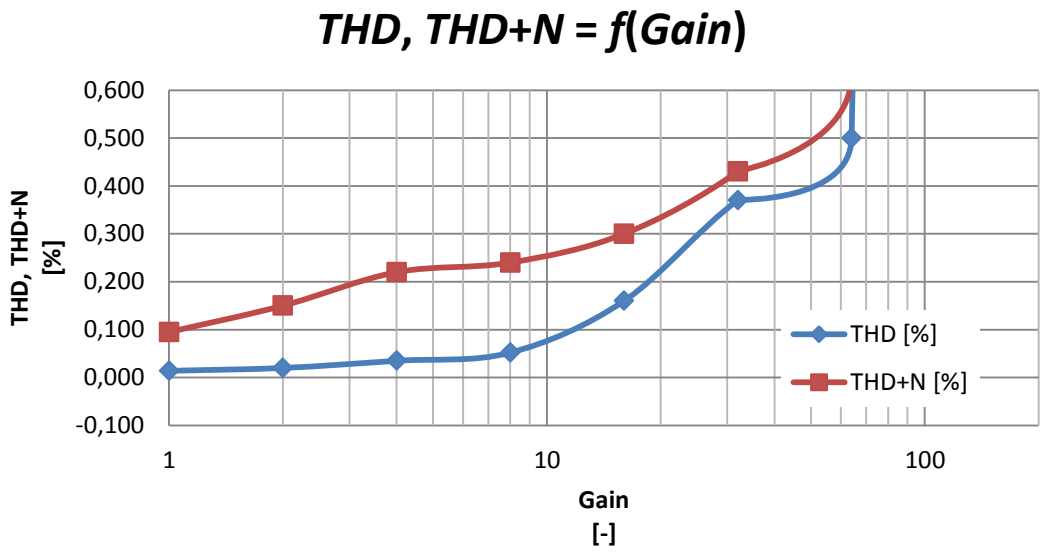

Fig. 17: THD and THD+N depending on the gain

On the graph (Fig. 18) is shown *THD* and *THD+N* waveform depending on the frequency. Measurement conditions were V_{in} = 100 mV_{PP}, G = 1. The THD values are under 0.025 % across the full range of frequency and at the frequency f = 1 kHz is *THD* = 0.013 %.

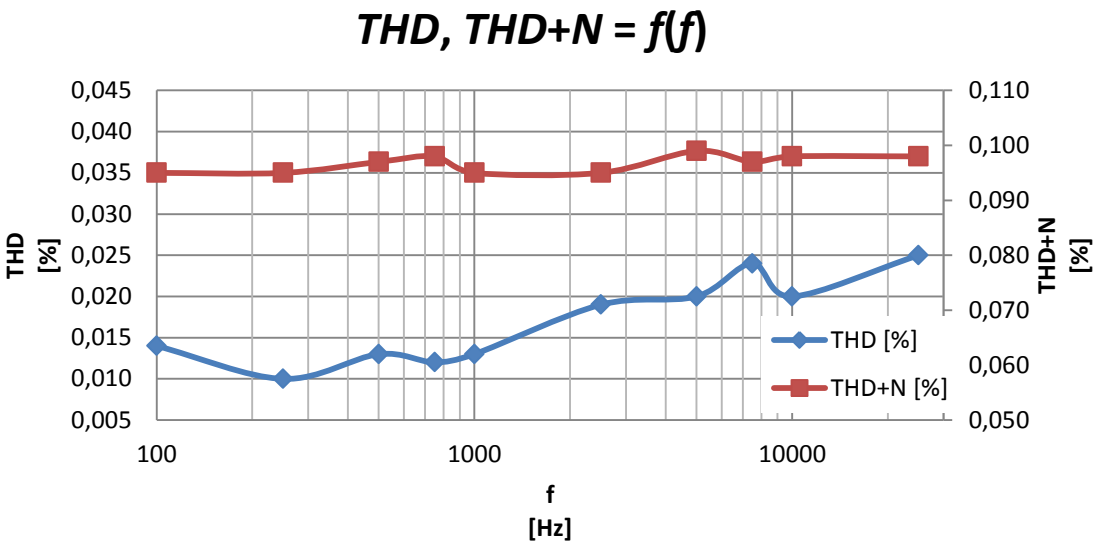

Fig. 18: THD and THD+N depending on the frequency

2.1.1.3 Test-signal generator

The generator of the testing signal provides a useful tool for audio path verification. It allows user to confirm the correct setting of the entire input audio path (or find possible mistakes in the configuration).

Two options of generator implementation were considered. The first one

was a usage of separate microprocessor with DDS algorithm. The second option was complete DDS IC from Analog Devices. Finally, the second solution was selected, as it offers easier implementation, better power consumption and *THD* performance. That outweighs the slightly higher price of such solution, especially for a small production.

AD9834 is 75 MHz low power complete DDS capable of producing high performance sine, triangular and square output. With 28bits frequency register and 75 MHz clock rate, the resolution 0.28Hz can be achieved.[13]

On the picture Fig. 19 schematic of the test-signal generator prototype board is shown. *THD* = 0.065 % was measured with available 48 MHz crystal oscillator. In the final measurements, lower values with recommended crystal oscillator are expected.

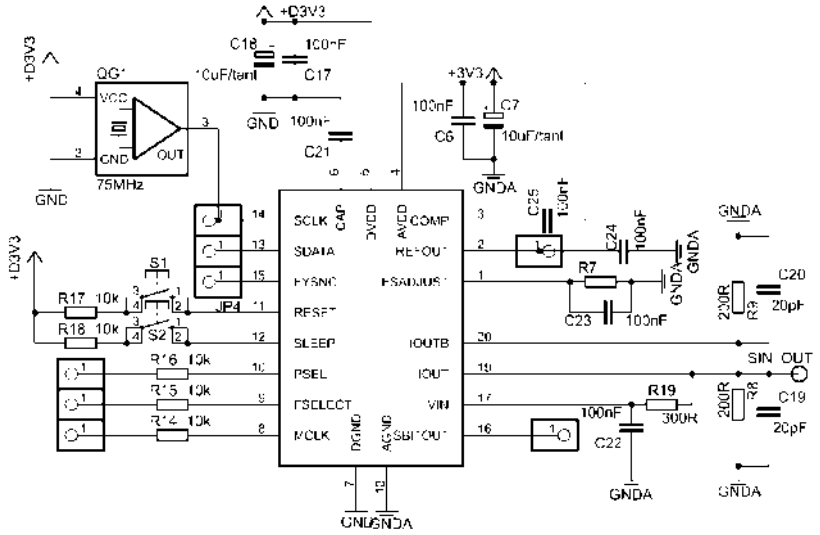

Fig. 19: Part of preamplifier schematic – Test-signal generator

2.1.2 Band filters

Different bandwidth in HF systems provides different hearing experience to participants of the call. Wideband audio offers high definition of voice and improvement in intelligibility due to extension of bandwidth from B_{NARROW} = 4 kHz (300 Hz to 3.7 kHz) to $B_{WIDEBAND}$ = 8 kHz (80 Hz to 7.7 kHz).[8]

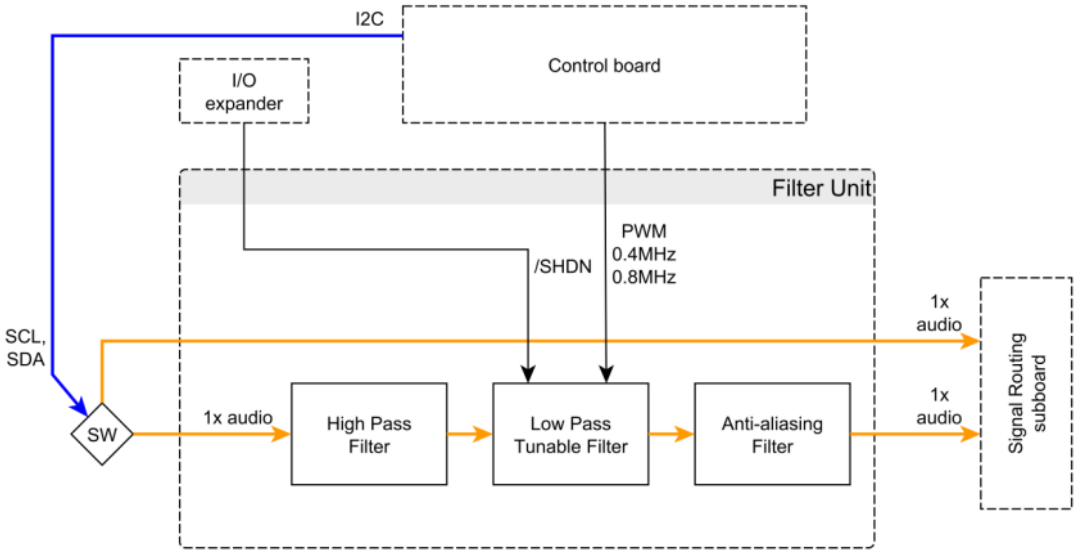

Fig. 20: Block diagram of the microphone filter unit

Bandwidth used in a final solution depends on customer requirements. In this reason tuning tool has to support various bandwidths. It may provide number of fixed and switchable filters. Or a much more adaptable solution with some tuneable (semi parametric) filter, which was finally adopted for this testing tool. The band-pass filter block consists of fixed high-pass and tuneable low-pass filter connected in series (Fig. 20). High-pass filter is the second order Sallen&Key filter with cut-off frequency f_C = 80 Hz. According to [14] cut-off frequency can be calculated by the formula (6). The design example of Sallen&Key filter is on the diagram of the filter unit (Fig. 22).

$$f_C = \frac{1}{2\pi\sqrt{R_1 C_1 R_2 C_2}} \qquad [\text{Hz}, \Omega, \text{F}] \qquad (6)$$

Calculated theoretical values were adjusted to producible form and simulated in SPICE simulator LTspiceIV. The resulting waveform of the simulation, for values of resistors R_1 = 300 kΩ, R_2 = 180 kΩ and capacitors C_1 = C_2 = 10 nF, is on the picture (Fig. 21). The read off value of the cut-off frequency is approximately f_{C1} = 77 Hz and slope -35 dB/dec.

On the completed prototype of the final filter design further adjustments were made. After several measurements the values of resistors R_1 = 330 kΩ, R_2 = 470 kΩ and capacitors C_1 = C_2 = 10 nF were selected. Measurement of this configuration was made by audio analyser Kenwood VA-2230A and the resulting module frequency characteristic is on the picture (Fig. 24) together with tuneable low pass filter. The resulting read off cut-off frequency of Sallen&Key is f_{c1} = 80 Hz.

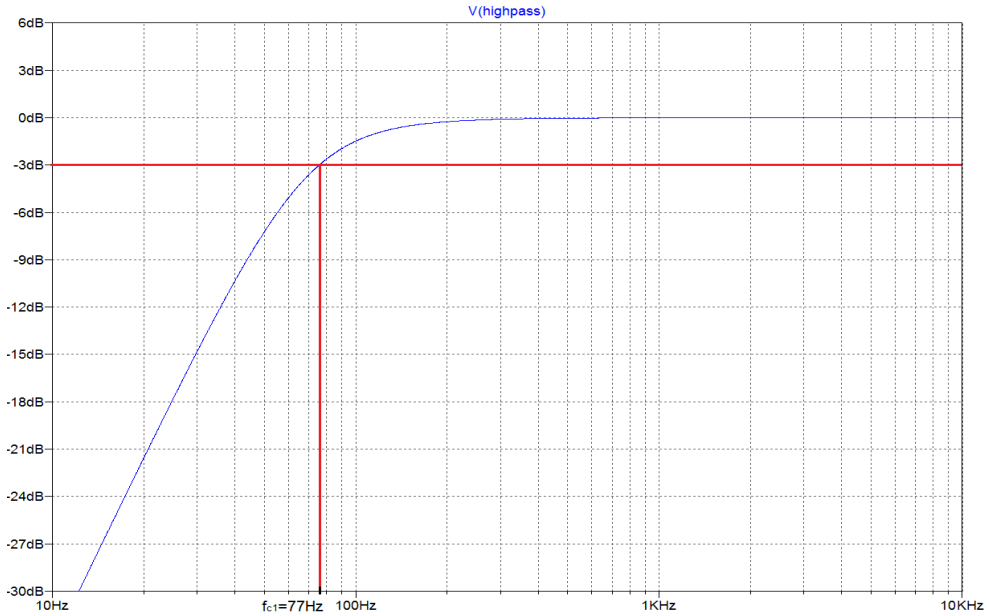

Fig. 21: Simulation result of the 2nd order Sallen&Key high-pass filter

The low-pass filter is realized by MAX7400 the 8th order, elliptic, switched-capacitor filter which allows corner frequencies from 1 Hz to 10 kHz. Two clocking options are available. The first option is self-clocking, through the use of external capacitor. But this option is not suitable, because the cut-off frequency is set by this capacitor. Set of the accurate cut-off frequency is impossible due to limited values of capacitors. The second clocking option is external clocking by PWM signal for tighter cut-off frequency control. The MAX7400 provide 82dB of stop band rejection and sharp roll-off with transition ratio of 1.5.[15]

External clock has frequency range from 100 Hz to 1 MHz with 40 % to 60 % duty cycle. CLK pin should be driven with CMOS gate powered from 0 V to V_{DD} = 5 V. Variation of the rate of the external clock adjusts the filter corner frequency:

$$f_C = \frac{f_{CLK}}{100}. \qquad \text{[Hz]} \qquad (7)$$

In case the filter unit is not used, it's possible to bypass the entire filter unit, and put the device into a shutdown mode. That is activated by driving shutdown pit to low. Placing the filter in shutdown mode reduces the supply current to 0.2 µA and places the output of the filter into a high-impedance state.[15]

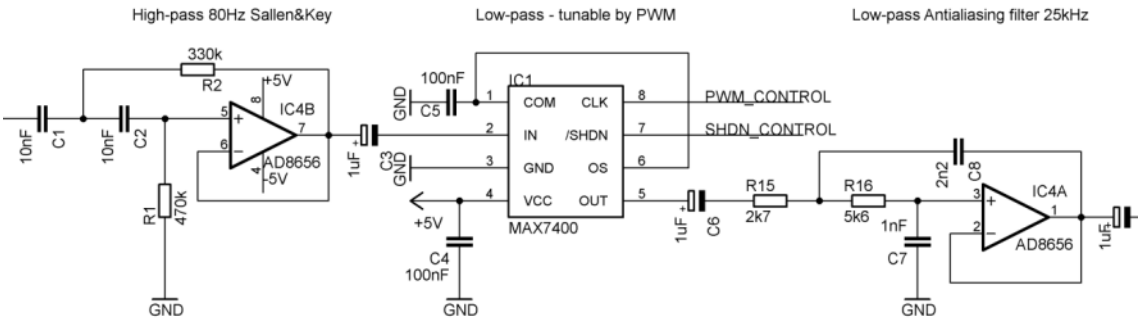

Fig. 22: Part of preamplifier schematic - Filter unit

The last part of the filter unit is the second order Sallen&Key low-pass anti-aliasing filter with cut-off frequency f_C = 25 kHz and slope approximately -40 dB. Simulation of the anti-aliasing filter is on Fig. 23. In this configuration, filter attenuate high frequency components that can appear as by-products of the preceding switched-capacitor tuneable filter operation.

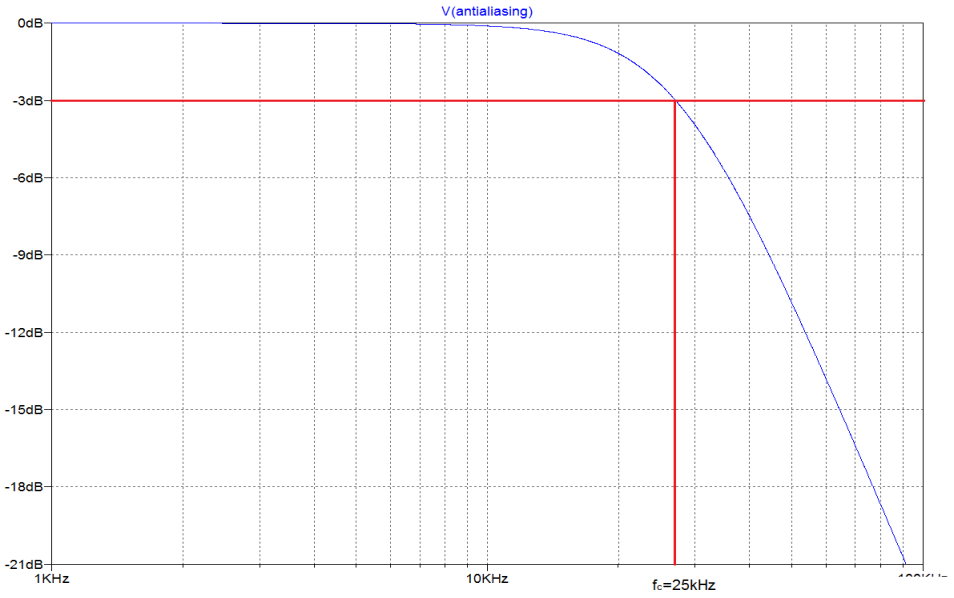

Fig. 23: Simulation result of the 2nd order Sallen&Key low-pass anti-aliasing filter

The prototype board of the complete filter unit was prepared and measured. The frequency response of the tuneable band pass filter is on the picture (Fig. 24). There are two waveforms. The blue one correspondents to narrowband pass filter with cut-off frequency approximately f_{C2} = 4 kHz. The red waveform correspondents to wideband pass filter with cut-off frequency f_{C3} = 8 kHz. To achieve the necessary corner frequencies PWM signal with frequencies f_{PWM1} = 400 kHz and f_{PWM2} = 800 kHz from 16-bit timer/counter was used.

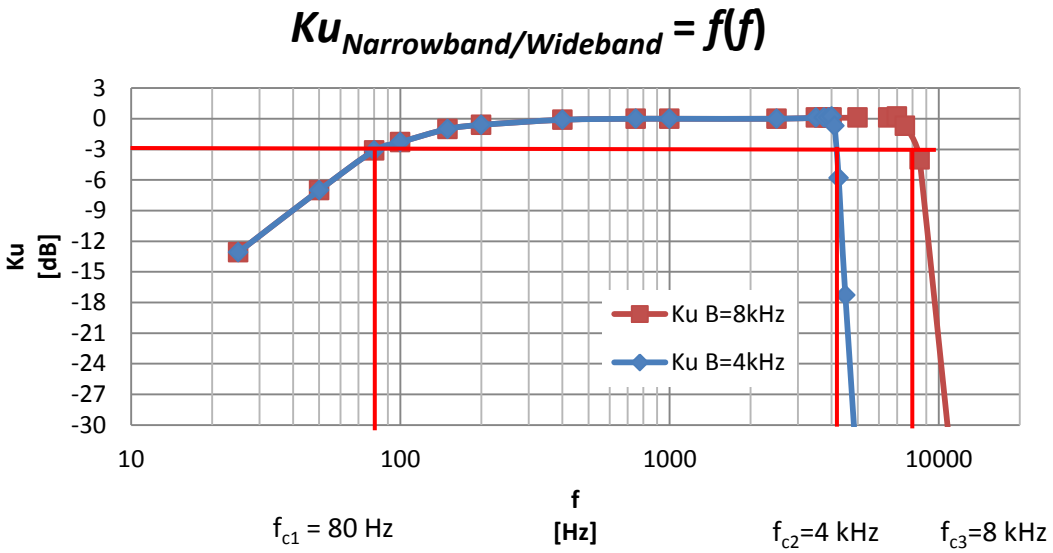

Fig. 24: Resulting frequency response of the band pass filter B = 4 kHz, B = 8 kHz

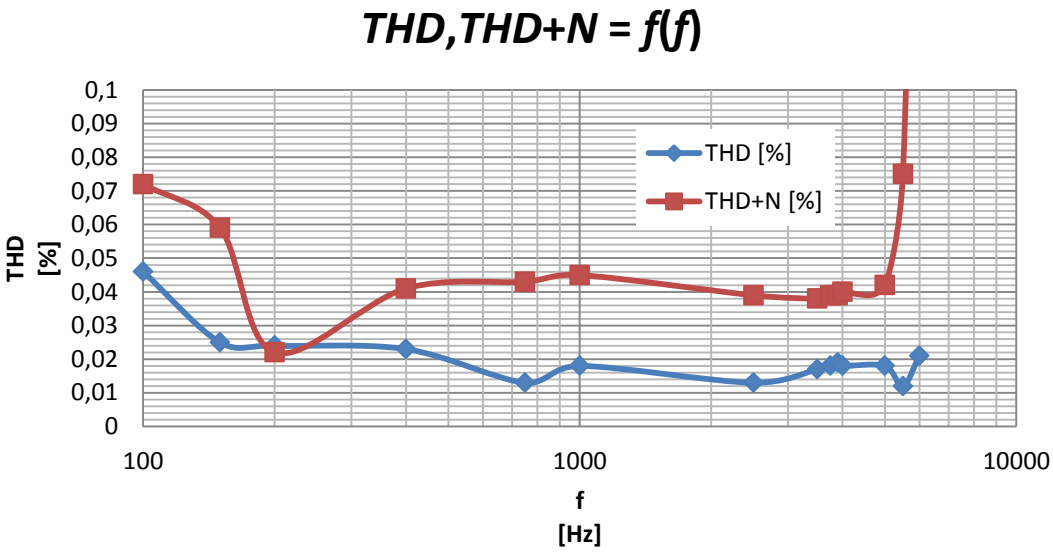

Fig. 25: Total harmonic distortion of the prototype filter unit (narrowband)

An important factor of audio chain is also total harmonic distortion. According to [16] the used capacitors in filter design influence total harmonic distortion. The ordinary X7R ceramic capacitors, also used in filter prototype, cause relatively large distortion. From this reason the least distorting common capacitors were selected for design of high-pass and anti-aliasing filters. But for testing tool capacitors with more suitable material such as COG ceramic capacitors or foil-film polypropylene capacitors and also more performance audio operational amplifier will be selected. This selection should cause better *THD* and noise performance of filter unit. Measurements were done again by audio analyser Kenwood for narrow band configuration. Measured values of the *THD* are in range from 0.012 % to 0.046 % (Fig. 25).

2.1.3 Microphone input – design

Second revision of the microphone input board was designed and manufactured. This revision connects and unifies all logical blocks (separate sub-boards from the first revision) to one board with design fitting into the tool case. All circuit schematics and PCB layouts are in appendixes A.1.1 and A.1.2. The microphone input board is closely connected with the external user interface, as the hardware part of the UI contains microphone input connectors and basic controls of the microphone biasing circuits.

The microphone signal comes to the board from the UI through the flat cable connector (K6 in the Fig. 51). Each audio wire in the flat cable is surrounded by ground wires on each side to reduce crosstalk between channels. First block in the audio path is the PGA (IC4 and IC5 in the Fig. 52), acting as a preamplifier, followed by mixing (IC18) and multiplexing unit (IC7 in the Fig. 54). This unit allows connection of the test-signal generator (IC6 in the Fig. 53) or bypass of the filter unit. After filtration, the audio signal is connected to the audio routing board by another flat cable.

Most of the analog and noise sensitive components are located on the top layer of the PCB (Fig. 56). The main audio path passes through the upper part. Voltage sources (LDOs) are located in the lower left-hand corner of the board Two of those sources (IC19, IC20) serve as voltage reference. Next source is using REF_{OUT} pin of the IC6 (AD9834), which provides V_{REF} = 1.18 V.[13] Pin header JP5 serves as a switch for selecting the one of three suitable solutions. Mixed analog/digital parts and circuits are located in the lower right-hand corner of the board. These circuits include test-signal generator and preparation for audio buffers of clipping indication unit (IC21 in the Fig. 55), realized by microcontroller ATtiny841 (IC23).

The second layer (Fig. 57) is reserved for analog supply rails (3.3 V, 5 V and 10 V) and voltage reference rail. The remaining audio traces, which could not be fit on the top, are also routed through this layer.

The third layer (Fig. 58) and bottom layer (Fig. 59) serve for digital signals and digital supply rails. There are I2C expanders (IC15, IC16 in the Fig. 48), oscillator of the test-signal generator and microcontroller connected to debug buttons (S5, S6) and LED1 and LED2 (Fig. 55). Test points were placed on microcontroller signal and IO traces to achieve maximum modularity during clipping indication development.

2.1.4 Microphone input – processed results

Measured data of the second revision of microphone input block is in appendix A.2.1. First preamplifier (IC4 PGA112) was measured to compare parameters between revisions. The frequency response comparison of the microphone preamplifiers from rev.1 and rev.2 is depicted in Fig. 26. As the graph shows, there is a small difference between revisions in the lower frequencies. But it makes only ΔKu = 0.3 dB.

The measurement of *THD* vs. PGA gain was performed with test sine signal with level V_{in} = -30 dBV and frequency f = 1 kHz. Resulting values of the total harmonic distortion are $THD \leq 0.05$ % below binary gain setting G = 32 (Fig. 115). However, relatively high level of noise influences *THD+N* measurement (Fig. 115 Fig. 116) with higher gain settings. It was confirmed that the noise of the microphone input board

is distributed by the V_{REF} rail. It is necessary to add resistor between voltage reference rail and each circuit using this reference to reduce current taken from voltage reference supply and attenuate processed signal. Resistor value may be about R = 15 kΩ as R25 and R26 in the Fig. 52.

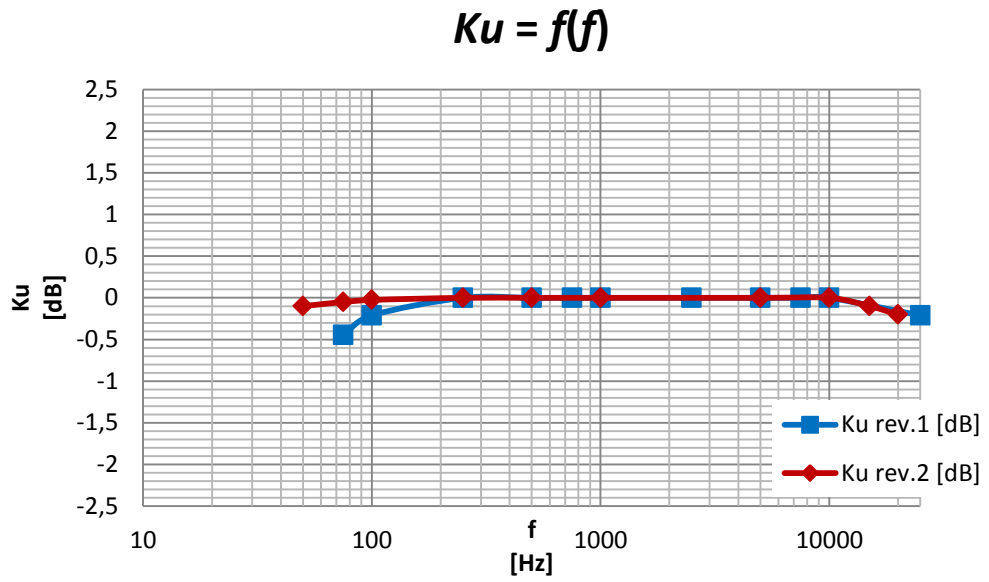

Fig. 26: PGA112's frequency response of the different revisions microphone input

In comparison with the first revision, a significant improvement of *THD* was achieved, especially for higher gain settings. It is caused by higher quality components used in whole audio path.

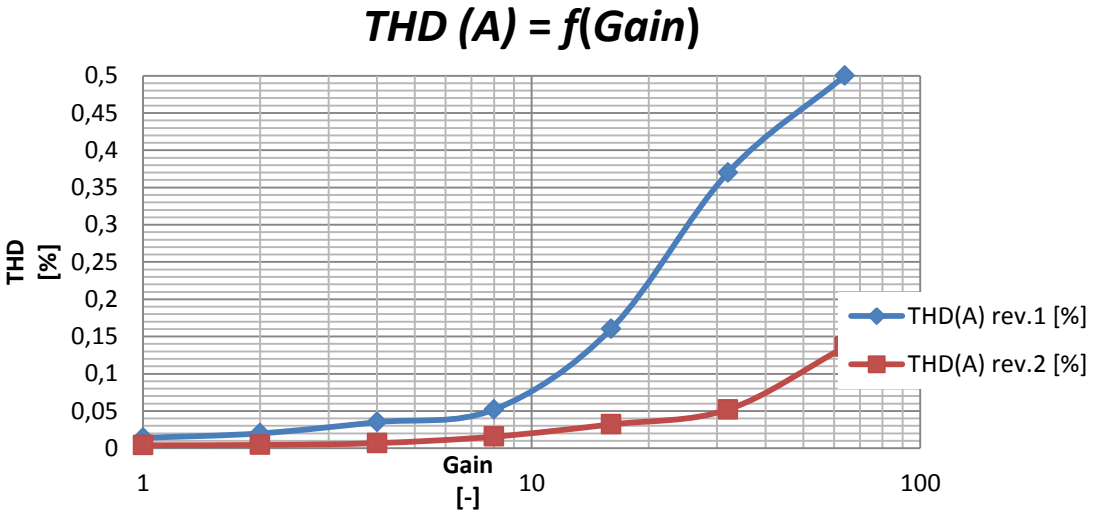

Fig. 27: PGA112's *THD* measurement of the different revisions depending on gain

Fig. 116 shows result of measurement PGA112's *THD* depending on frequency. Values fluctuate about THD = 0.04 %, with testing parameters of signal V_{in} = -0.5 dBV and gain setting G = 1 (Tab. 7).

Tab. 5 includes measurement results of the whole audio path. Total harmonic distortion, measured at 1 kHz, reach value THD = 0.036 %

Frequency response of the whole audio path (Fig. 114) corresponds well with measured first revision. PWM frequency f_{PWM} = 740 kHz is required to achieve low-pass corner frequency f_{c2} = 7.7 kHz. It makes error Δf = 30 kHz compared with data in product documentation.[15]

Last measured unit at microphone input second revision board is DDS (IC6 in the Fig. 53). Output level of the analog sine signal is V_{out} = -14.8 dBV and the generated f = 1 kHz signal has THD = 0.055 % with 48 MHz oscillator (Tab. 8).

Next modifications of this board will be focused primarily on eliminating problems with the voltage reference rail.

2.2 Duplex multichannel converter

The duplex multichannel converter provides connection of all function blocks together. It has two main tasks. The first one is signal routing, which allows connection of arbitrary input to arbitrary output. The second task is conversion of analog signal to digital and vice versa.

2.2.1 Audio routing

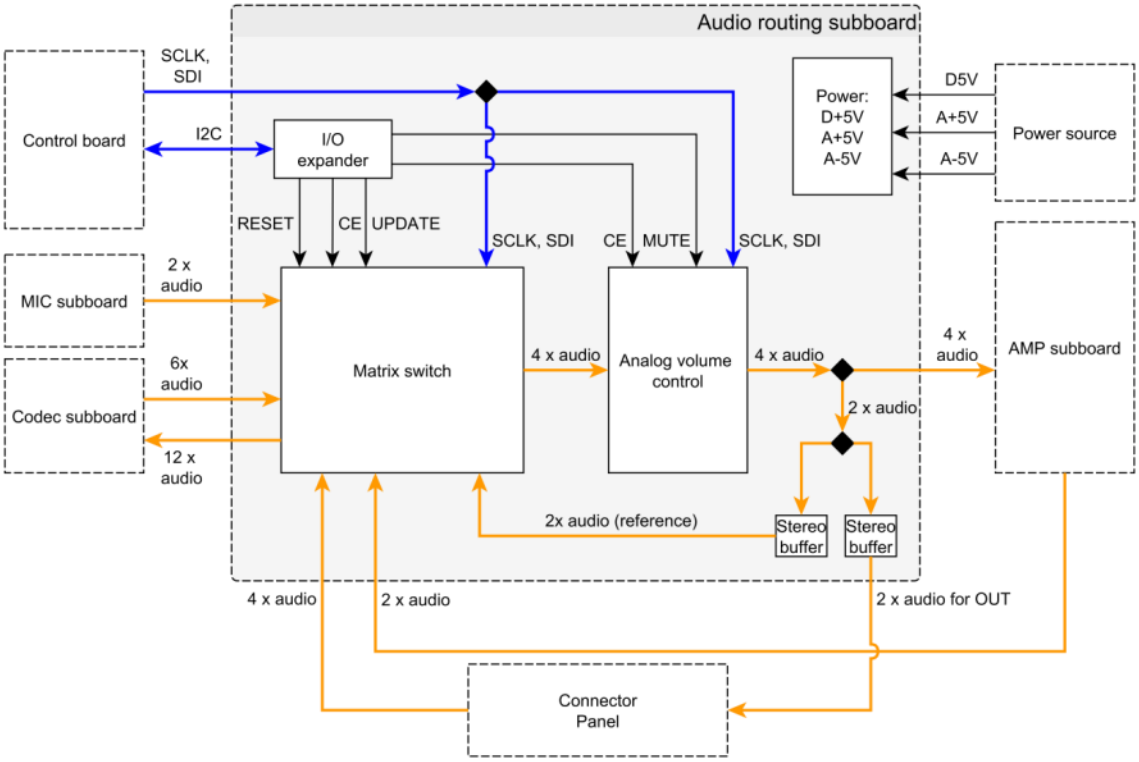

Fig. 28: Block diagram of the audio routing sub-board

The matrix switch has the most important function in this sub-board. The audio routing block diagram (Fig. 28) shows all possible analog inputs and outputs.

Two microphone channels, two stereo line input channels, three stereo inputs from codec sub-board and two stereo audio references required for the EC running on the DUT are connected to the matrix switch. Outputs of the matrix switch include three outputs connected to codec sub-board and one output to the volume control. Each output has stereo front and rear channels (together it takes 16 line outputs).

Analog volume control is provided by PGA4311 from Texas Instruments. The PGA4311 is a high performance, four channel programmable gain amplifier designed for high-end audio system. It has low additive noise and low THD = 0.0004 % at f = 1 kHz and gain G = 0 dB. Gain and attenuation range is wide from +31.5 dB to -95.5 dB with gain step ΔG = 0.5 dB. Gain and mute is controlled by 3 wire serial control interface (SPI). Mute function is also controlled by hardware /MUTE input pin.[17]

The switch function is provided by 16x16 high speed nonblocking switch array AD8113. The manufacturer promises low $THD \leq 0.002$ % at f = 20 kHz $V_{in\text{-}max}$ = 20 V_{PP}. Low crosstalk of -83 dB and bandwidth $BW_{\text{-}3dB}$ = 60 MHz. Each output can be connected to any of the 16 inputs. Organised by output row, 16 switchable stages are connected to each output buffer in the form of 16 to 1 multiplexer. Each of the 16 rows is wired in parallel to the 16 inputs pins, for total array of 256 transconductance stages. Anywhere from zero to 16 transconductance stages can be sharing one input pin, so there is a varying amount of bias current supplied through the source impedance driving the input. For audio systems with larger source impedances, this has the potential of creating large offset voltages, audible as pops when switching between channels.

2.2.1.1 Audio routing design

Complete design documentation is in the appendix A.1.6 and A.1.7. Layout of this board was formed with respect to evaluation board AD8113.[17] The evaluation board is also reference with the best possible results of audio performance. It provides the ideal star layout of inputs/outputs (without crossing) terminated with 75Ω BNC connector. The input/output traces are placed on one layer separated from each other by ground plane. This limits capacitive coupling and improves measured audio parameters, at the cost of PCB size, which is rather large (26 x 31 cm). Due to relatively small dimension of the tool case and different functions of the inputs/outputs, it was necessary to use two layers (with crossing). All reference data are in manufacturer product documentation.[17]

The top layer of the PCB (Fig. 83) is used for placement of all noise sensitive integrated circuits. There are also necessary audio signals and the linear voltage regulators for an analog supply. Rest of the top layer is shielding plane connected to the analog ground.

The second layer (Fig. 84) is used for most of the analog signals. There is the analog ground between each wire to reduce channel crosstalk. During design and routing of this layer, the emphasis was put on the reduction of capacitive coupling and optimal signal shielding.

The third layer (Fig. 85) is reserved for power supply traces. Large part of the copper plane is also connected to the analog ground.

The bottom layer (Fig. 86) is accommodates digital interface consisting of the I^2C

port expander PCF8574. There are also additional components supporting function of the AD8113.

Electronics circuit of the matrix switch (Fig. 80 in A.1.4) was prepared according to the manufacturer's recommendations. The resistors R_1~R_{16} = 10 kΩ determine input impedance. There are decoupling capacitors C_4~C_{20} = 10 nF placed on the bottom layer as close as possible to AD8113. There are decoupling capacitors C = 100 nF and C = 10 uF for each supply line placed on the top layer.

The volume control IC (PGA4311) needs minimum of external component (Fig. 52). There are only six decoupling capacitors for separated digital and analog voltage supply.

The stereo audio references consist of the four operational amplifiers ADA4075 connected as simple audio buffers. The ADA4075 reaches also good audio performance. For example low distortion THD = 0.0002 % and noise N = 2.8 nV/√Hz (typ.), declared by the manufacturer.[18]

As with other boards there are ribbon connectors for the audio inputs and outputs. Each audio wire is surrounded by ground wire on each side.

2.2.1.2 Audio routing – processed results

First revision of this PCB was manufactured and measured. Appendix A.2.2 contains all measurement results. Frequency response is really flat. The maximum difference is ΔKu = 0.3 dB (Fig. 117 in A.2.2). But this difference is caused by low-pass filter activated in the audio analyser with corner frequency f_c = 20 kHz. Fig. 117 shows measured frequency response. Extent vertical axis of the graph is only 1 dB.

Total harmonic distortion (Tab. 12) was measured with activated psophometric A-weighted filter. Frequency of the input signal was f = 1 kHz and level Vin = 1.5 dBV, output was unloaded. Value of measured THD = 0.0025 % is similar to the manufacturer's specification of THD = 0.002 % under test conditions f = 20 kHz, R_L = 600 Ω, Vin = 20 V_{P-P}. The conditions are not directly comparable, but with regards to the application, a measurement at 20 kHz was not optimal and therefore had not been conducted.

Crosstalk specified by manufacturer is V_{CROSS} = -67 dB with input signal f = 20 kHz. With lower frequency signal value of the crosstalk is better. Crosstalk of the designed prototyped board was measured between input/output channels 5 and 4. Even though the testing signal had lower frequency (f = 1 kHz), the value of crosstalk was measured V_{CROSS} = -60.7 dB (Tab. 11). Worse parameters are caused by suboptimal layout, limited by the PCB dimensions. Measured values are however sufficient for the application purposes.

Fig. 133 and Fig. 134 show mounted PCB of the audio routing from top and bottom side.

2.2.2 Codec sub-board

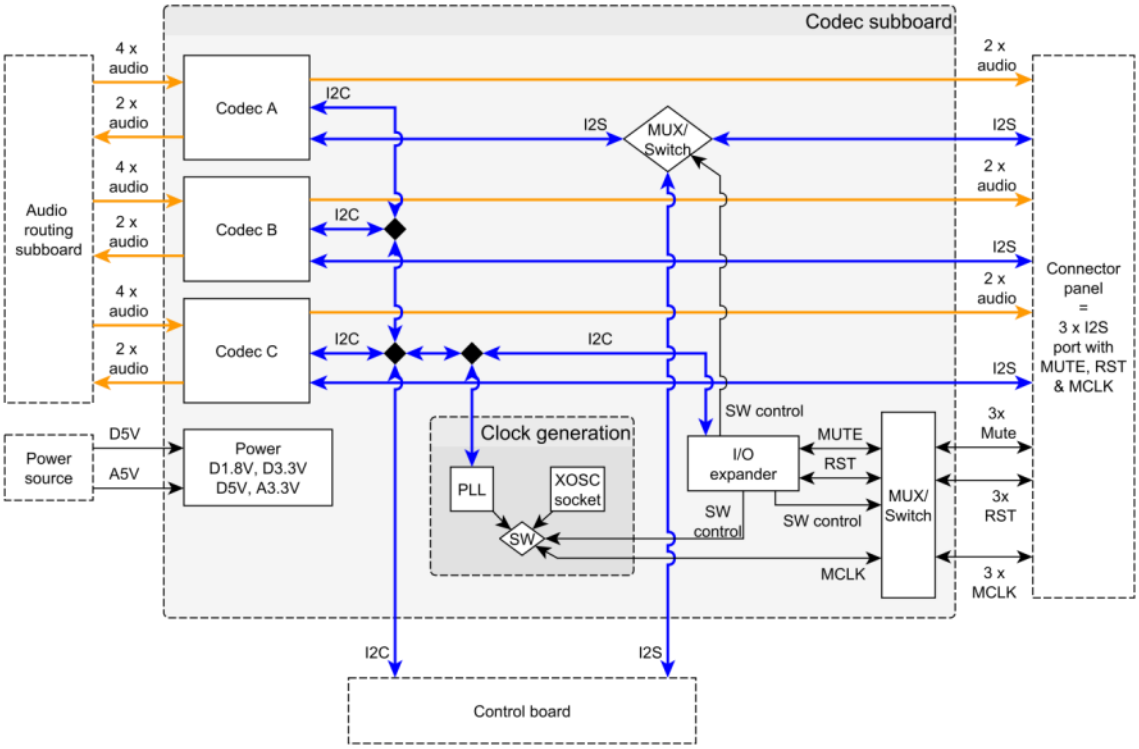

Fig. 29: Block diagram of the codec sub-board

The codec sub-board is based on three TLV320AIC33 codec ICs. It is low power stereo audio codec with multiple inputs and outputs programmable in single ended or fully differential configurations. Power consumption under 14mW with supply 3.3 V makes it ideal for portable battery-powered audio and telephony applications. The stereo audio ADC and DAC supports sampling rates from 8 kHz to 96 kHz. The serial protocol bus supports SPI or I2C protocols, while the serial audio data bus is programmable for I2S, left/right-justified, DSO, or TDM modes. A highly programmable PLL is included for flexible clock generation and support for all standards audio rates from a wide range of available MCLKs. For more accurate but fixed MCLK XOSC socket is included into the design.[20]

2.3 Class D amplifier

Power amplifier integrated into the testing tool is crucial part of the system for several reasons. Being able to bypass the amplifier system built into the car means maintaining the entire audio output chain (except speakers) constant, which is important for benchmarking. As explained in chapter 1.2, nonlinear distortion in a power amplifier presents major source of EC problems. Therefore it's necessary to use hi-quality/low-distortion amplifier to achieve the best possible EC performance. Finally, integrated amplifier stage is useful for demonstrations in case the infotainment system including amplifier has been removed from the test vehicle for one reason or another.

Amplifier selected for this tool is TAS5414 four channel digital audio amplifier

designed for use in automotive amplifier modules. It's a product aiming for high-level segment of infotainment systems, but still belongs into the commonly used automotive parts.

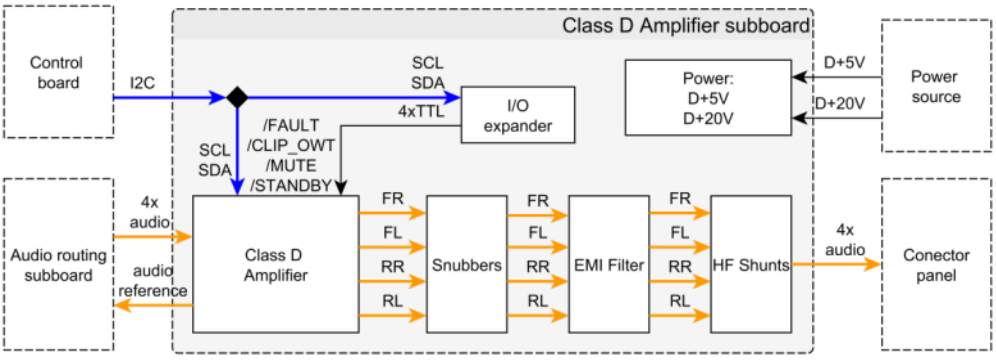

Fig. 30: Block diagram of the class D amplifier

TAS5414 can drive four channels with 4 Ω loads at 58 W (max.). According to [21] amplifier reaches efficiency about 90 % with 4 Ω load at 23 W. With power supply V_{DD} = 21 V, output power 1 W and excitation signal f = 1 kHz, it achieves *THD+N* of 0.02 %. TAS5414 has integrated preamplifier with configurable gain G = (12, 20, 26, 32) dB per channel. It has built-in load diagnostic functions for detecting and diagnosing misconnected outputs to help to reduce test time during the tuning process. Protection and monitoring functions provide over-and-under supply voltage conditions, current and over-temperature protection, dc level and clip detection. Current state of the amplifier can be read via I2C bus. Alternatively, four hardware pins can be used to capture fault events in real time.

- /FAULT is output pin that indicates presence of a fault condition. Under this condition amplifier goes automatically into Hi-Z mode or standby mode and will stay in standby until fault log is read by I2C interface. As the selected voltage source (charge pump) has slower power-on voltage ramping, TAS5414 would report under voltage fault at V_{DD} event when it is turned on. For this reason, this false fault log must be at the end of the amplifier power-up sequence.
- /CLIP_OWT pin is configured by the user to indicate overtemperature warning or the detection of clipping. The configuration is selected via I2C bus.
- /MUTE is input/output pin used for hardware hard control/detection of the mute state for all four channels. For pop- and click- free operation a capacitor is connected to this pin. Capacitor value influence time constant for the gain ramp.

/STANDBY pin has a large influence on the power consumption, among others. When it is asserted, the device goes into a complete shutdown, and current draw is limited to 2 μA.[21]

To reduce interference in the AM radio band, the TAS5414 has the ability to change the switching frequency via I2C commands. This can eliminate tones that can appear in radio signal due to switching frequency being demodulated by the AM tuner circuits.

The TAS5414 amplifier outputs are driven by high-current LDMOS transistors in an H-bridge configuration. The resulting output signal is PWM with duty cycle that is proportional to the amplitude of the audio signal. The main purpose

of the second-order LC filter (reconstruction filter) is to attenuate the high-frequency components of the output signal.[21]

2.3.1 Class D amplifier - design

All circuit schematics are in appendix A.1.8. The preamplifier of the TAS5414 has high input impedance. It allows the use of low cost (class 2) input capacitors C = 1 uF made of the Y5V material (Fig. 89). Snubbers are connected to inputs to prevent high-frequency interference signals (automotive EMI). EMI snubbers consist of the resistor R_{18} = 499 Ω and capacitor C_{43} = 1.2 nF forming the low-pass filter with corner frequency f_C = 150 kHz and –and slope 20 dB per decade. For this application of high frequency filtering, film capacitors from Polyphenylene Sulphide (PPS) were selected. Capacitors from this material have small temperature and frequency dependence and are thus suitable in frequency-determining applications.[22] The input snubbers were placed on the top PCB layer in highest possible proximity to the TAS5414 to achieve the best performance. Resistors $R_{18\text{-}21}$ = 49.9 kΩ represent input impedance for Audio Routing sub-board. Fig. 31 depicts simulated frequency response of the input filters.

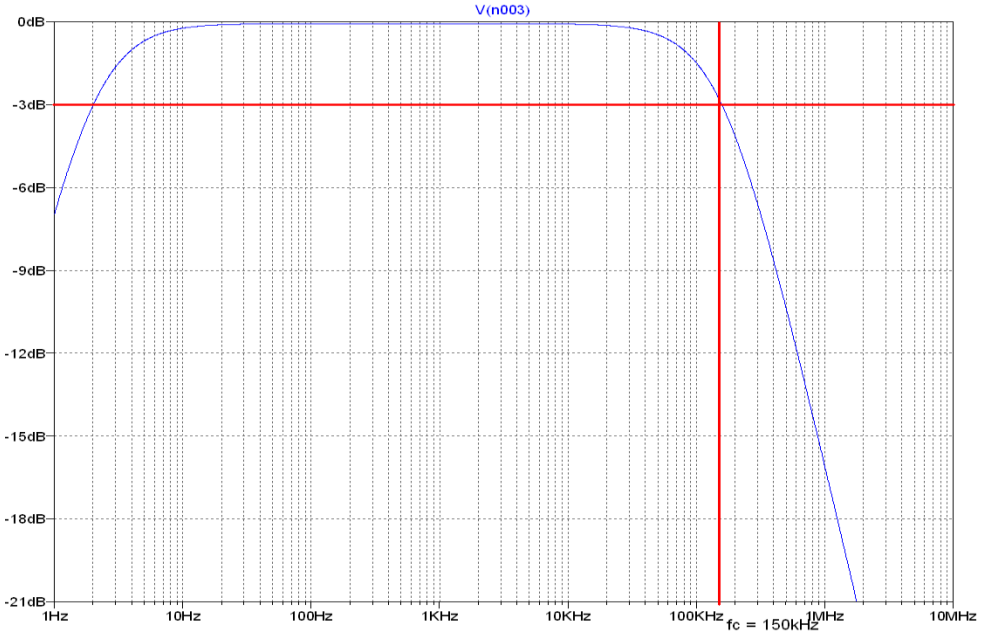

Fig. 31: Simulated frequency response of the input EMI filter

According to the manufacturer's recommendations, a second order reconstruction filter was used to recover the audio signal from square-wave output signal. The main purpose of the output filter is to attenuate high frequency components of the output. The output filter consists of snubbers, EMI and demodulation filters and HF shunts. Simulated frequency response of the output filter is depicted in Fig. 32 A corner frequency of the recommended reconstruction filter is f_C = 42 kHz and the slope is -40 dB per decade. Film PPS capacitors with 1 nF, 150 nF and 470 nF values were selected for the implementation.

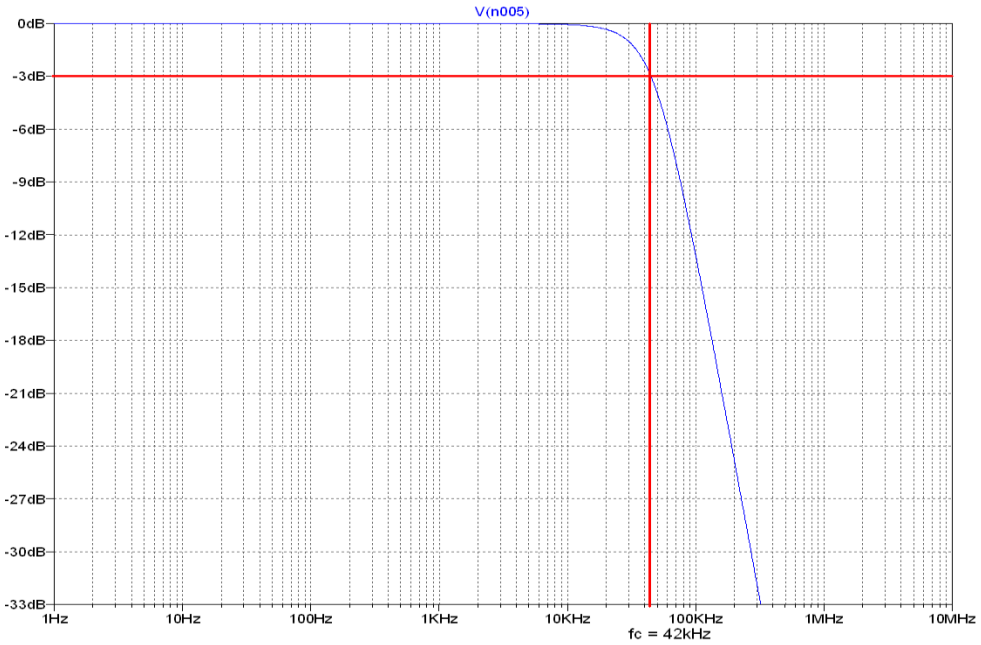

Fig. 32: Simulated frequency response of the output reconstruction filter

The Audio Reference Unit is the next noise sensitive block at the Power Amplifier sub-board. A conversion from balanced audio outputs of the power amplifier to unbalanced audio signals is the main task of this unit. These signals are used as audio reference for echo suppression algorithms used in the device under test. Operational amplifier (IC4 in Fig. 91) is connected as difference amplifier. The best common-mode rejection (CMR) parameter can be achieved with identical gain at both channels. Therefore OZ INA2134 was selected. It includes laser trimmed precision resistors to achieve accurate gain and highest CMR. The CMR of typical device designed with INA2134 is about 74 dB as specified by the manufacturer. This OA is also features low distortion $THD+N$ = 0.002 %.[23]

There is a digital potentiometer, which allows adjust output level. The potentiometer AD5242 from Analog Devices, Inc. was selected with nominal value R = 10 kΩ. It has I^2C interface and includes two resistors with 256 positions.[24]

There is also I^2C expander for saving GPIO pins at the Raspberry Pi. It drives and senses the power amplifier's control pins, (/mute, /standby etc.).

2.3.2 Class D amplifier – processed results

First revision of the power amplifier board was manufactured and measured against 4 Ω loads. All measured results are included in appendix A.2.3. There is frequency response of the amplifier for each build-in preamplifier setting of gain G = (12, 20, 26, 32) dB. As Fig. 33 shows, curves of frequency response are flattened with maximum difference ΔKu = 0.4 dB for gain 12 dB and ΔKu = 1.5 dB for gain 32 dB in the measured range. Therefor attenuation -3 dB could not be marked. Maximum gain-error is G_{err} = 0.6 dB. These errors meet requirements. Values of gain error are 2 dB according to product documentation.[21]

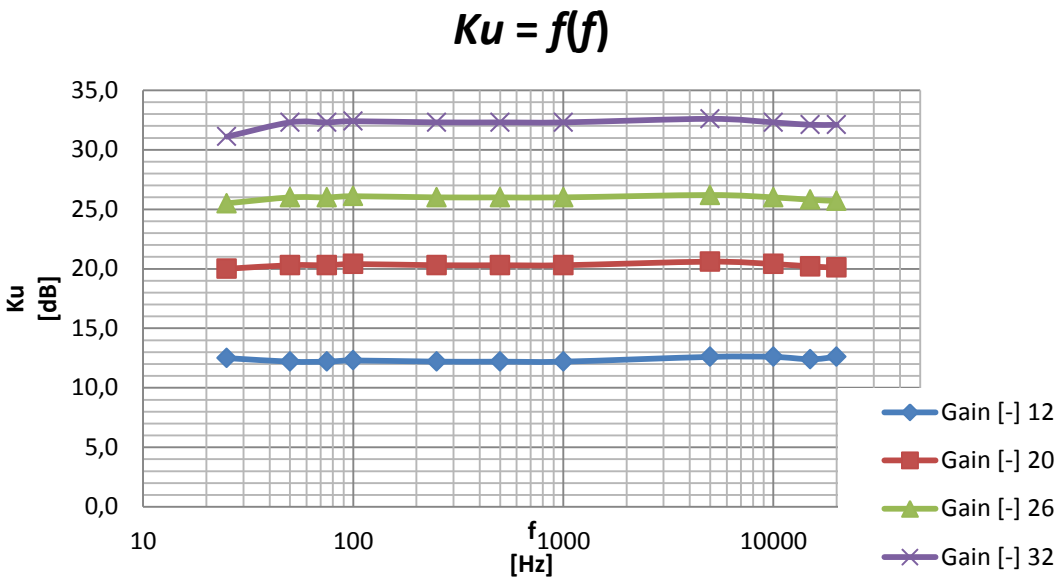

Fig. 33: Frequency response of power amplifier

Values of total harmonic distortion were measured with psophometric A-weighted filter, which takes into account the physiological characteristics of the human ear and is common for measurements of telephony and voice-communication equipment. The first graph shows *THD* on the level of the input signal with gain set to 12 dB. Fig. 34 shows that acceptable values of the *THD+N* ≤ 0.05 % are achievable for maximum input level V_{in} = -5 dBV (V_{in} = 0.56 V_{RMS}). With higher levels of input signal total harmonic distortion started climbing steeply over values *THD*+N = 0.2 % (V_{in} = 0 dBV). Depending on gain (Fig. 120) values of *THD+N* varies in the range from 0.052 % to 0.24 %. Level of input signal was V_{in} = -5 dBV.

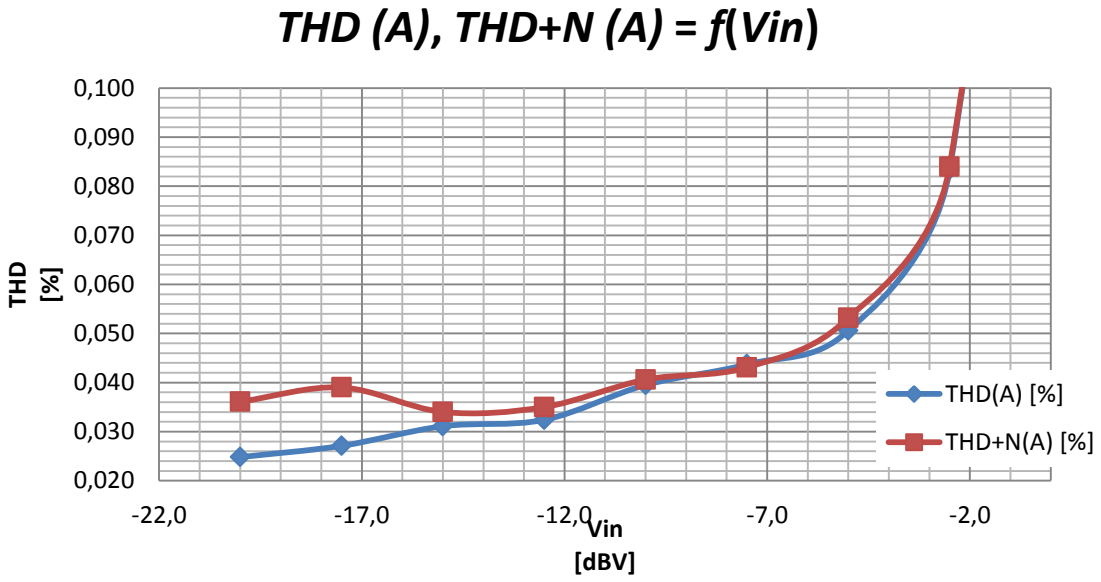

Fig. 34: *THD*, *THD+N* of power amplifier depending on input signal level

It’s difficult to match these results with data from manufacturer, as the measurement conditions were not the same. Measurements were conducted to verify performance at conditions relevant to the application. Therefore levels of input signals were chosen with regard to clipping of the output signal, well below the clipping boundaries. Datasheet values for THD+N range from 0.02 % to 0.1 % under following conditions P = 1 W, G = 26 dB, f = 1 kHz. Output power P = 1 W correspondents with V_{in} = -12 dBV.[21]

Crosstalk was measured between channel 3 and 4 into 4 Ω load at output power approximately P_{out} = 10 W (V_{in} = -10 dBV, G = 26 dB) depending on frequency. Fig. 121 shows a plateau at the level of V_{CROSS} = 35.5 dB. Tab. 17 contains measured data. This table also includes measurement of crosstalk level depending on the output power. Values are in the range from -60.2 dB (P_{out} = 0.4 W) to -40.3 dB (P_{out} = 39 W). These results are sufficient in comparison with manufacturer value range of crosstalk from 75 dB to 60 dB with output power P_{out} = 1 W.[21]

Measurements of the Audio Reference block were not conducted yet because of scheduling limitations.

Next revision will be focused at better mechanical layout, especially with regards to installation and mounting into the case.

2.4 Control board

The control board consists only of Raspberry Pi module. The Raspberry Pi is single-board computer developed in the UK by the Raspberry Pi Foundation with the intention of promoting the teaching of basic computer science in schools. The Raspberry Pi has a Broadcom BCM2835 system on chip, which includes an ARM1176JZF-S with FPU, VideoCore IV GPU and 512 MB of RAM. It uses an SD card for booting and long-term storage. For the purpose of this project was chosen Raspberry Pi model B revision 2.0. Operating system is Raspbian Linux distribution. [25]

The model B features two USB ports and 10/100 Ethernet controller, which serves as programming and tool setting interface. There are other useful peripherals such as 8x GPIO, I2C bus, SPI bus and I2S audio bus. These peripherals are connected to others sub-boards as shown on the picture Fig. 35. 12 devices are connected to I2C bus, 8 devices are connected to SPI bus and one device is connected to I2S bus for which is used for debug and verify of the I2S audio.

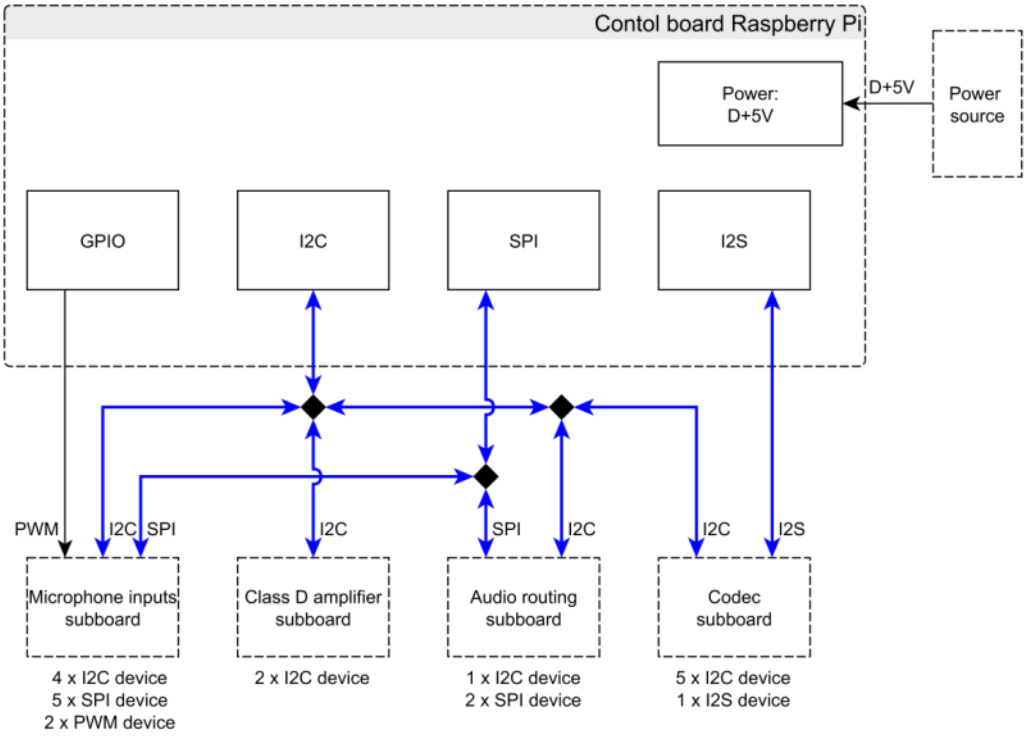

Fig. 35: Block diagram of the control board

2.4.1 Control board – design

The function of the Control board is to provide interconnection between Raspberry Pi (RPi) and the rest of the test tool system – other boards as well as the tool case (temperature control), UI and DUT. Control board layout in its first revision (in appendix A.1.10 and A.1.11) was designed specifically to allow easy debugging. It is expected that future revisions will be optimized in terms of trace routing, connector design etc.

In order to connect RPi to the board in the shortest and mechanically robust way, it was necessary to move the RPi connector P1 to the other side of the RPi board and add pin headers for connector P5.

All GPIO signals are routed to pin headers in the upper part of the control board, complemented by several GND and voltage supply rail pins. (P1 in the Fig. 98). These pin headers can be used as debug pins, or for some future hardware extension.

Input/output pins of two I2C port expanders (PCF8574 IC1 and IC2 in the Fig. 98) are placed near the debug pin headers. Next to them are three connectors (K8, 10, 11) for temperature sensor DS18B20. There are other connectors on the left side of the control board, which are used for connection of other boards to common busses (see Fig. 136). There are also two supply connectors (K12 and K13) for +5 V and +12 V digital rails. The +12 V rail serves for supply and control ventilator placed on the rear wall of the tool case by transistor Q1.

Real Time Circuit connector, a pair of the I2C port expanders and connector for I2S audio (K6) are placed on the bottom layer. Ethernet and USB will be lead out to connectors for panel mounting via cables directly from RPi.

2.5 Power sources

Testing tool uses automotive 12V system as the primary power source. DC-DC convertors on the power sources sub-board provide supply voltage for digital ICs. Necessary analog supply sources are supplied by LDOs on individual sub-boards to reduce noise and interferences. Detailed block diagram of power distribution among sub-boards is shown in Fig. 36

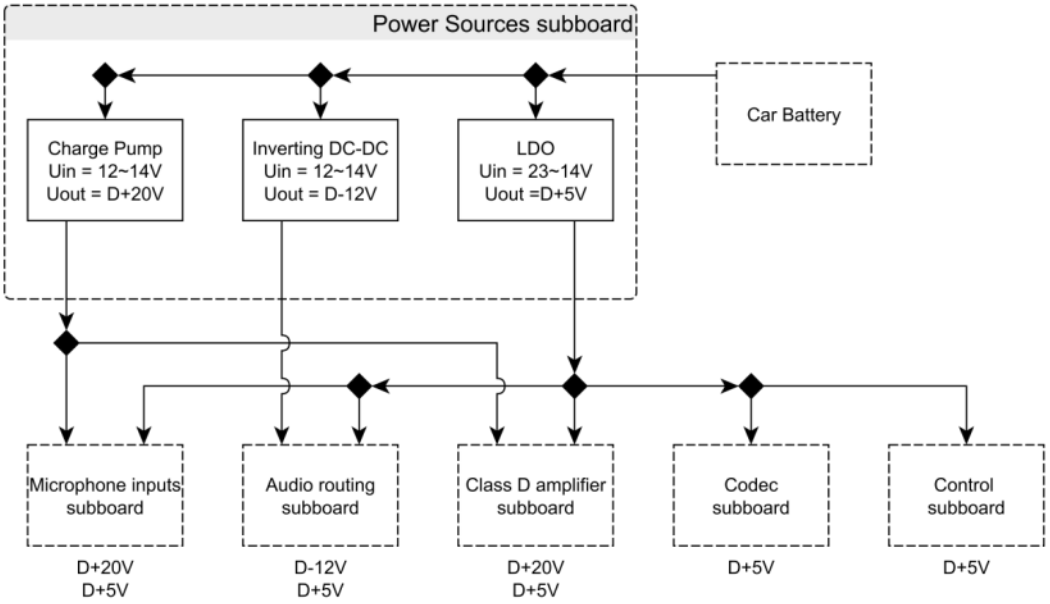

Fig. 36: Block diagram of the power sources sub-board

The design of power source module is an important aspect of the system. Parameters of the power source affect all sub-boards and influence the audio performance. In noise-sensitive applications, such as an analog audio system, low noise and low output impedance are necessary to achieve desired quality and performance.

2.5.1 Utilization of modular power supplies

A design of suitable power source for the entire system is difficult and time-consuming task. For this project, which will result in only several pieces of constructed units, it is sensible to utilize ready-made third party solutions, as long as the technical parameters are sufficient and the solution is cost-effective.

For that reason, cost-effective solutions available on the market were tested for each required power supply block. Original designs were used only when it could be confirmed that no solution on the market will be able to provide sufficient parameters for the application at a given cost.

Each of the following sections therefore begins with comparison of ready-made commercial solutions (most of them are products popular for prototyping).

2.5.2 Power sources for low-voltage circuits

In the process of investigating available commercial solutions, several samples from Chinese manufacturers (Fig. 41) were measured and compared. Unfortunately, DC-DC module No. 2 did not work and therefore was excluded from the results.

Power supply for the low-voltage circuits is provided by common D+5 V rail. In this case a DC-DC step-down converter topology is used. Benefits include small dimensions, good stability, and high efficiency. This reduces heat dissipation inside the tool enclosure, thus reducing cooling and temperature stabilization requirements. Two step-down (buck) DC-DC modules and one step up/down (buck-boost) module were tested (Fig. 37). All important parameters provided by the manufacturer are in the Tab. 1. The task was to verify the data and to decide about suitability for use in the designed testing tool.

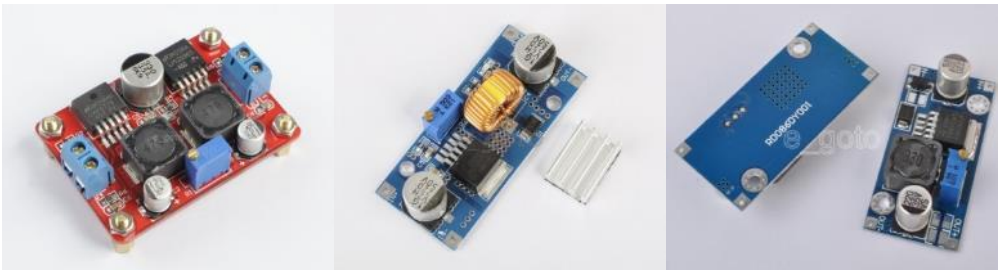

Fig. 37: Purchased DC-DC modules (No. 1 [26], No. 2 [27], No. 3 [28])

Tab. 1: DC-DC modules specifications [26], [27], [28]

		No. 1	No. 2	No. 3
Topology	[-]	BUCK-BOOST	BUCK	BUCK
Input voltage	[V]	3,5-28	4-38	4-35
Output voltage	[V]	1,25-26	1,25-36	1,23-30
Output current (max)	[A]	3	5	3
Efficiency (max)	[%]	Unspecified	96	92
Output ripple	[mV]	Unspecified	Unspecified	30

Output ripple and unwanted additive noise of higher harmonics frequencies are important parameters for the noise-sensitive applications. Output ripple and propagation of higher harmonics on the power rail are common properties of DC-DC converters. These unwanted phenomena may rules them out as a power option for many use cases.

Power sources requirements are nominal input voltage V_{in} = 12 V, output voltages V_{out1} = 5 V V_{out2} = 3.3 V and the lowest possible noise level. DC-DC modules measurements (Fig.38) were performed in the laboratory of student creativity at DREL, BUT (Brno University of Technology).

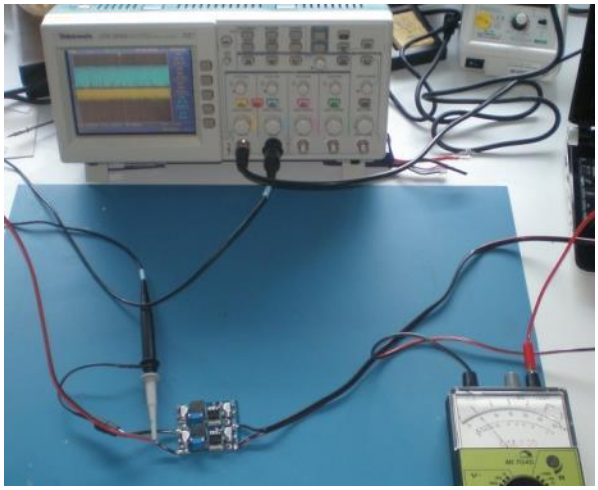

Fig.38: Measuring workplace, DC-DC module No. 1

Used measurement setup and relevant measured data are included in appendix (A, Tab. 1). Fig. 39 and Fig. 40 show the most interesting results with regards to the testing tool design. The worst case of output ripple voltage and the high frequency additive noise was always measured. This curve is named $V_{pp\text{-}out}$ [mV] = $f(I_{out})$. In this measurement Diametral P230R51D was used as input power source and set to 12 V.

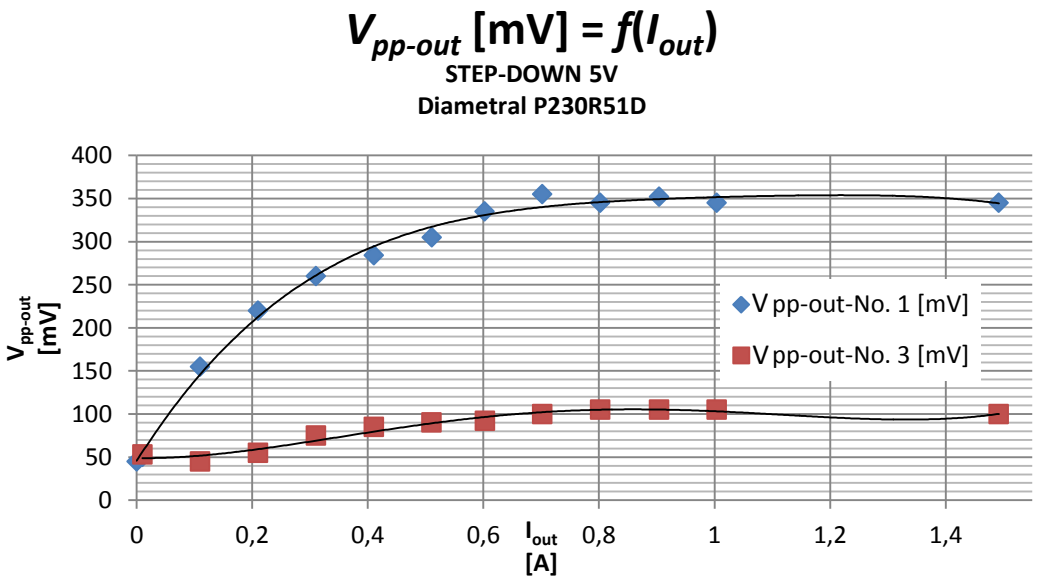

Fig. 39: DC-DC modules measured output noise, V_{out} = 5 V

Output voltage of the DC-DC modules was 5V in the first case. On the Fig. 40 is graph of the same measurement, this time with V_{out} = 3.3 V.

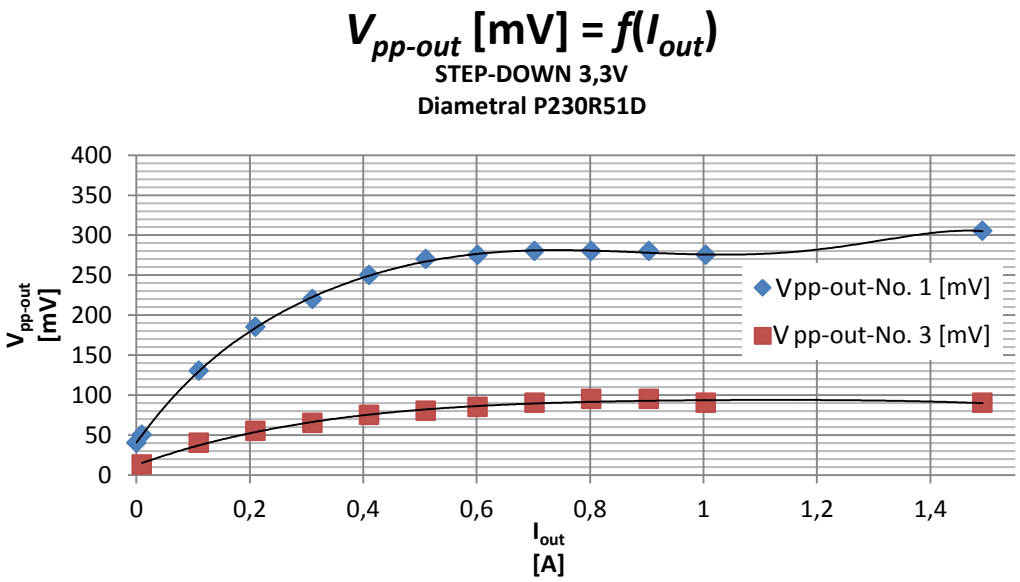

Fig. 40: DC-DC modules measured output noise, V_{out} = 3.3 V

From the upper plots we can see that module No. 3 has better noise performance. The measured noise is about $V_{pp\text{-}out}$ = 100 mV for output current I_{out} = 1 A, this value does not change significantly with the output voltage. DC-DC Buck-Boost module has output noise about $V_{pp\text{-}out}$ = 350 mV at V_{out} = 5 V and $V_{pp\text{-}out}$ = 280 mV at V_{out} = 3.3 V with output current I_{out} = 1 A. These results are not sufficient for direct supply of analog circuits. For this reason LDO and filtration capacitors are used at each sub-board which contains analog circuitry.

We can see fairly constant output voltage over a range of load in appendix results (A). Conversion efficiency is plotted in Fig. 124 and Fig. 125. Efficiency of module No.1 does not exceed 66 % under test conditions. No. 3 has better efficiency, but η = 78 % is the maximum value. Such value does not correspond to values specified by the manufacturer.

In the testing tool two DC-DC Buck convertors (No. 3) are used for digital and analog +5 V rail. One DC-DC is used for +12 V rail, to prevent direct connection of internal circuits to the vehicle's electric network.

Supply source with V_{out} = -12 V is also needed. To fulfil this requirement, a supply source based on Linear Technology's LT1931A IC was designed. LT1931A allows to designing simple switcher with minimum external components and provides low noise performance exactly as stated in the datasheet.

2.5.3 Power source for the class D amplifier

A supply for power amplifier implies specific set of requirements. . Audio amplifier requires supply voltage of 20 V and supply current of 11 A (peaks) for maximum output power without significant nonlinear distortion. Since only 12 V system is available in the vehicle, a DC-DC converter with step-up topology is necessary. Charge pump system is more suitable for audio equipment due to better possibilities for output noise filtering. However, commonly offered boost charge pump do not reach the maximum

output current I_{out} = 11 A in peaks. Therefore step-up DC-DC convertor with inductance was selected for supply TAS5414 (car audio amplifier).

As a reference power source was selected DC-DC converter (based on LT1680) used in previous version of the testing tool as power supply for TAS5424.

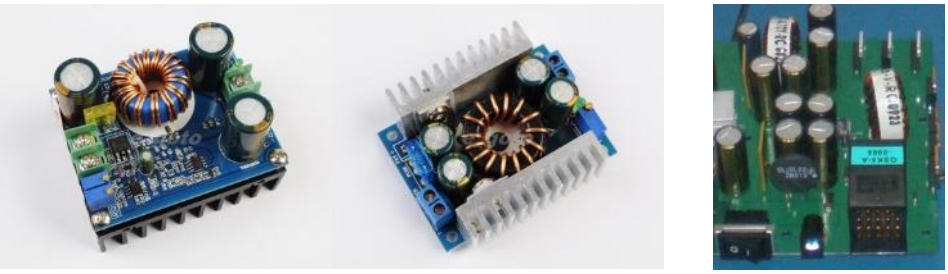

Fig. 41: Purchased DC-DC modules (No. 4[29], No. 5 [30], No. 6)

Measurements were conducted in the laboratory of student creativity at DREL, BUT. The peak currents required by the use-case prohibited using the laboratory power supplies. Therefore LiPo battery pack was selected as the input power source. Measurement focused on output voltage ripple, noise performance and dynamic characteristic of the source for switching load. Complete measured and processed data are described in appendix (A.2.4).

Tab. 2: DC-DC step-up modules specifications [29], [30], [31]

		No. 4	No. 5	No. 6
Topology	[-]	BOOST	BOOST	BOOST
Input voltage	[V]	12-60	8-32	-0,3-20
Output voltage	[V]	12-80	9.46	20
Output current (max)	[A]	12	16	11
Efficiency (max)	[%]	95	95	93
Output ripple	[mV]	Unspecified	Unspecified	Unspecified

In the case of the No. 4 and No. 5 values in Tab. 2 are complete module specifications from manufacturer. Specifications for No.6 can be achieved with IC LT1680.

At first, the output voltage dependency on output current was measured (Fig. 126). DC-DC modules No. 4 and No. 5 have good output voltage stability in increasing the load current. Maximum continuous load current for all modules was $I_{out\text{-}MAX}$ = 7 A. Modules from Chinese manufacturers exhibit output voltage decrease of approx. 1 V at full load. Source No. 6 shows decrease of approx. 6 V at full load, which is not a good result with regards to the amplifier's maximum output power. However, the expected output current for the intended use-case is about 3 to 5 A for normal operation conditions. Within this range, all sources work equally well, with output voltage decrease of only approx. 0.5 V.

Results of conversion efficiency (Fig. 127) are again almost identical for modules No. 4 and No. 5. They reach values over η = 90 %. Power source No. 6 performed at the efficiency of approx. 80 % over the entire load range.

Only power source No. 6 has output low-pass LC filter. This filter reduces high frequency artefacts generated by all DC-DC sources. As simulations and measurements show, this output filter hast the most significant negative influence to the output power and efficiency. At the same time, measurements of the ripple voltage and output HF noise show its main advantages. Fig.42 includes the most interesting curve for noise sensitive applications. Again, the worst case of output noise was measured.

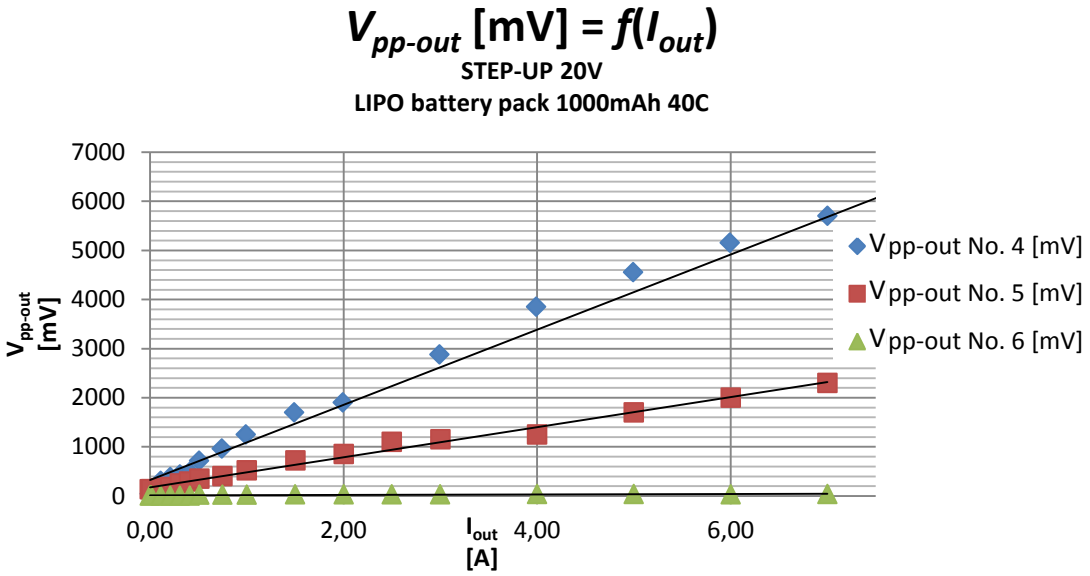

Fig.42: Amplifier power sources measured output noise

The worst case of output noise was measured with source No. 4, $V_{pp\text{-}out}$ = 5.7 V at full load, as depicted in Fig.42. Taking into account that output voltage is 20 V, such output noise value is extreme. For this reason, module No. 4 was excluded from further considerations. Module No. 5 performs slightly better, but 2.3 V_{PP} noise at full load is still insufficiently high. Power source No. 6 has clearly best noise performance. Fig. 128 is focused on the No. 6 output noise. It shows that values do not exceed $V_{pp\text{-}out}$ = 35 mV.

Output load switching was also measured as a typical dynamic factor. Output load current was set to value higher than 1 A and switched by frequency f_{SW} = 30 Hz and f_{SW} = 1 kHz.

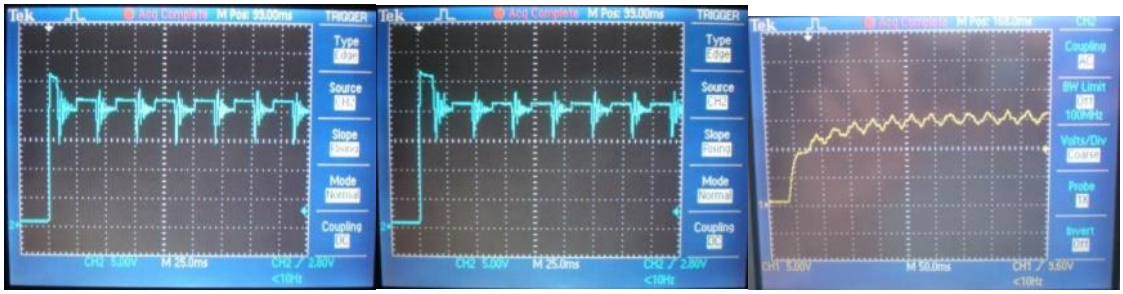

Fig. 43: Output load switching curves f_{SW} = 30 Hz(No. 4, No. 5, No. 6)

Fig. 43 and Fig. 44 show all tested power sources and their respective ripple output

voltages under switching load. Again, module No. 6 shows the most acceptable waveform. The start-up curve can be observed on these pictures. Slow ramp voltage of No. 6 prevents annoying sounds during power amplifier start-up.

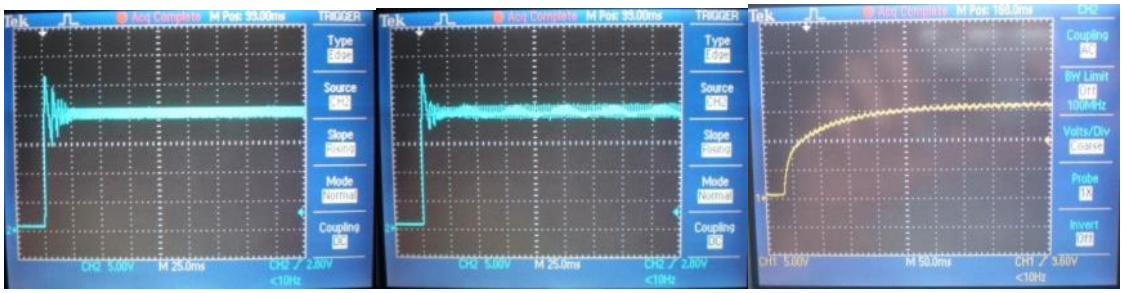

Fig. 44: Output load switching curves f_{SW} = 1 kHz (No. 4, No. 5, No. 6)

As a conclusion, the measurement indicated that modules from Chinese manufacturers are not suitable for use in designed testing tool. Therefore, power supply concept No. 6 was adopted for the design. The concept was further improved by using newer type of MOSFET transistors with lower R_{DSon}.

In future revision of the testing tool, it would be appropriate to use a power source based on IC LT1738 (ultra low noise DC-DC controller). This IC has a slew rate control feature. It allows design power source with output voltage ripple and noise about 100mV without use of the output LC filter and 400uV with LC output filter according to manufacturer documentations. This statement was checked and compared in the simulation program LTspiceIV.

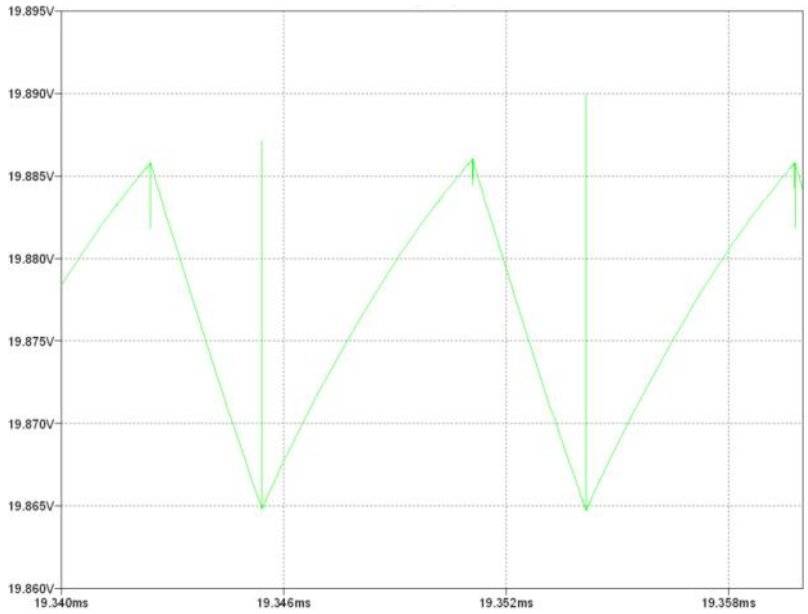

Fig. 45: Simulation of the output ripple voltage (power source No. 6)

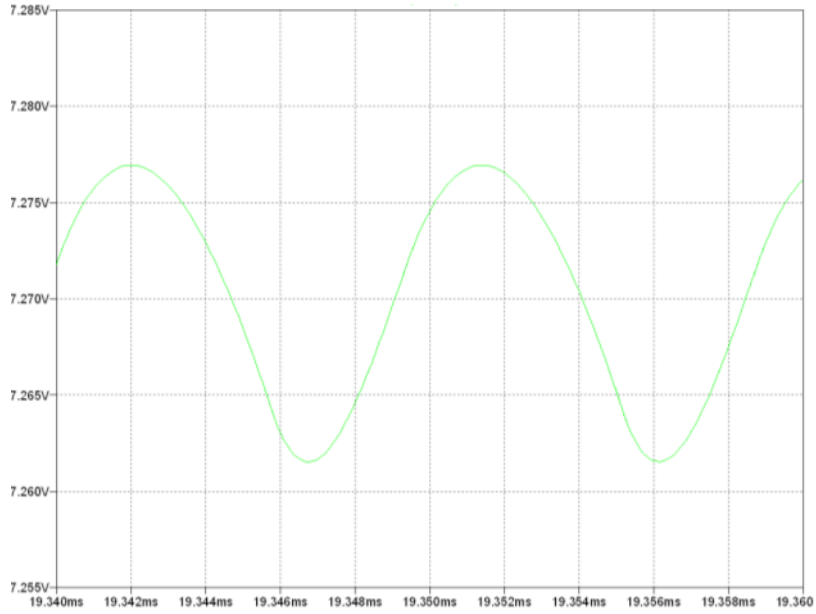

Fig. 46: Simulation of the output ripple voltage (LT1738)

Simulation curve on the Fig. 45 belongs to power source No. 6 (based on LT1680). Curve on the Fig. 46 belongs to reference design power source from LT manufacturer (based on LT1738). These waveforms demonstrate the effect and importance of slew rate control. Rounded curve shape indicates decreased production of the high frequency harmonics and therefore lower output noise level. Power source based on LT1738 could improve audio performance of the power amplifier.

2.6 User interface

User interface (UI) can be divided into hardware and software part. Block diagram of the hardware or external user interface is on the picture Fig. 8. There are two connectors for microphones and four mechanical switches. Two of them are used for bias resistance selection and the two others are used for bias voltage connection to the separate microphone pin or as phantom power to signal pin of the microphone. External UI could include also the connector panel consisted of three I2S ports, three stereo line outputs, two stereo inputs and Ethernet interface.

The software part of the UI will be as web site with specific options for suitable setting of the whole testing tool. Parameters will be changed through connected PC or notebook. Communication between web site and testing tool will be provided by Raspberry Pi module, which is programmed by Ethernet interface. All libraries and interfaces are coded with Python programming language.

2.7 3D model of the testing tool

For each functional block allocation of the final DPS is necessary to know, how much space can be used. Connections between them, interferences, mechanical mounting, air flow and others must be included in considerations. For this reason 3D model of testing tool was made.

The testing tool will be placed in a case with handle for easy handling. The case external dimensions are approximately L = 48 cm, W = 20 cm, H = 24 cm. There will be mounted boards of the testing tool covered by connector panel and external UI in one half of the case. Small fan sustains about the suitable air flow and power amplifier active cooling. In the second half will take place device under test. Cables for connection to existing car audio chain and Ethernet interface will be only outputs from the case. On the pictures (Fig. 47) is a 3D model drawn in AutoCAD.

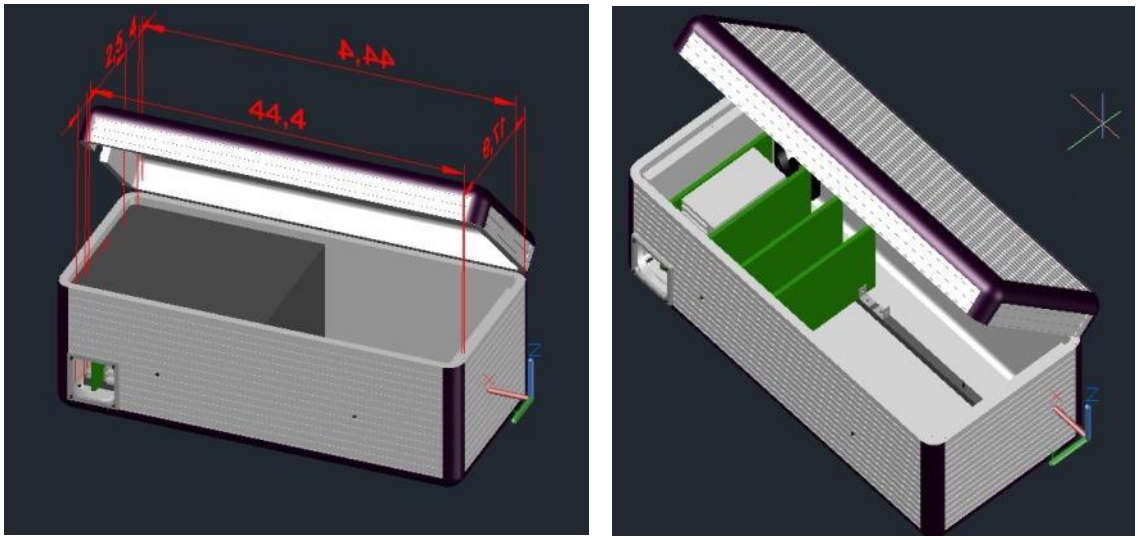

Fig. 47: 3D model of the testing tool

3 SUMMARY

The result of this master's thesis is a functional first revision of hardware platform for an automotive Hands-Free module testing tool.

Motivation for construction of such a tool, as well as theory behind the technical requirements with regards to Acoustic Echo Cancellation and Noise Reduction methods were explained in the first chapter.

The entire system was broken down in top-down manner to separate functional blocks, represented by hardware sub-boards. Design of each block was discussed separately in the text, together with considerations for each design choice in case when more than one suitable solution was available. For most parts, an early prototype had been constructed prior to the first revision of the PCB design.

The mechanical aspect of the system, including transportation case, layout and mounting of PCB and user interface, was also designed and implemented.

For a relatively extensive project (770 parts on 6 boards) with expected small amount of realizations, utilization of third-party modular solutions was considered to increase the design efficiency. Such options were always considered against original design. This is represented particularly in the discussion of power supply block.

PCBs for each block had been produced, populated, measured and tested for application-relevant parameters, with focus on analog parameters. When applicable, the measurement results were compared to measurements of early prototypes, and to product specifications of parts used in the design.

On the whole, the functionality of the basic analog path until codec interface was confirmed. However, some parameters, such as Power Amplifier voltage supply stability or noise on the microphone inputs, are not yet sufficient for the required application. In cases when result does not meet the requirements, possible causes or methods of improvement are suggested. Some parts, including audio reference path from the amplifier and digital-audio path after ADC, had not been yet confirmed due to limited time.

The project at its current state is ready to serve as a platform for control software development based on Raspberry Pi platform, and for further improvements of hardware parameters with respect to future revisions.

The author of this thesis remains closely involved in the project and plans to reach the final solution matching all specifications in the next hardware revision.

BIBLIOGRAPHY

[1] HETHERINGTON, P., MOHAN, A. *Essential Ingredients of a Quality Hands-Free Solution.* QNX Software Systems, 2011.

[2] *How to Choose an Acoustic Echo Canceller.* Polycom, Inc, 2004.

[3] AKG ACOUSTICS. *AKG Q500Series AKG 501T.* 2004.

[4] SINHA, P. *Speech Processing in Embedded Systems*. Springer, 2009.

[5] VLACHÝ, V. *Praxe zvukové techniky*. Praha: Muzikus, 2000.

[6] DŽBÁNEK, L. Kompenzace akustického echa a jeho implementace. *Elektrorevue* [online.]. 2002 [cit. 10. 11. 2013] available at: www:http://elektrorevue.cz/clanky/02071/index.html

[7] ITU-T. Acoustic Echo Controllers, Recommendation G.167. *General Characteristics of International Telephone Connections and International Telephone Circuits.* Telecommunication standardization sector of ITU, 1993.

[8] ITU-T. Series P. Telephone Transmission Quality, Telephone, Installations, Local Line Networks P.110. *Narrow-band hands-free communication in motor vehicles*. Telecommunication standardization sector of ITU, 2008.

[9] Microphone. *Wikipedia* [online.]. 23.7.2013 [cit. 20. 11. 2013] available at: www:http://en.wikipedia.org/wiki/Microphone

[10] VDA. *VDA-Specification for Car Hands-Free Terminals*. Frankfurt: 2008.

[11] TEXAS INSTRUMENTS. *Quad 10-Bit, Low power, Voltage output, I2C interface digital to analog converter DAC6573.* TI, 2003. [cit. 11.10. 2013] available at: http://www.ti.com/general/docs/lit/getliterature.tsp?literatureNumber=slas402

[12] TEXAS INSTRUMENTS. *Zero drift programmable gain amplifier with MUX PGA112.* TI, 2008. [cit. 3.10. 2013] available at: http://www.ti.com/lit/ds/sbos424b/sbos424b.pdf

[13] ANALOG DEVICES. *20mW Power, 2,3V to 5,5V, 75MHz Complete DDS AD9834.*Analog Devices, 2011. TI, 2008. [cit. 5.11. 2013] available at: http://www.analog.com/static/imported-files/data_sheets/AD9834.pdf

[14] BRANČÍK L., DOSTÁL T. *Analog Electronic Circuit*. Electronic textbook. FEKT VUT in Brno, 2008. Available at: https://www.vutbr.cz/www_base/priloha.php?dpid=21222

[15] MAXIM INTEGRATED PRODUCTS. *8th-order, Lowpass, Elliptic, Switched-capacitor Filters MAX7400*. Maxim, 1999. [cit. 28.11. 2013] available at: http://datasheets.maximintegrated.com/en/ds/MAX7400-MAX7407.pdf

[16] BATEMAN, C. Capacitor sound? *Electronics World*. 2002.

[17] ANALOG DEVICES. *Audio/Video 60 MHz 16 x 16, G = 2 Crosspoint Switch AD8113.* AD, 2003. [cit. 28.11. 2013] available at: http://www.analog.com/static/imported-files/data_sheets/AD8113.pdf

[18] ANALOG DEVICES. *Ultralow Noise Amplifier at Lower Power ADA4075-2.* AD, 2008. [cit. 7.5. 2014] available at: http://www.analog.com/static/imported-files/data_sheets/ADA4075-2.pdf

[19] TEXAS INSTRUMENTS. *4-channel audio volume control PGA4311*. TI, 2002.

[cit. 10.12. 2013] available at: http://ti.com/lit/ds/sbos230a/sbos230a.pdf

[20] TEXAS INSTRUMENTS. *Low Power Stereo Audio CODEC for Portable Audio/Telephony TLV320AIC33.* TI, 2008. [cit. 18.12. 2013] available at: http://ti.com/lit/ds/slas480b/slas480b.pdf

[21] TEXAS INSTRUMENTS. *Four-channel automotive digital amplifiers TAS5414.* TI, 2007. [cit. 8.12. 2013] available at: http://ti.com/general/docs/lit/getliterature.tsp?literatureNumber=slos514a

[22] *Film capacitor,* Wikipedia, 2014. [cit. 30.3. 2014] available at: http://en.wikipedia.org/wiki/Film_capacitor#Polyphenylene_sulfide_.28PPS.29_film_capacitors

[23] TEXAS INSTRUMENTS. *Audio differential line receivers 0dB (G = 1, INA2134).* TI, 1997. [cit. 5.7. 2014] available at: http://www.ti.com/lit/ds/sbos071/sbos071.pdf

[24] ANALOG DEVICES *C-Compatible, 256-Position Digital Potentiometers. AD, 2001.* [cit. 5.7. 2014] available at: http://www.analog.com/static/imported-files/data_sheets/AD5241_5242.pdf

[25] Raspberry Pi. *Wikipedia* [online.]. 13.12.2013 [cit. 17. 12. 2013] available at: http://en.wikipedia.org/wiki/Raspberry_Pi

[26] Ebay.com. *DC-DC Converter Step Up/Down Module 3.5-28V to 1.25V-26V.* [cit. 22.3.2014] available at: http://www.ebay.com/itm/121141246236?ssPageName=STRK:MEWNX:IT&_trksid=p3984.m1497.l2649

[27] Ebay.com. *DC-DC Step Down Power Module 4V-38V to 1.25V-36V 5A Adjustable good.* [cit. 22.3.2014] available at: http://www.ebay.com/itm/370940933915?ssPageName=STRK:MEWNX:IT&_trksid=p3984.m1497.l2649

[28] Ebay.com.*2pcs LM2596 DC-DC Buck Converter Step Down Module Power Supply Output 1.23V-30V.* [cit. 22.3.2014] available at: http://www.ebay.com/itm/130945548152?ssPageName=STRK:MEWNX:IT&_trksid=p3939.m1497.l2649

[29] Ebay.com. *DC-DC 600W Step Up 12V-60V to 12V-80V Power Apply Module High-Power Good.* [cit. 22.3.2014] available at: http://www.ebay.com/itm/130976725283?ssPageName=STRK:MEWNX:IT&_trksid=p3984.m1497.l2649

[30] Ebay.com. *DC-DC 150W Step Up 8V-32V to 9V-46V Power Apply Module High-Power good.* [cit. 22.3.2014] available at: http://www.ebay.com/itm/121191153988?ssPageName=STRK:MEWNX:IT&_trksid=p3939.m1497.l2649

[31] Linear Technology. *High Power DC/DC Step-Up Controller.* LT, 1997. [cit. 22.3.2014] available at: http://cds.linear.com/docs/en/datasheet/1680fa.pdf

LIST OF INCLUDED APPENDIXES

A DESIGN OF THE TESTING TOOL

A.1 Design documentation

A.1.1 Microphone input - schematic

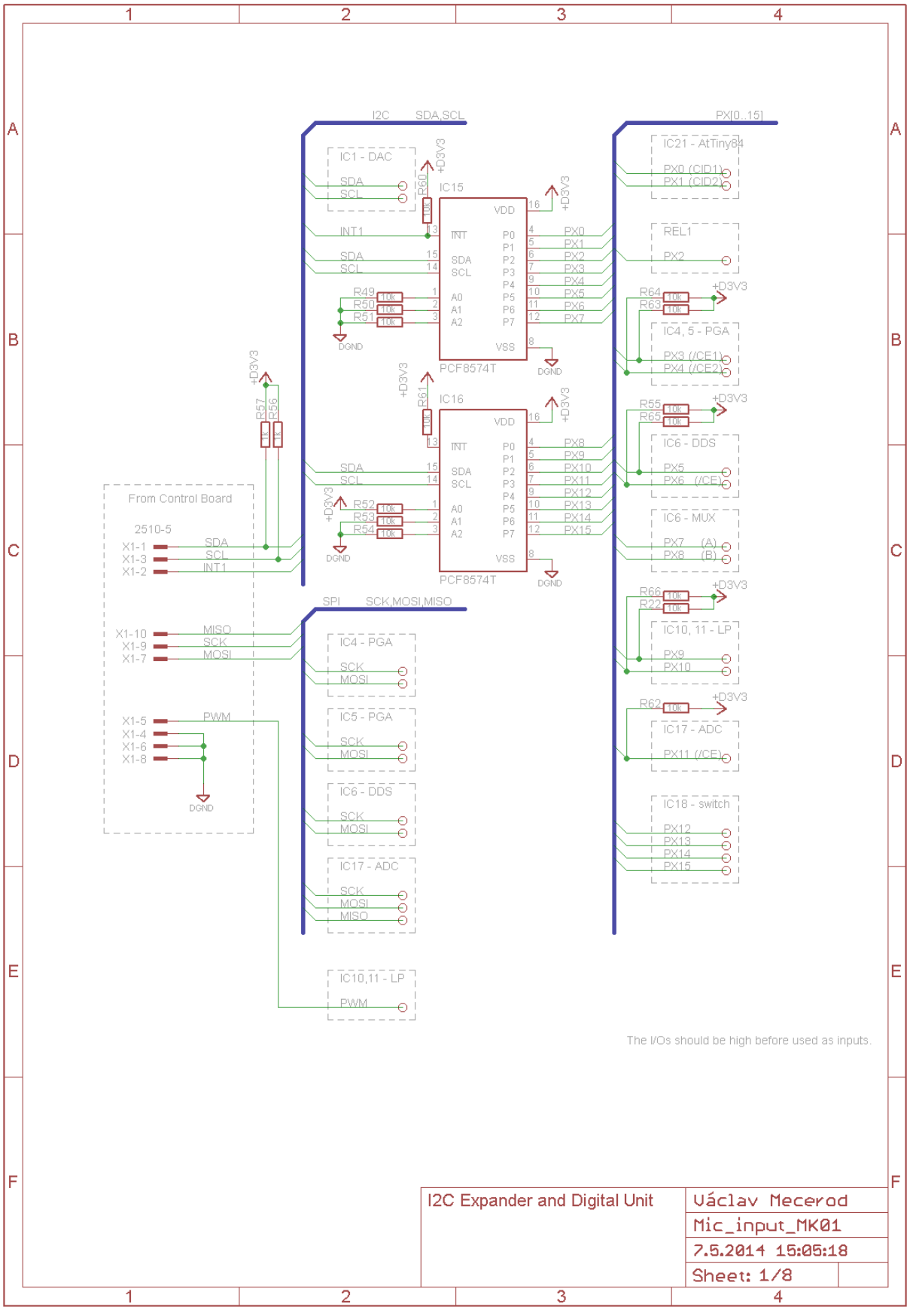

Fig. 48: I^{2}C expander and Digital interface unit

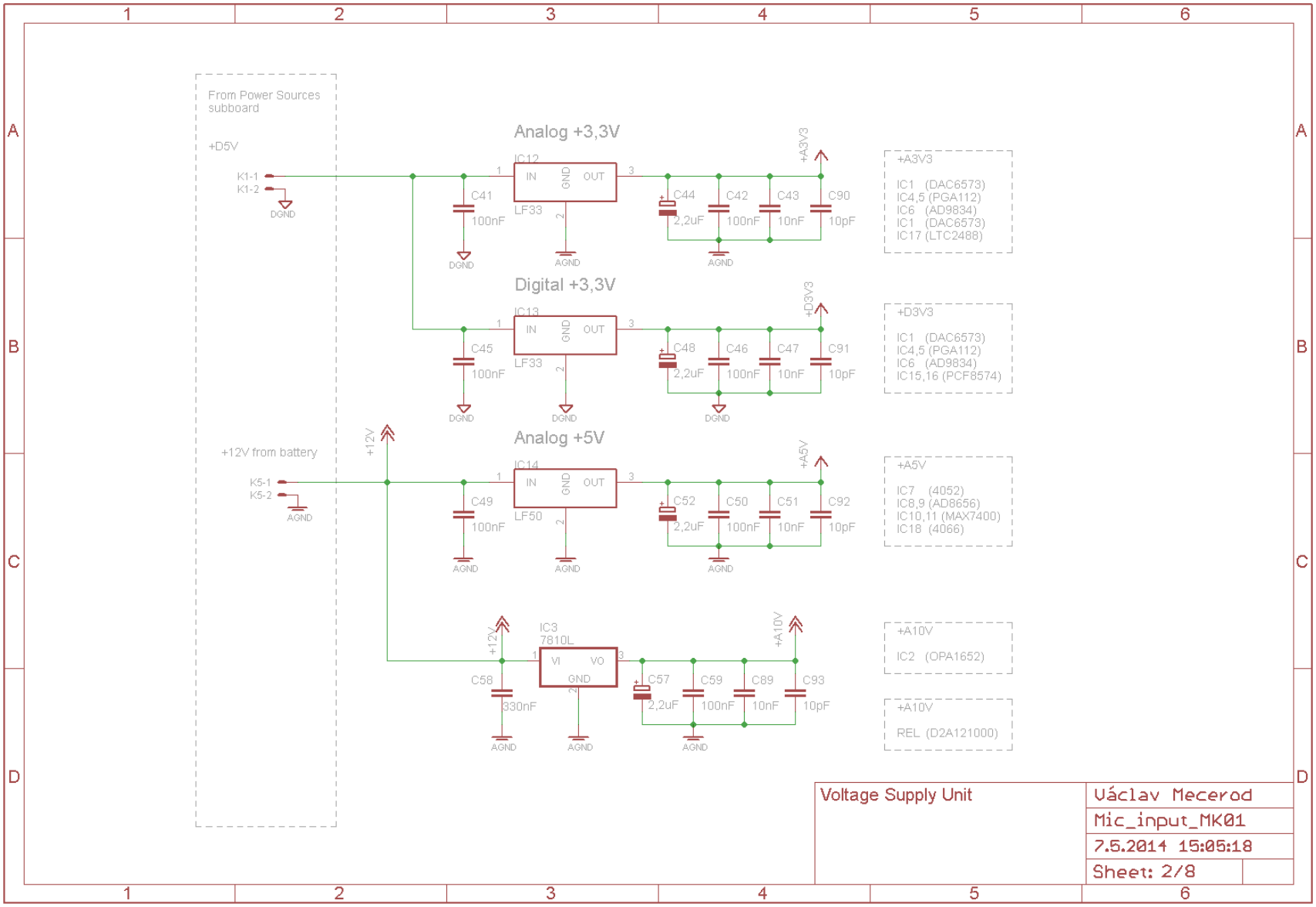

Fig. 49: Voltage supply

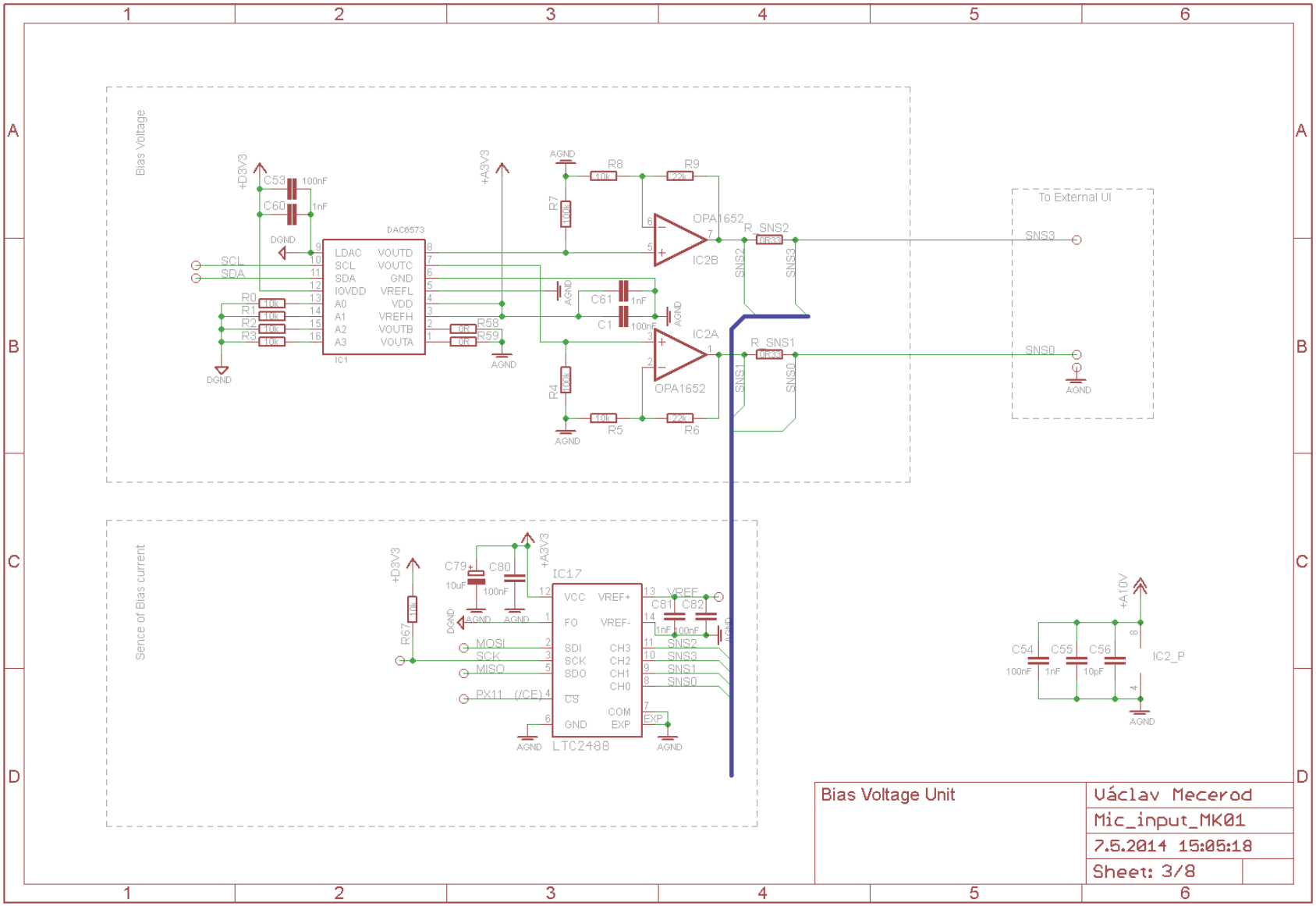

Fig. 50: Bias voltage unit

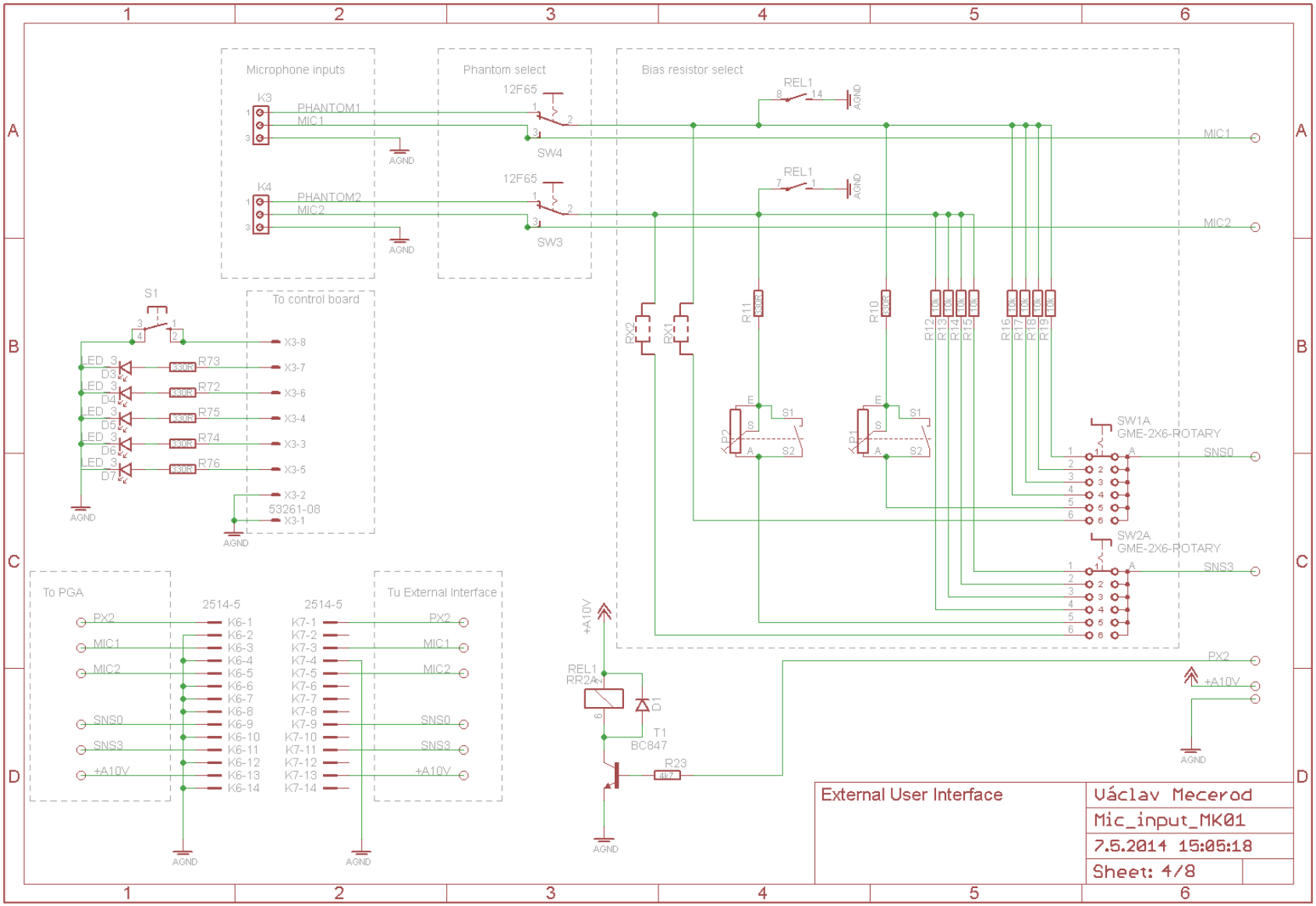

Fig. 51: External user interface

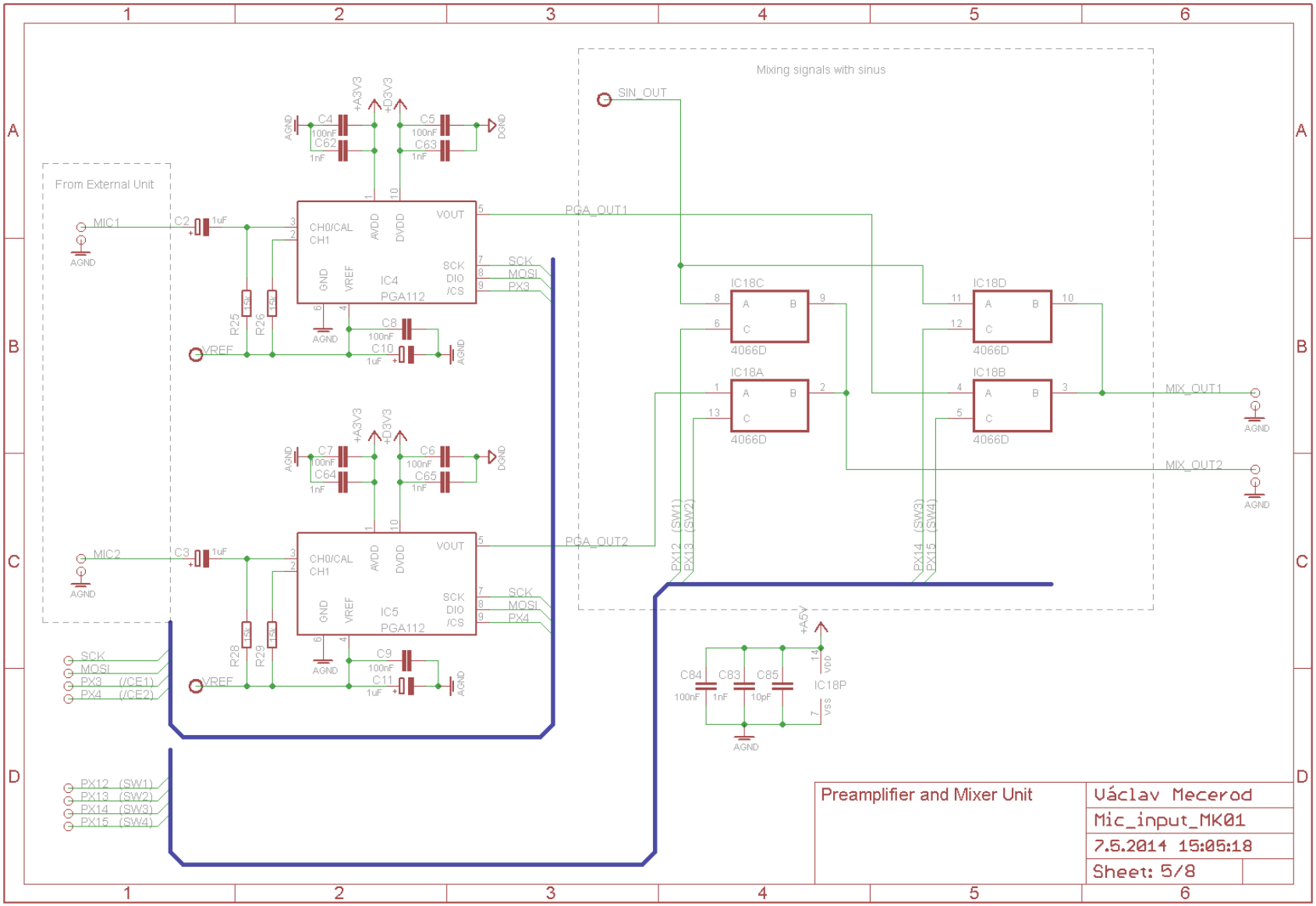

Fig. 52: Preamplifier unit

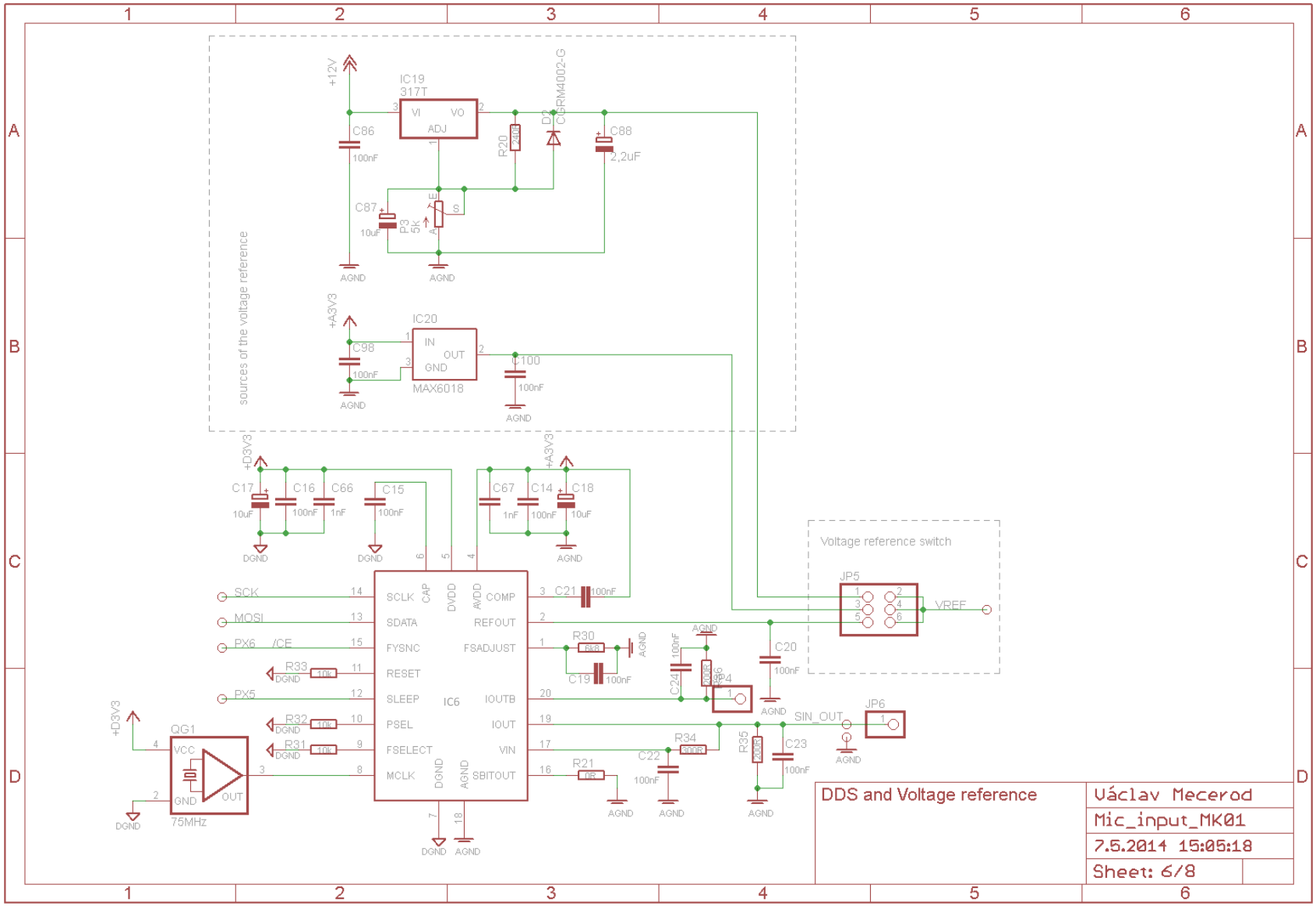

Fig. 53: Test-signal generator

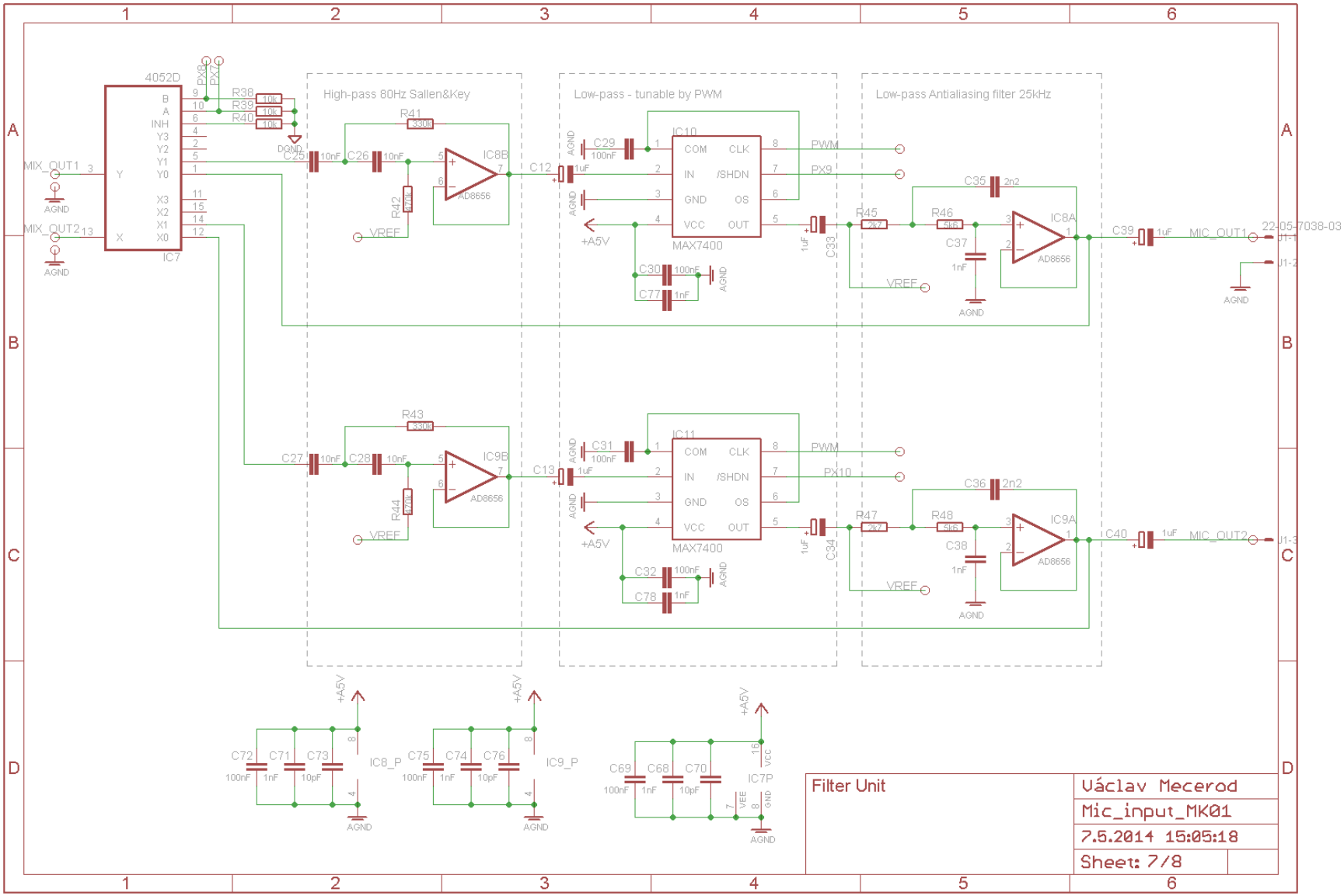

Fig. 54: Filter unit

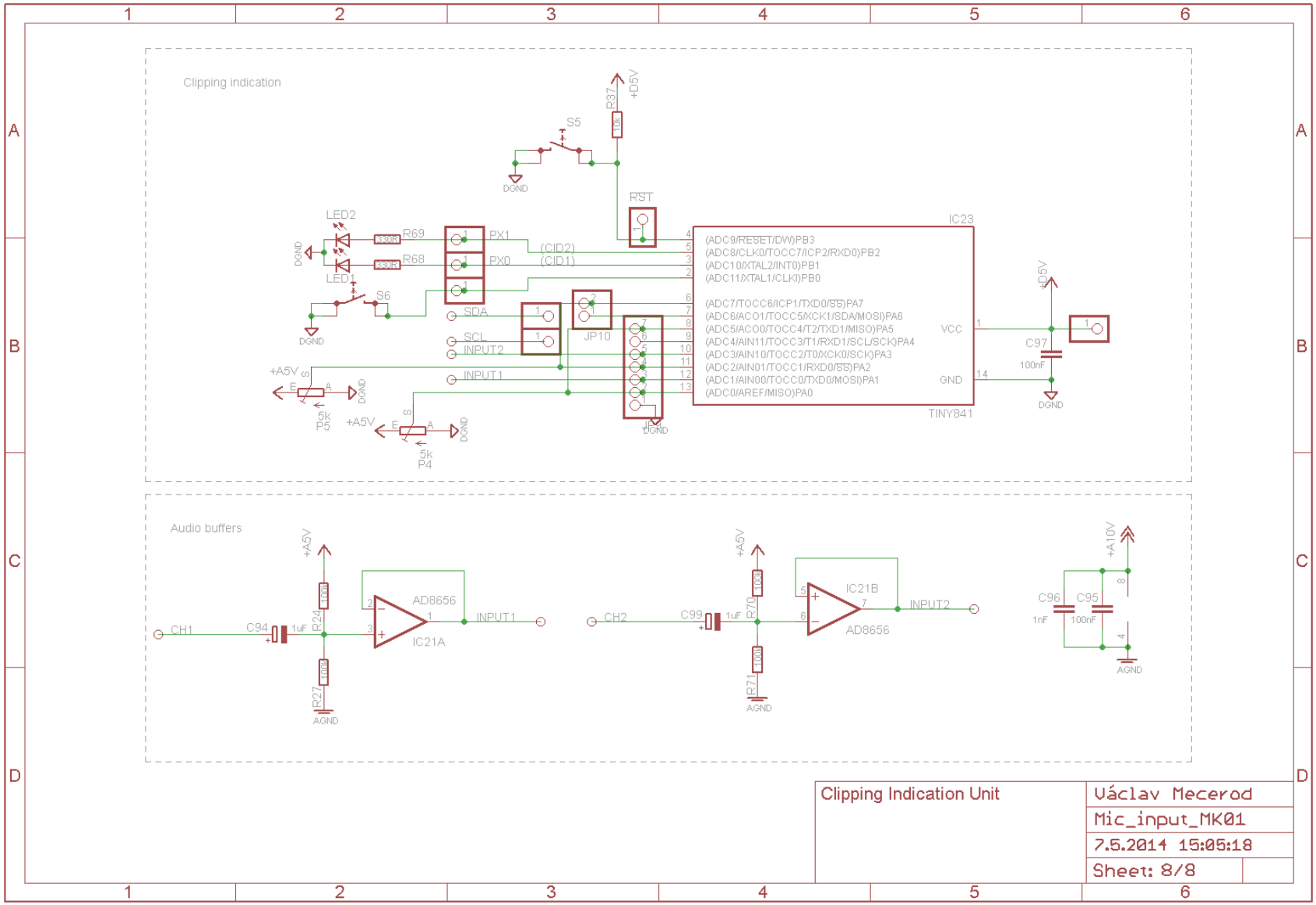

Fig. 55: Clipping indication

A.1.2 Microphone input – PCB

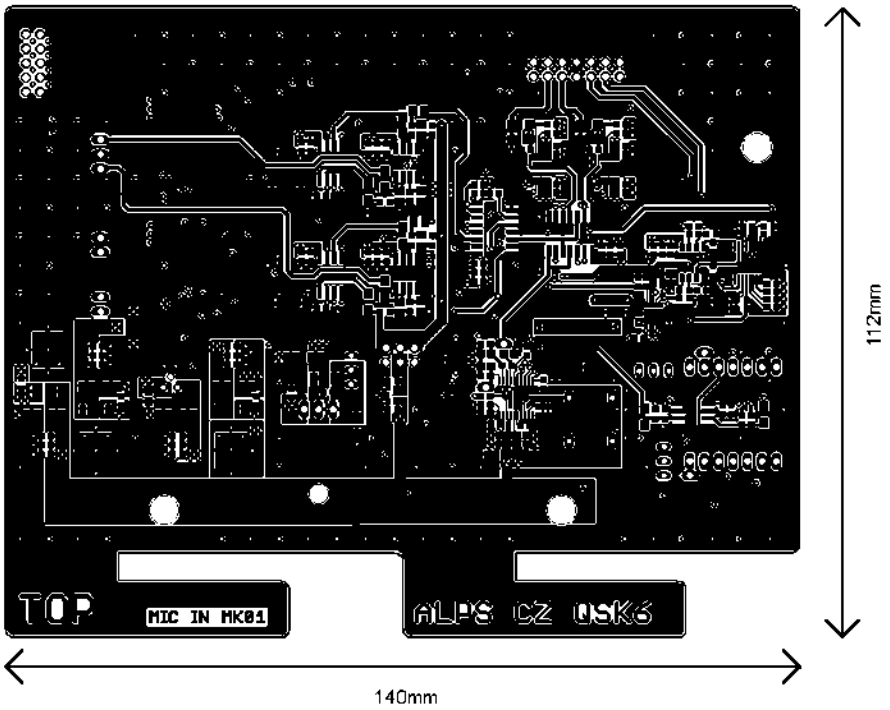

Fig. 56: Microphone input – top layer

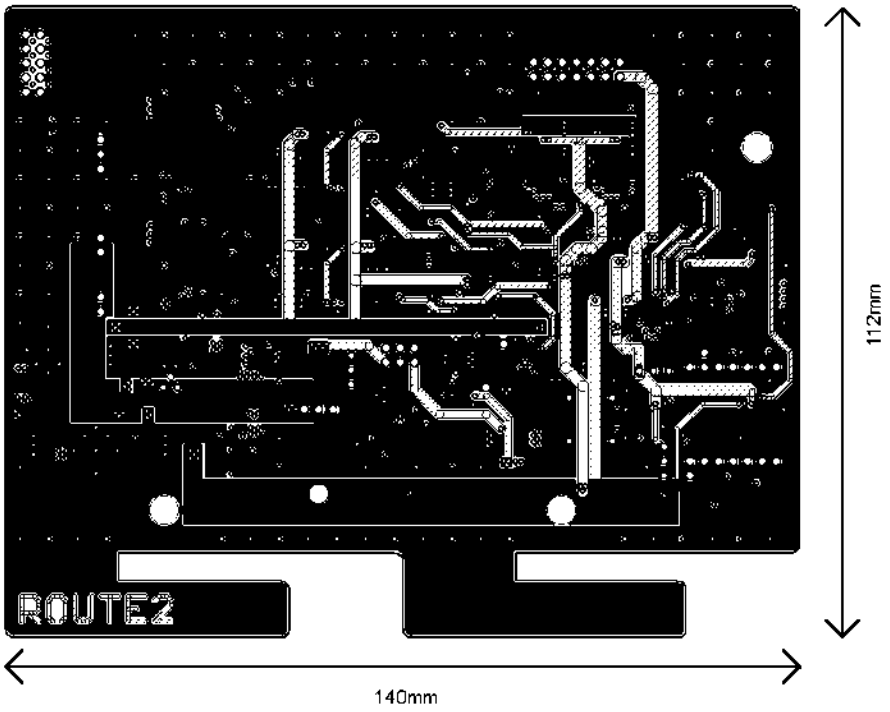

Fig. 57:Microphone input – second layer

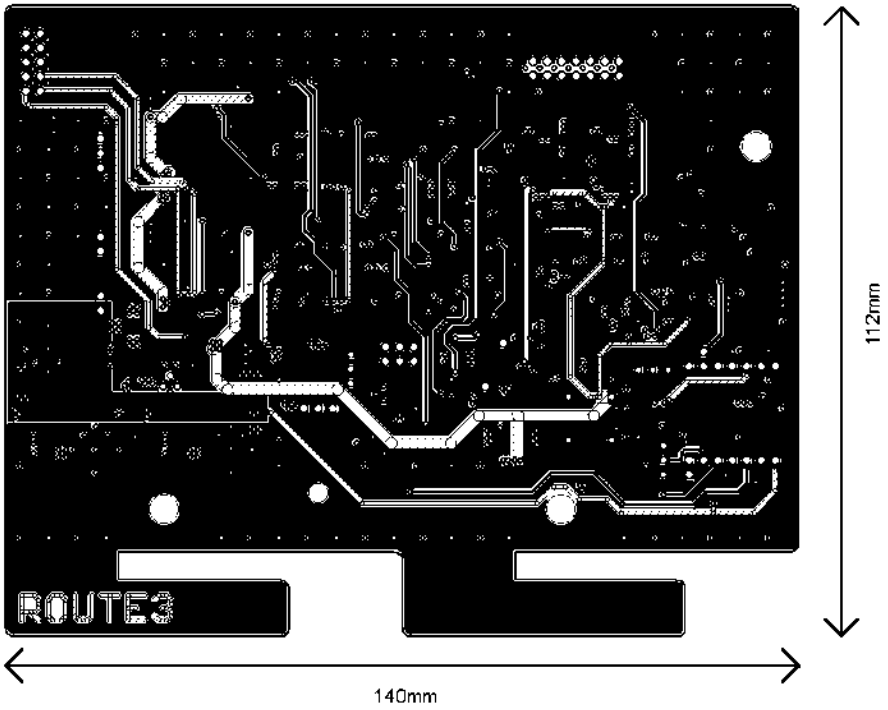

Fig. 58: Microphone input – third layer

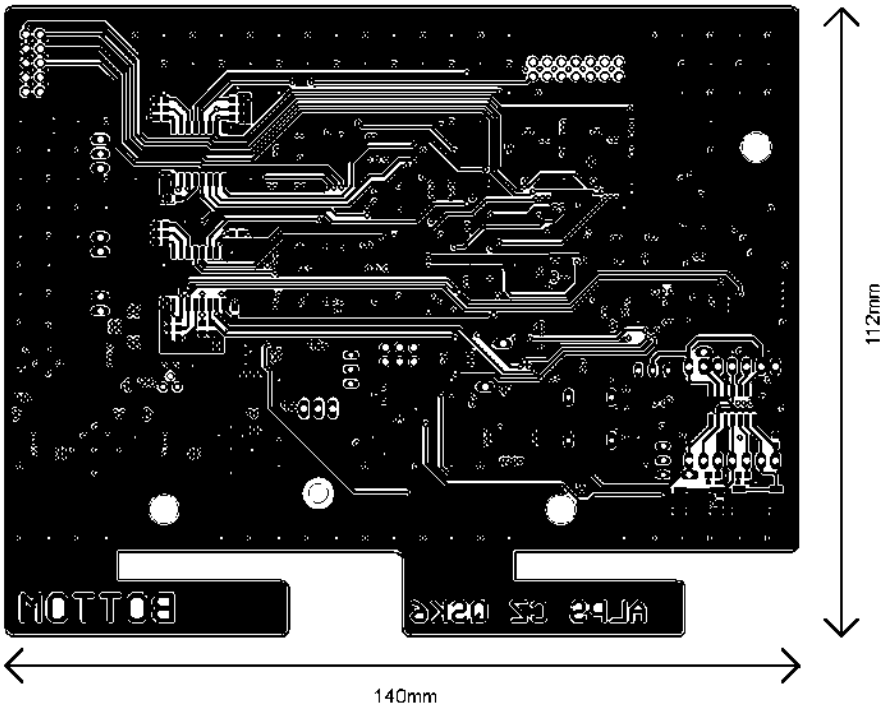

Fig. 59: Microphone input – bottom layer

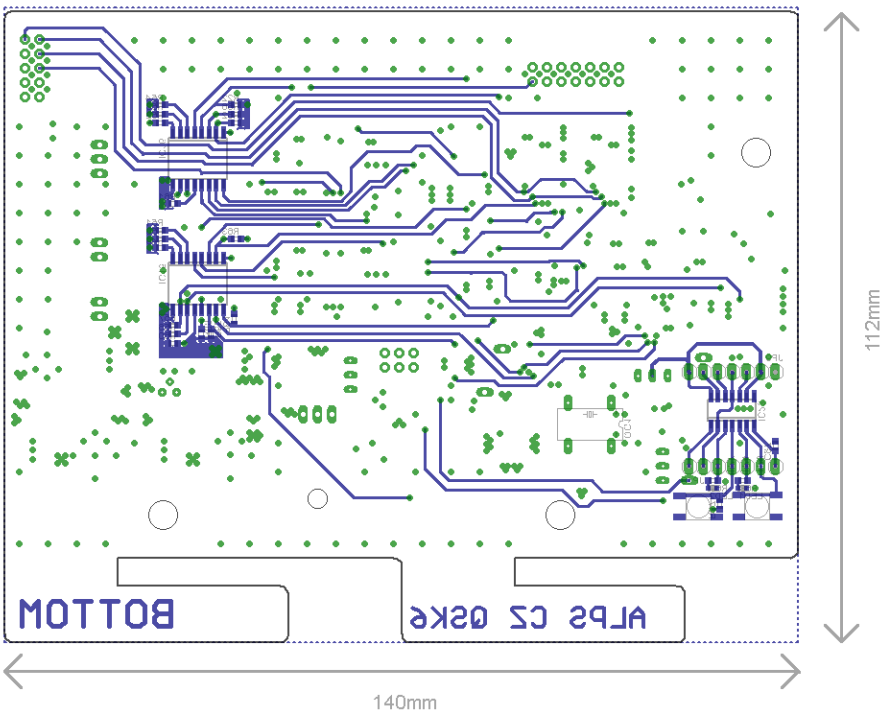

Fig. 60: Microphone input – layout of components - bottom

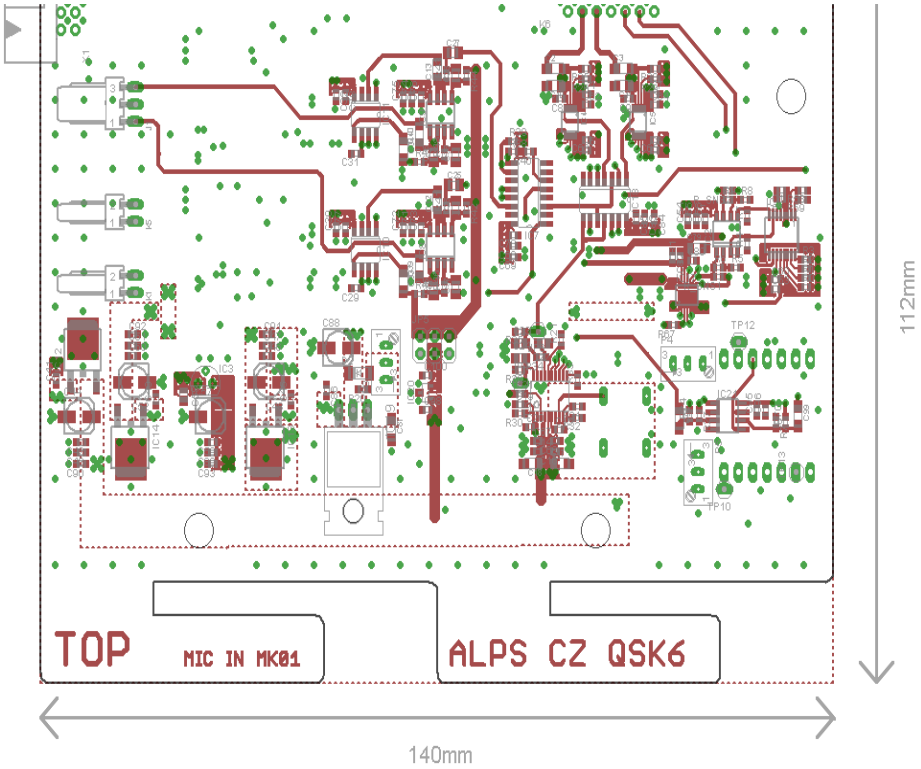

Fig. 61: Microphone input – layout of components - top

A.1.3 External User interface – PCB

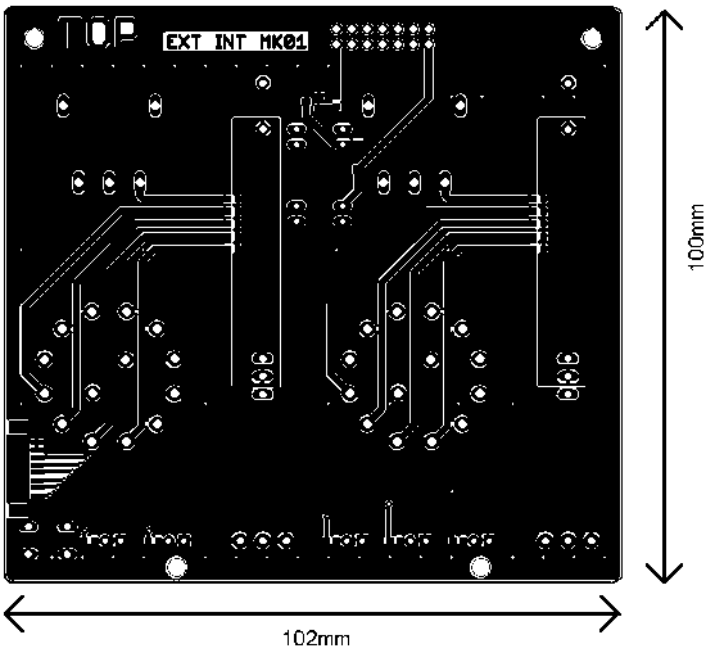

Fig. 62: External user interface – top layer

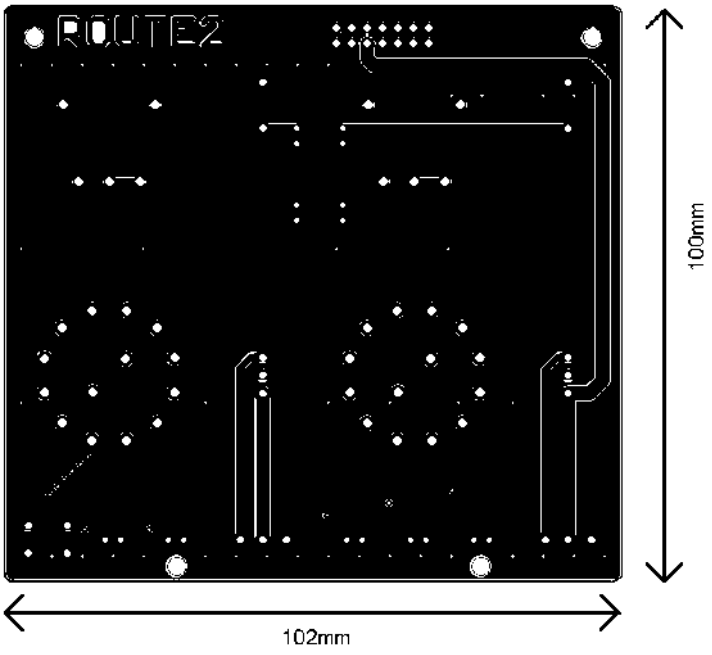

Fig. 63: External user interface – second layer

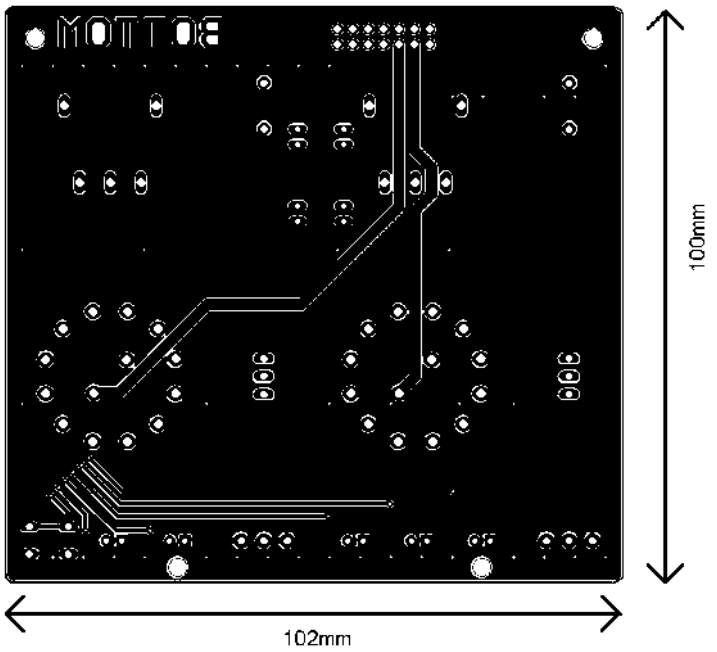

Fig. 64: External user interface – third layer

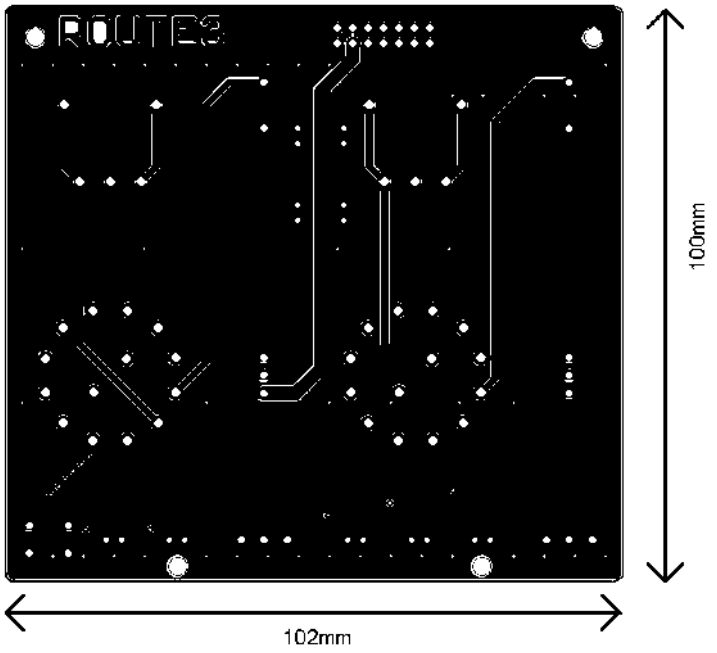

Fig. 65: External user interface – bottom layer

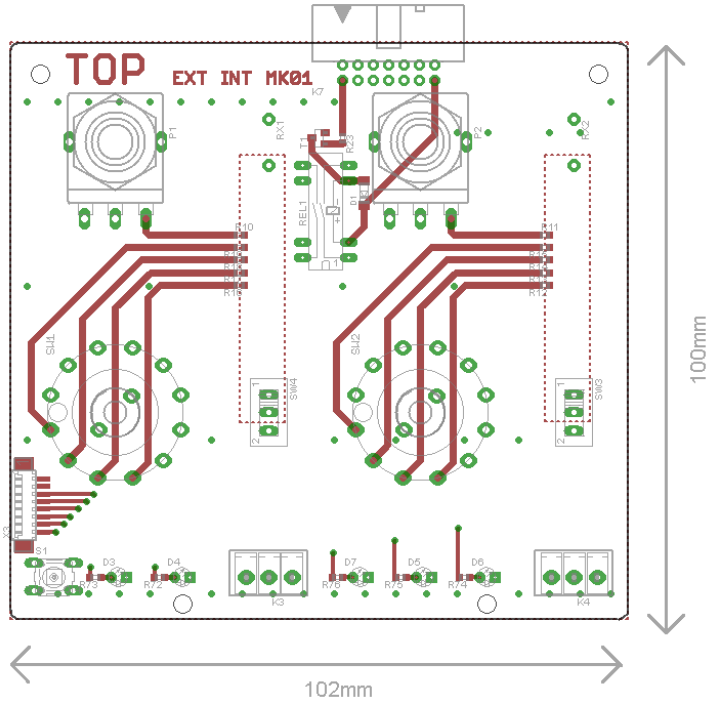

Fig. 66: External user interface – layout of components

A.1.4 Codec board – schematic

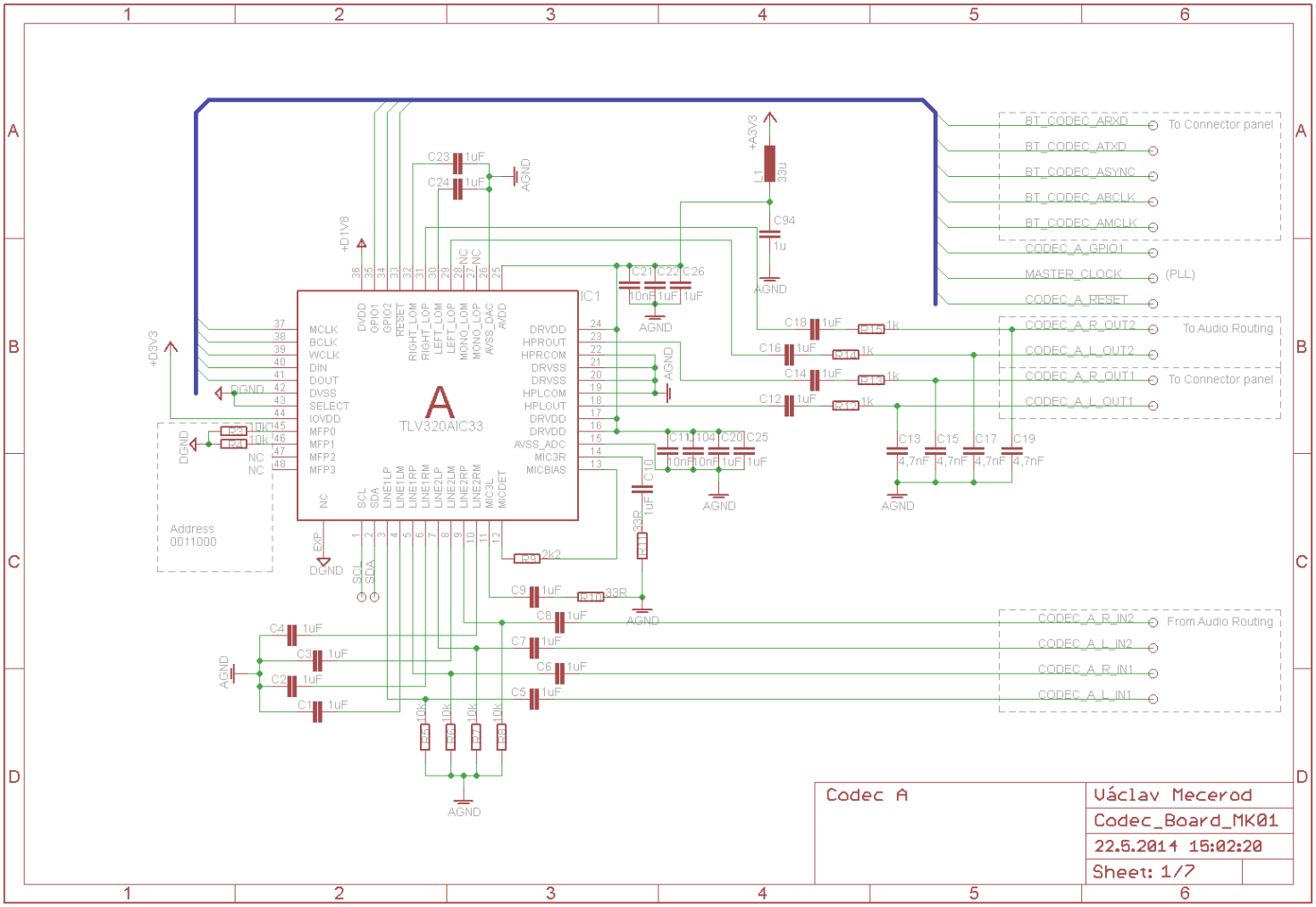

Fig. 67: Codec A

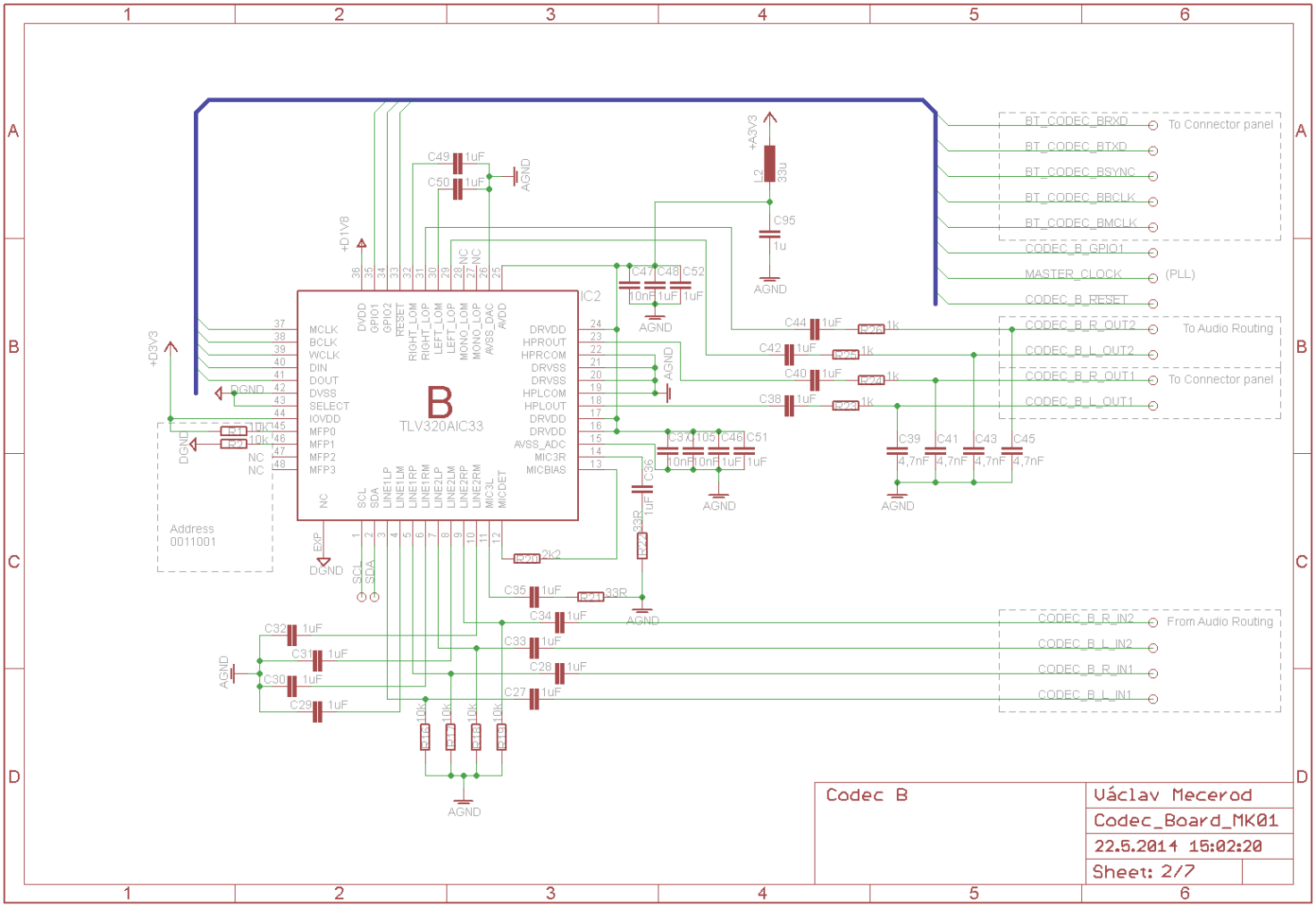

Fig. 68: Codec B

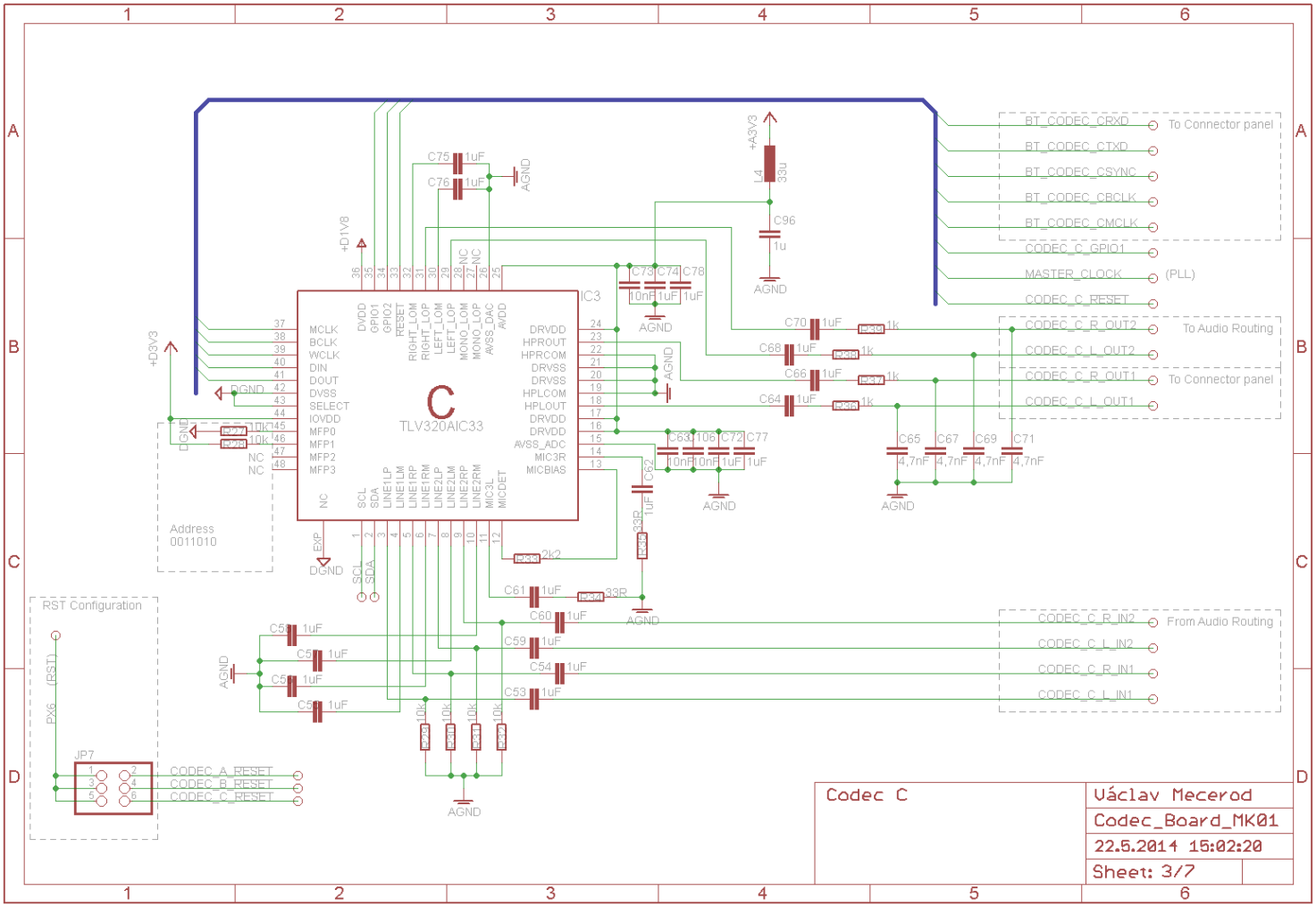

Fig. 69: Codec C

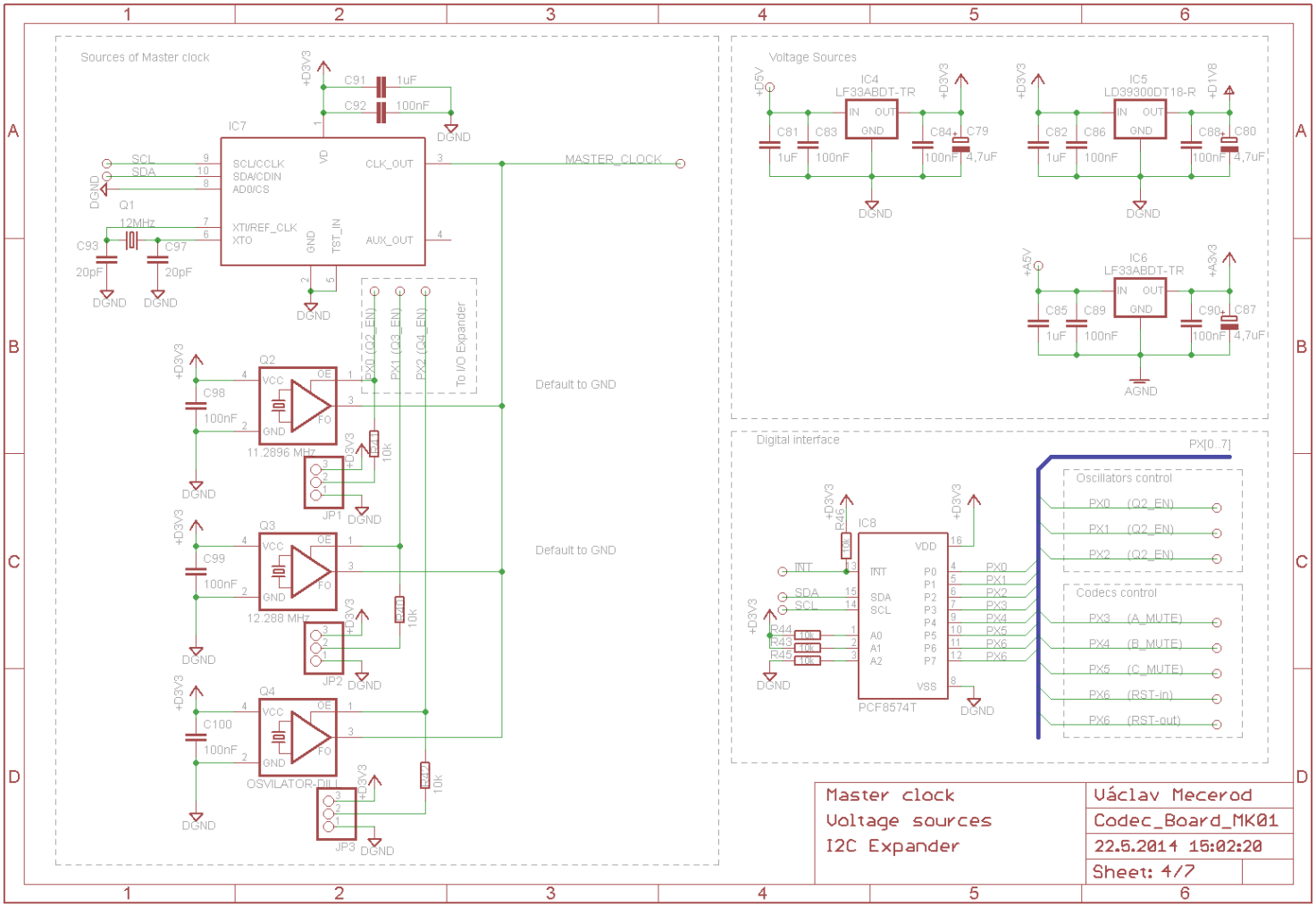

Fig. 70: Master clock generation

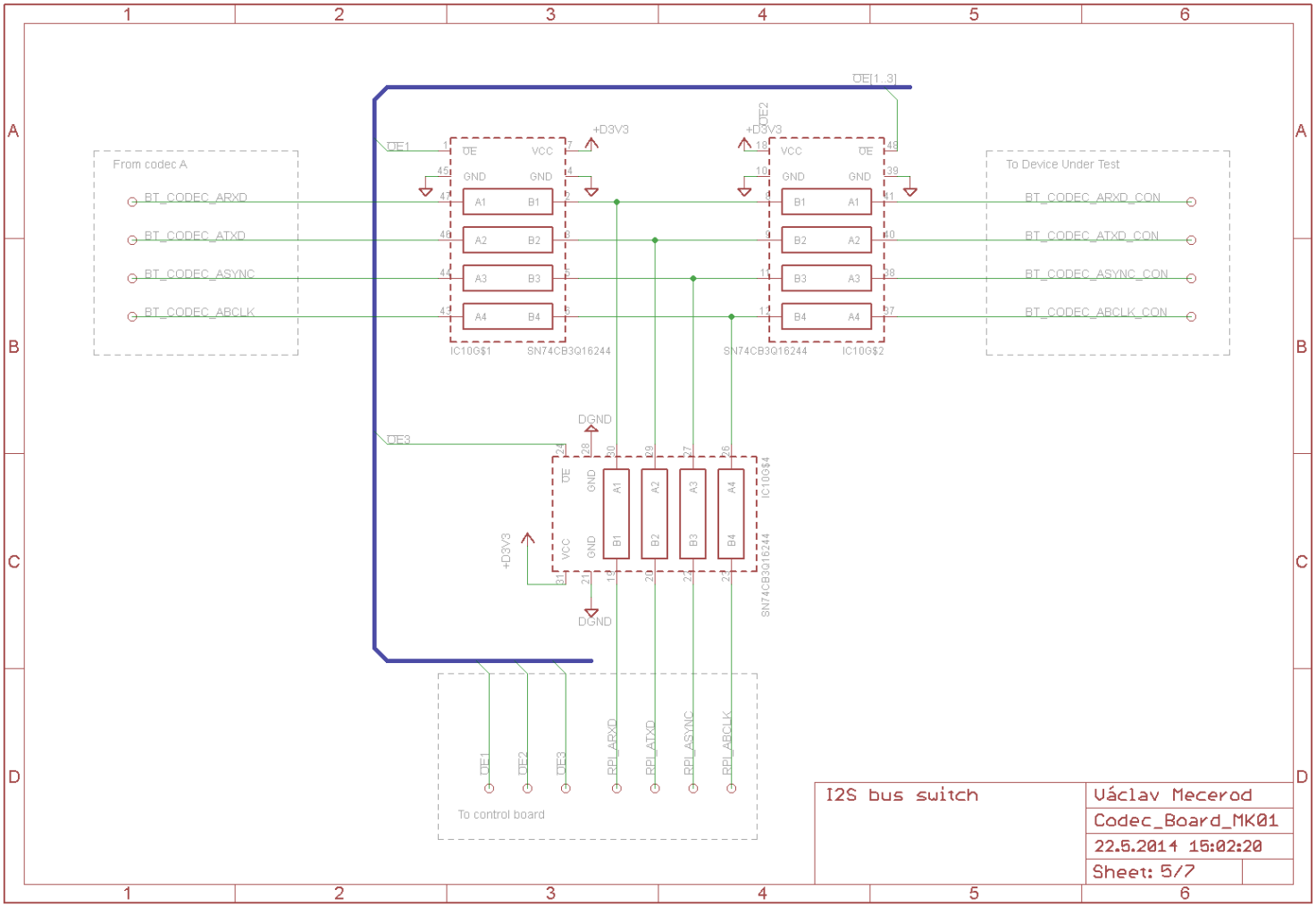

Fig. 71: I2S bus switch

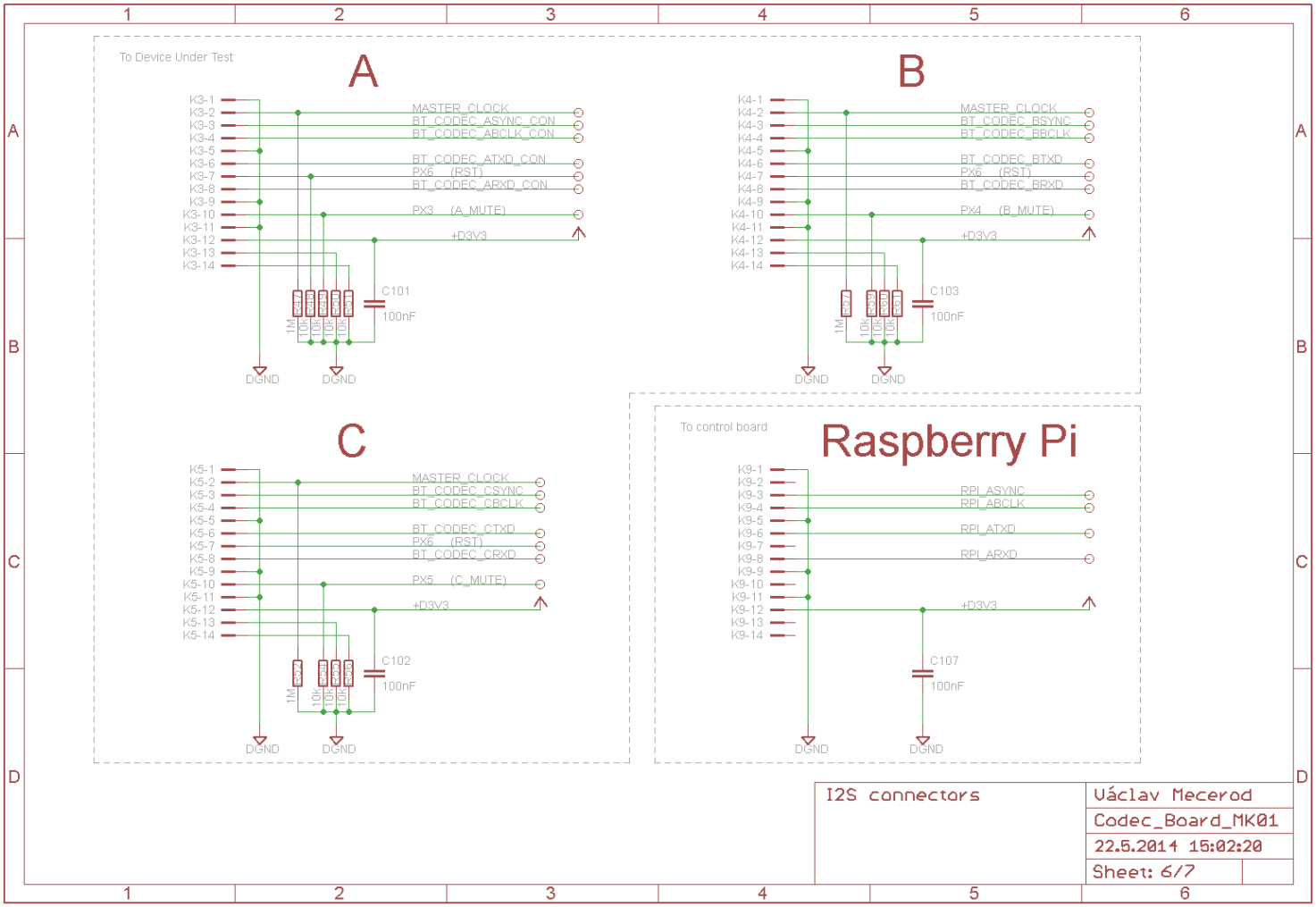

Fig. 72: I2S connectors

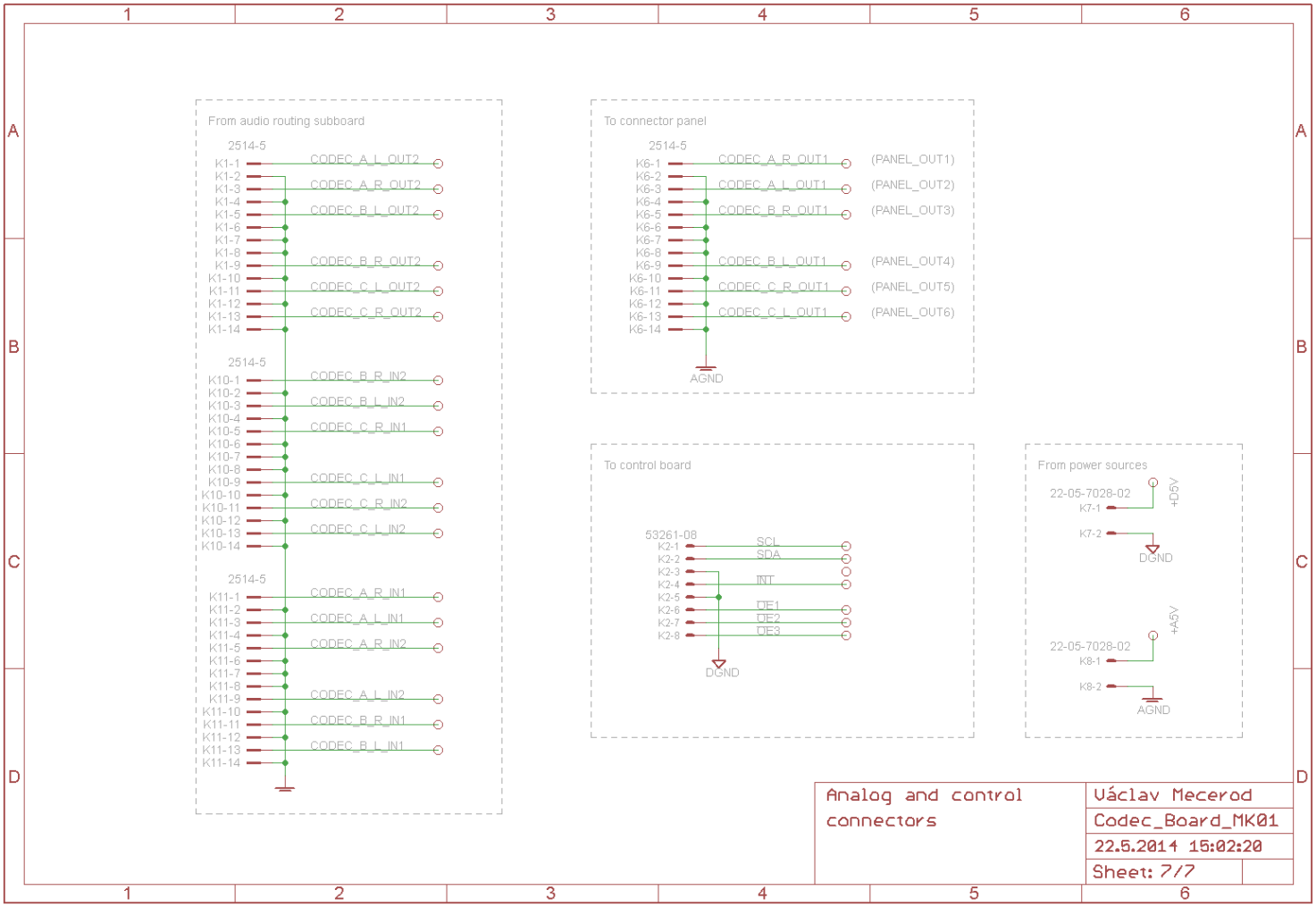

Fig. 73: Codec board connectors

A.1.5 Codec board – PCB

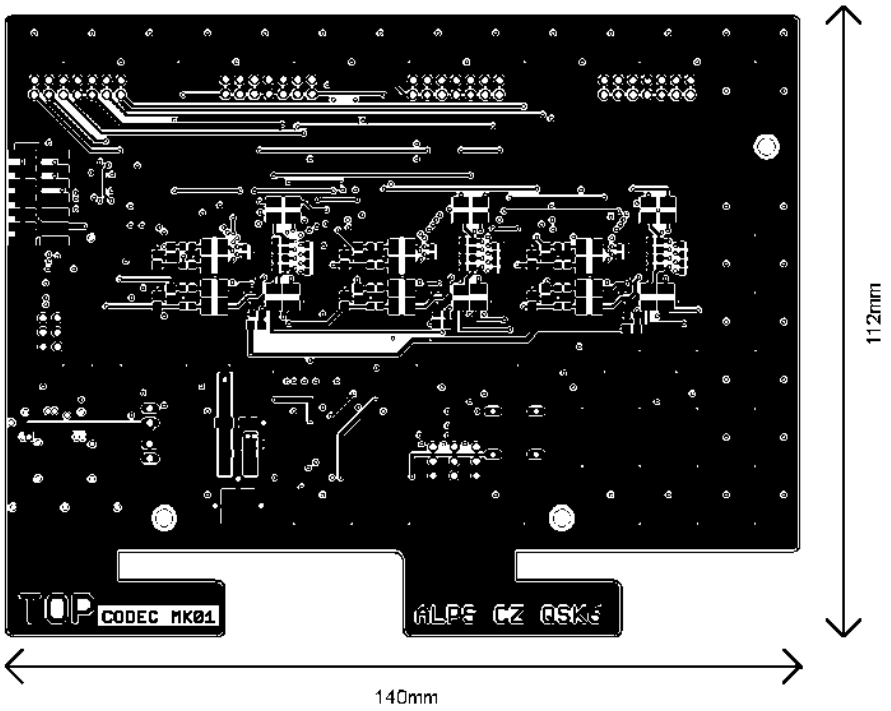

Fig. 74: Codec board – top layer

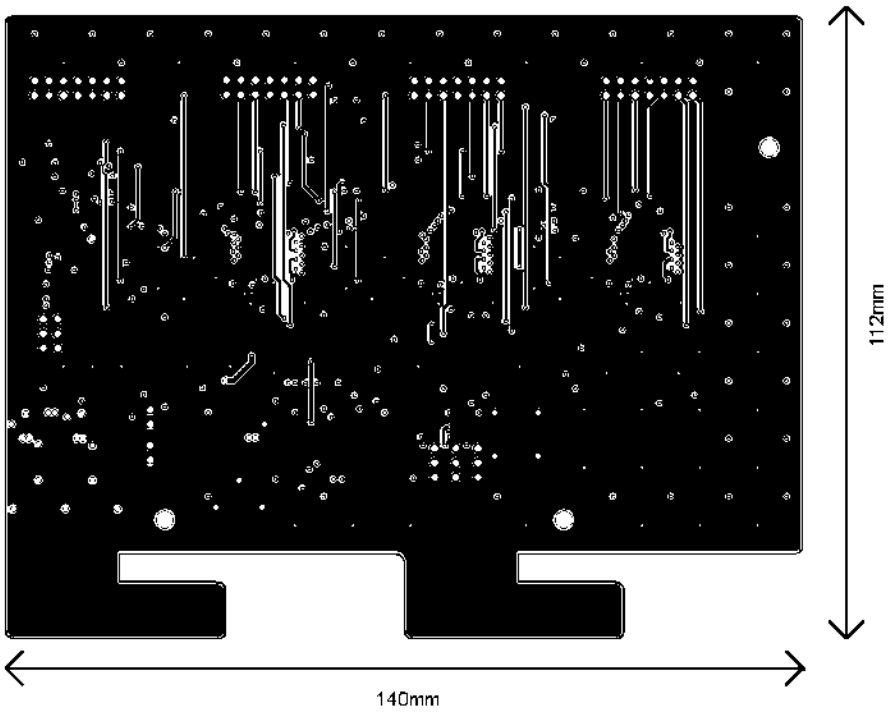

Fig. 75: Codec board – second layer

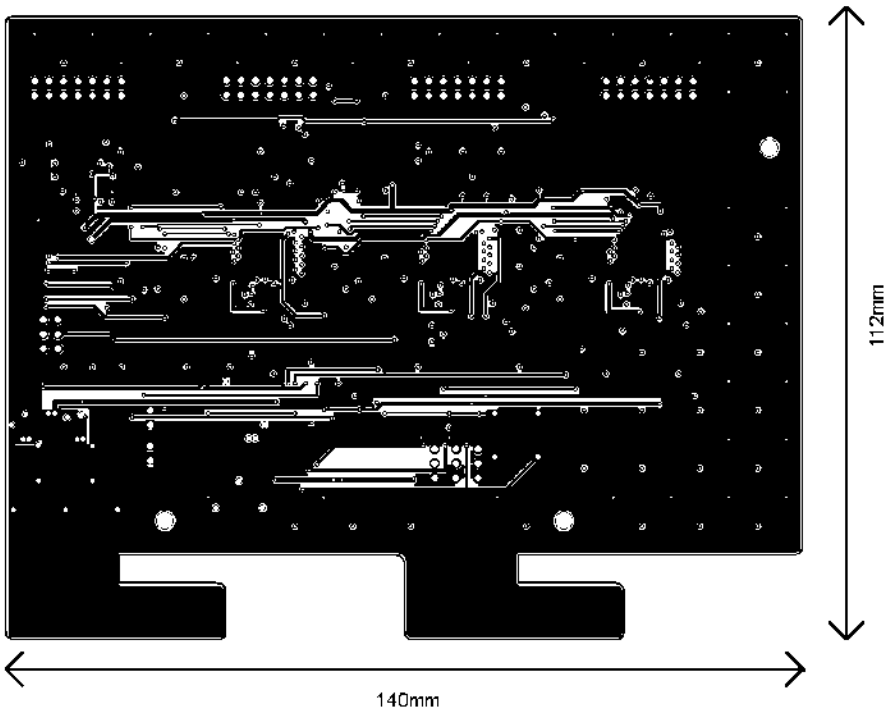

Fig. 76: Codec board – third layer

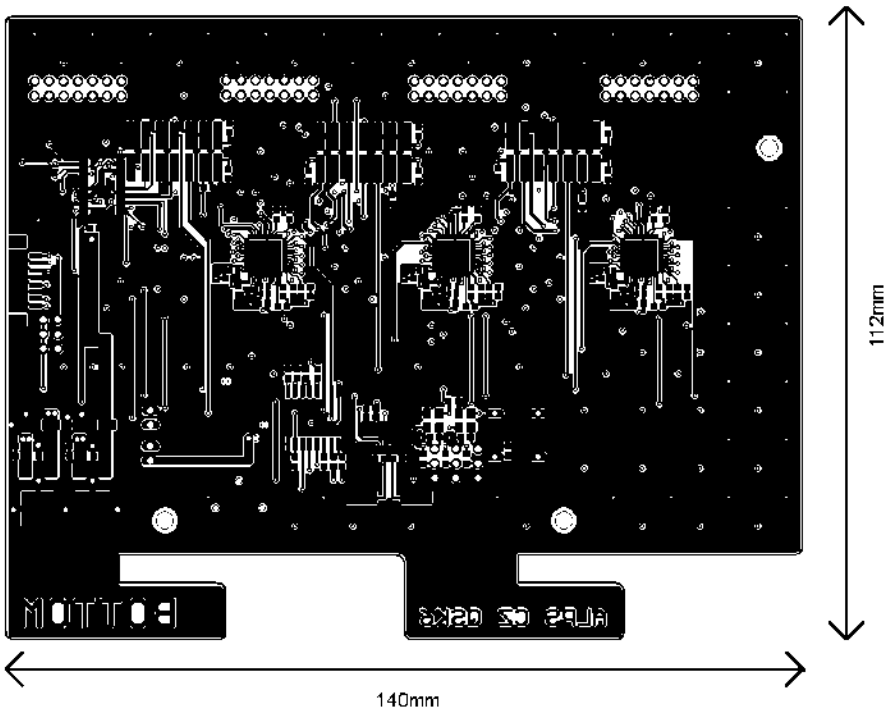

Fig. 77: Codec board – bottom layer

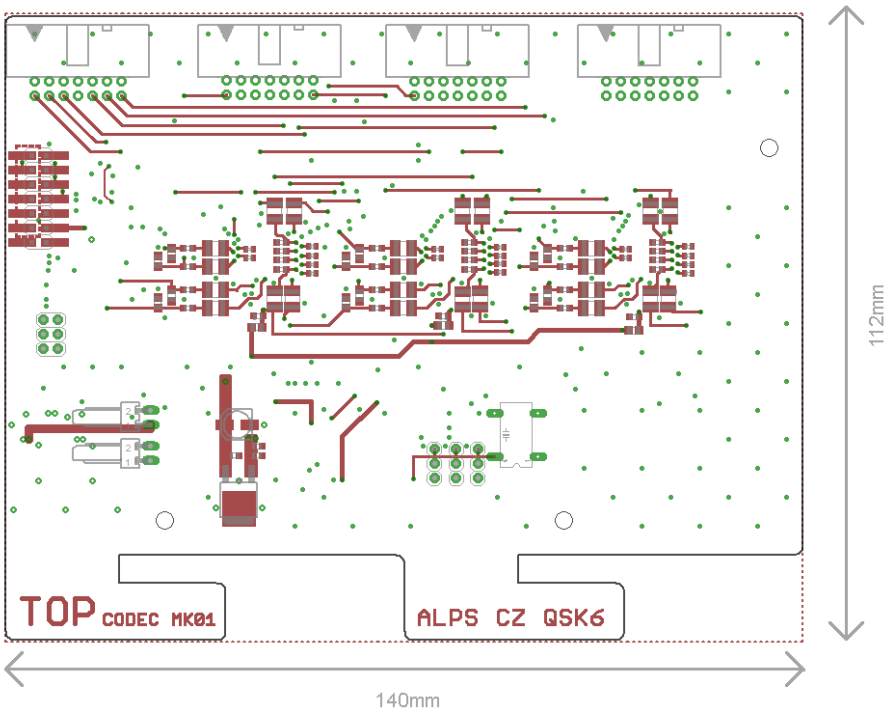

Fig. 78: Codec board - layout of components - top

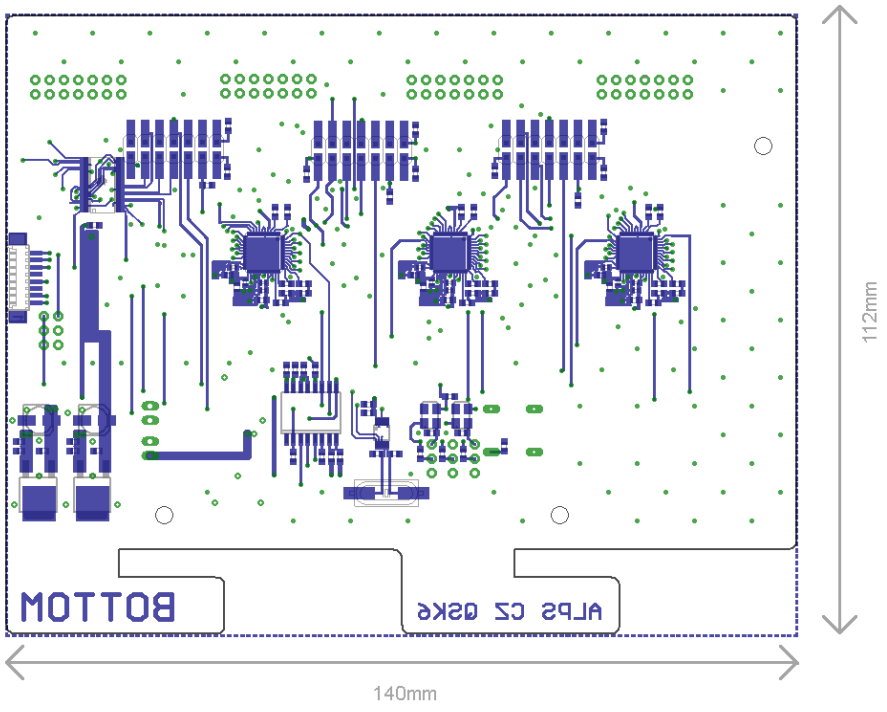

Fig. 79: Codec board - layout of components - top

A.1.6 Audio routing – schematic

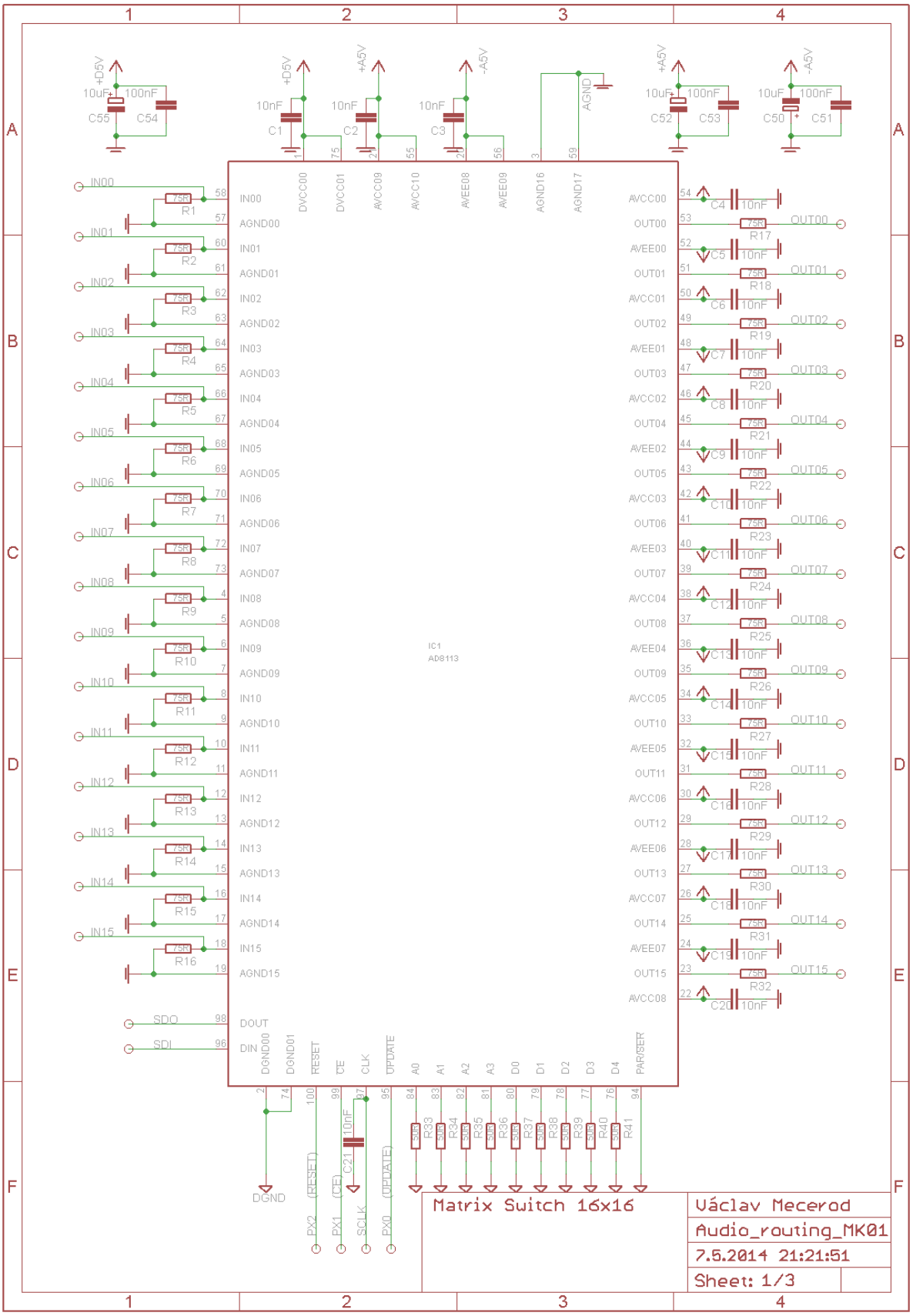

Fig. 80: AD8113 matrix switch

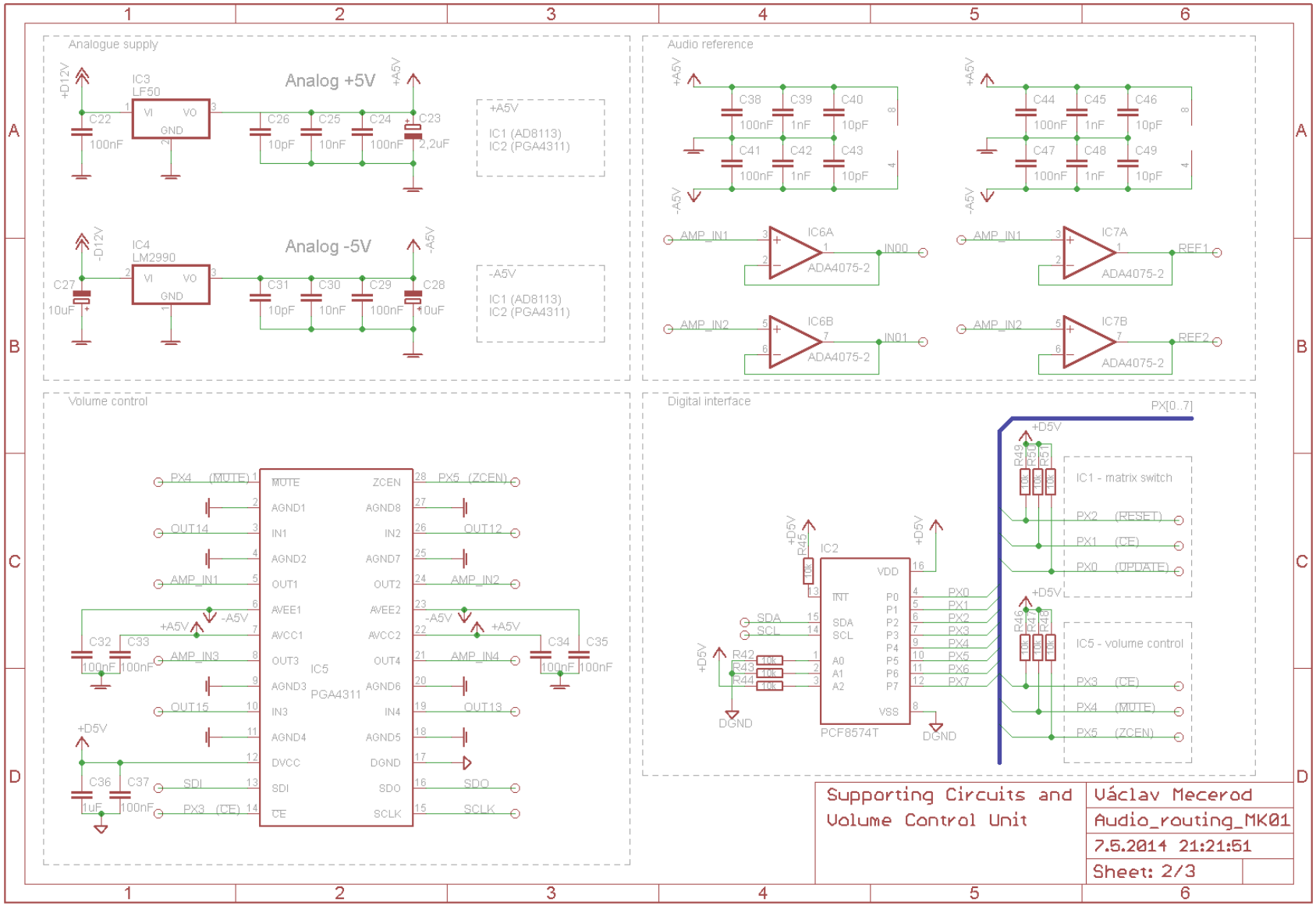

Fig. 81: Voltage supply, Audio reference, Volume control and Digital interface

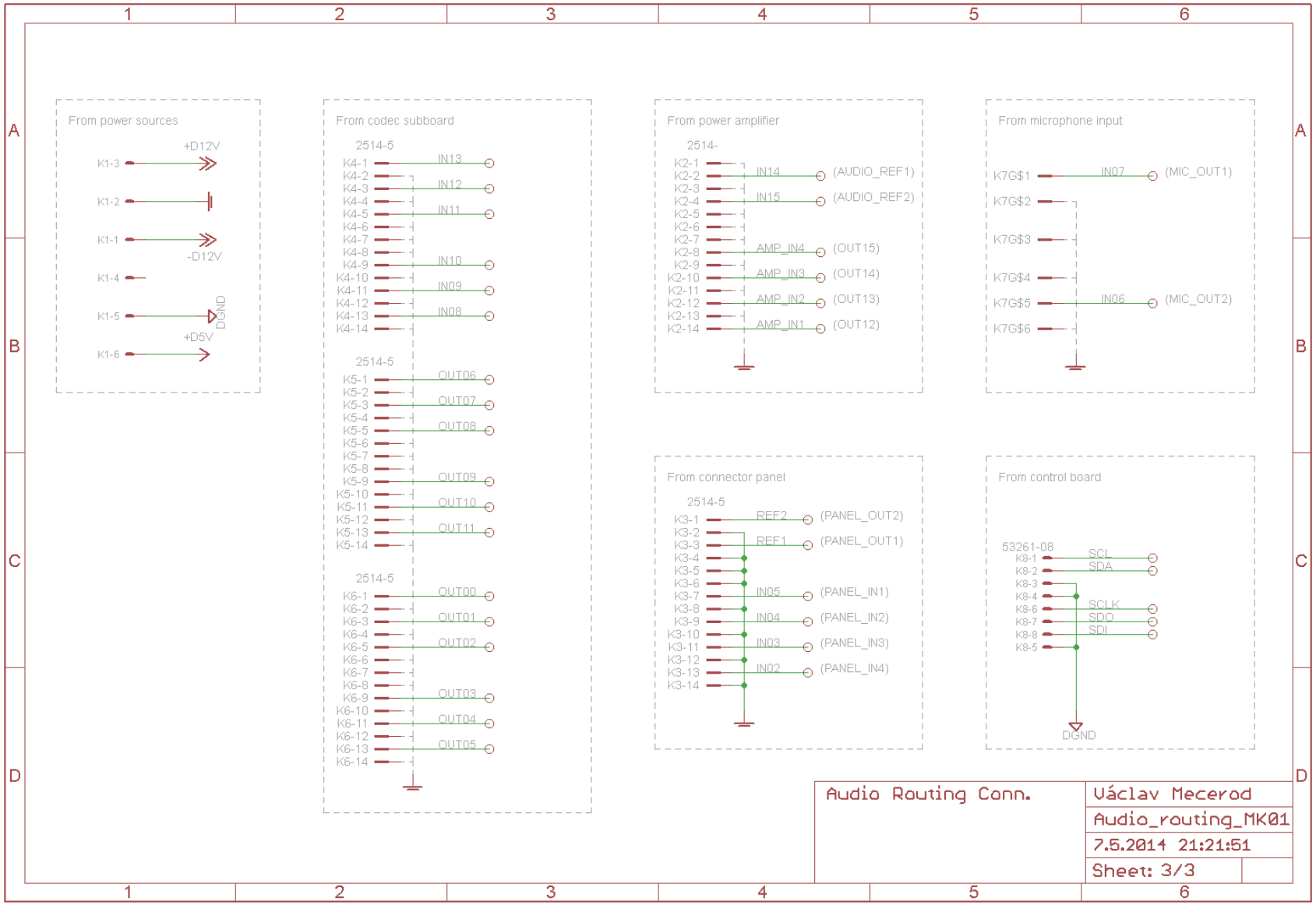

Fig. 82: Audio routing connectors

A.1.7 Audio routing - PCB

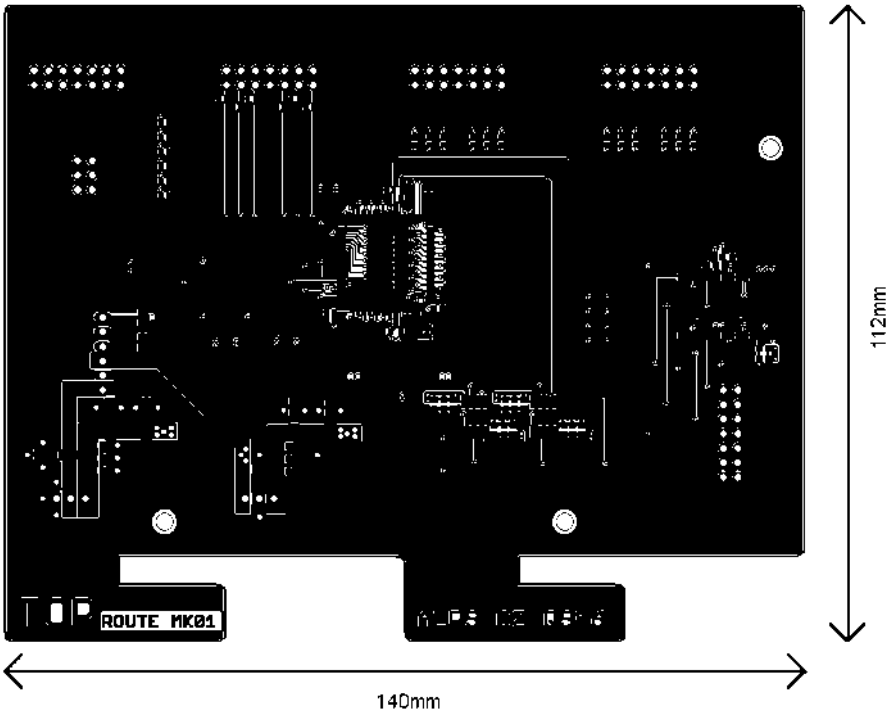

Fig. 83: Audio routing – top layer

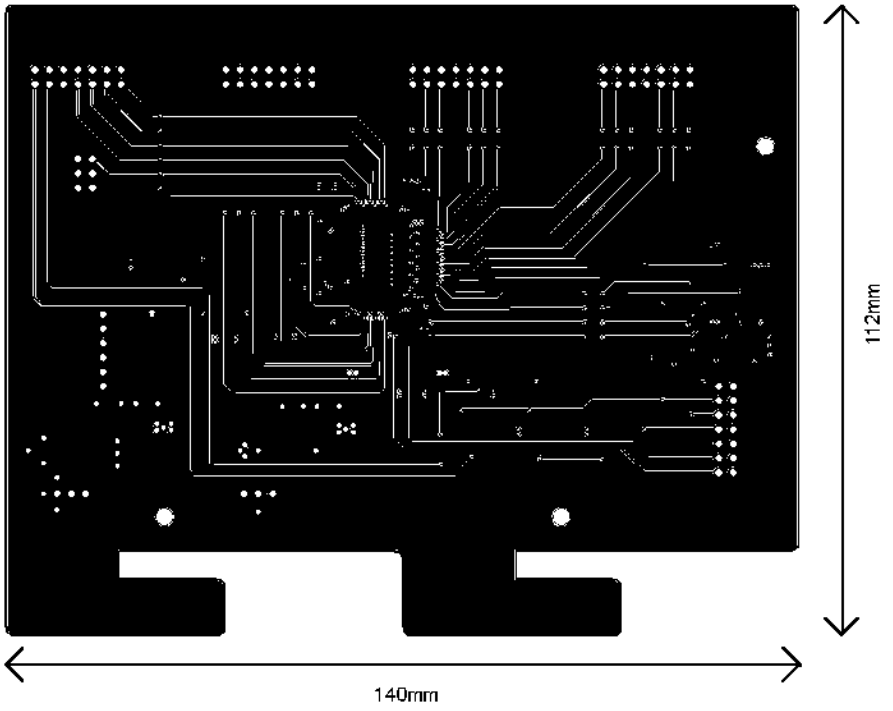

Fig. 84: Audio routing – second layer

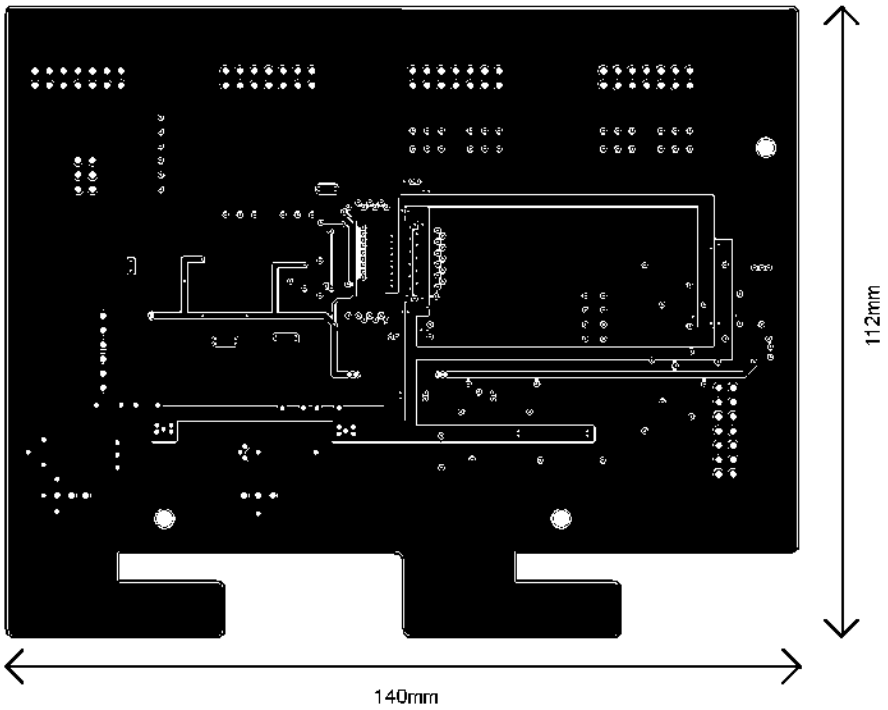

Fig. 85: Audio routing – third layer

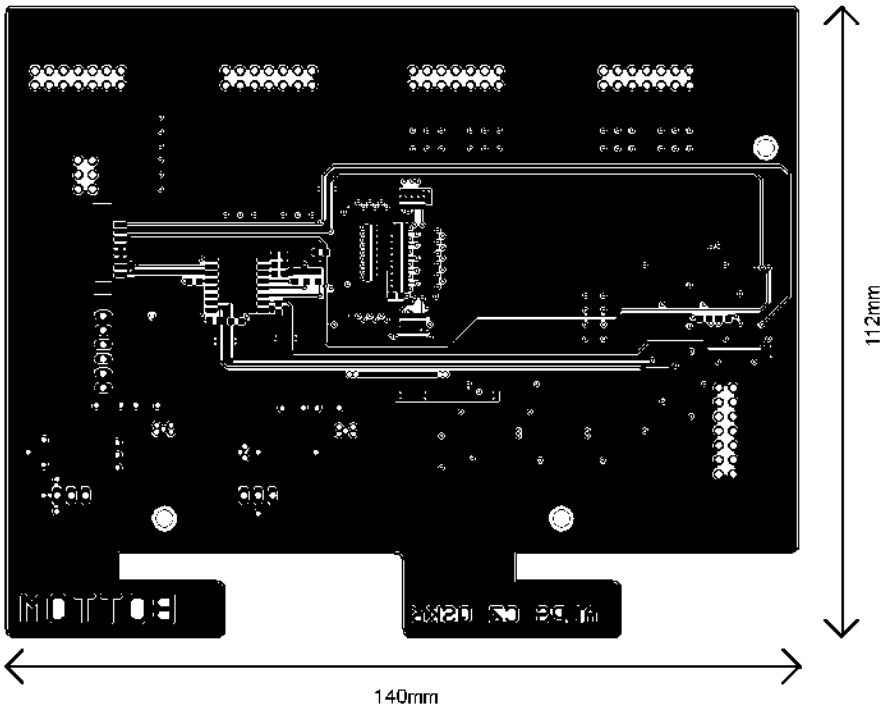

Fig. 86: Audio routing – bottom layer

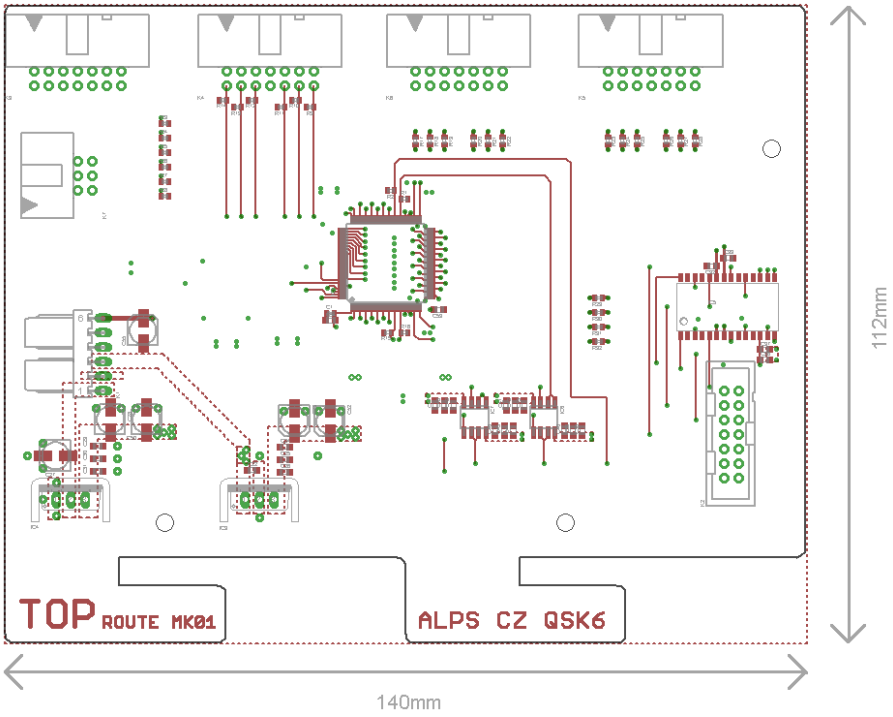

Fig. 87: Audio routing – layout of components - top

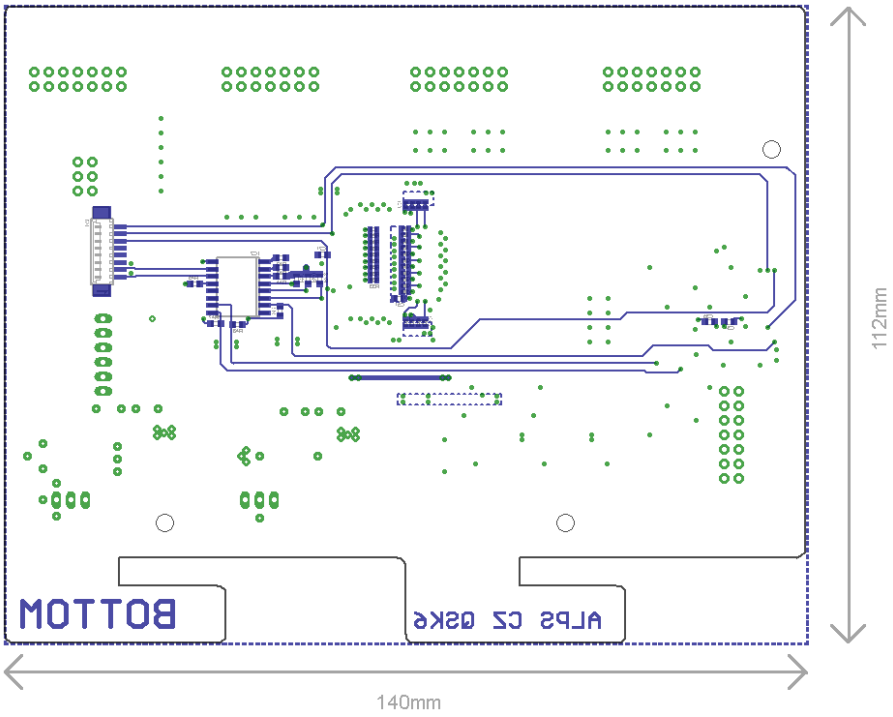

Fig. 88: Audio routing – layout of components - bottom

A.1.8 Cass D Amplifier – schematic

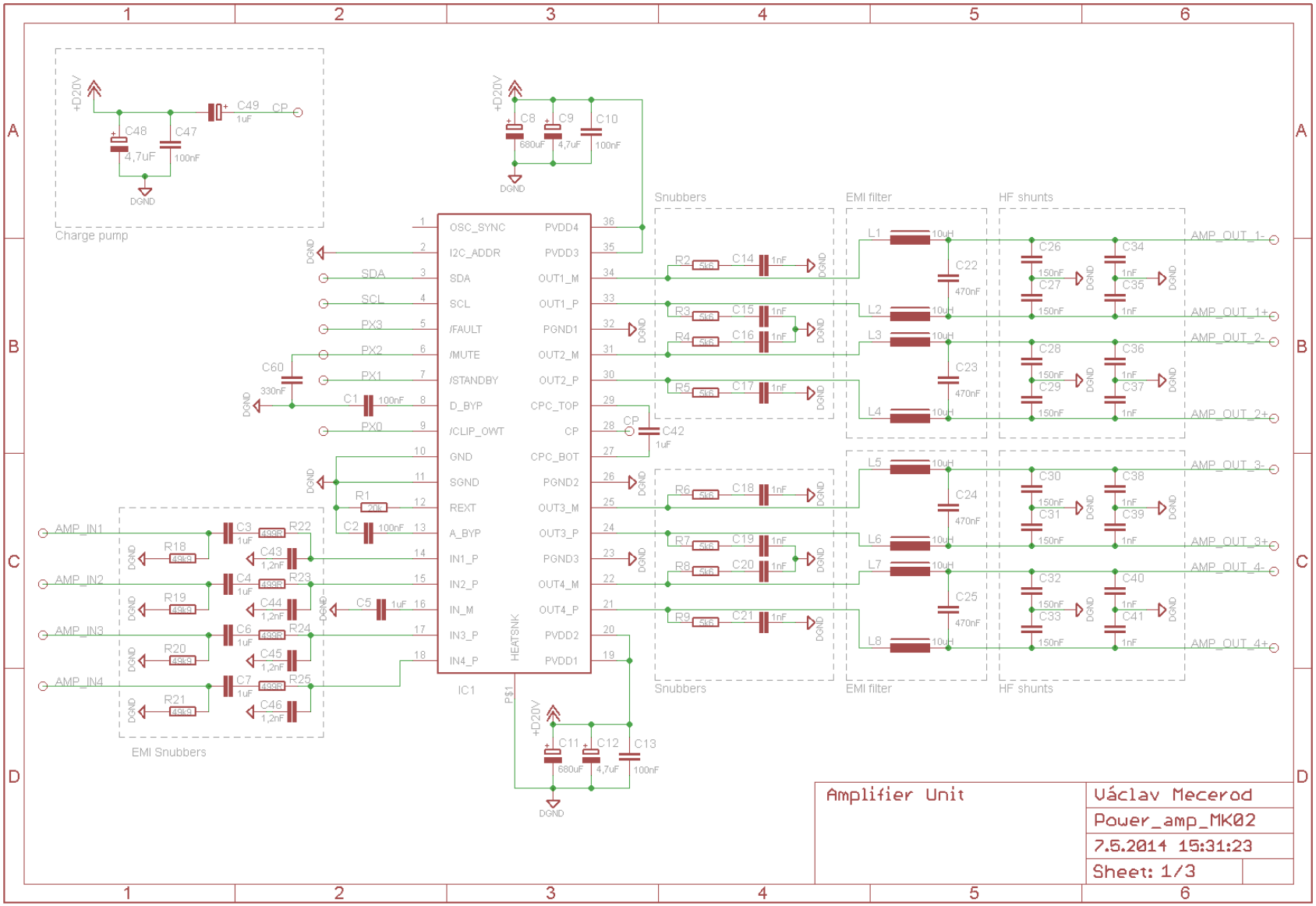

Fig. 89: Class D amplifier

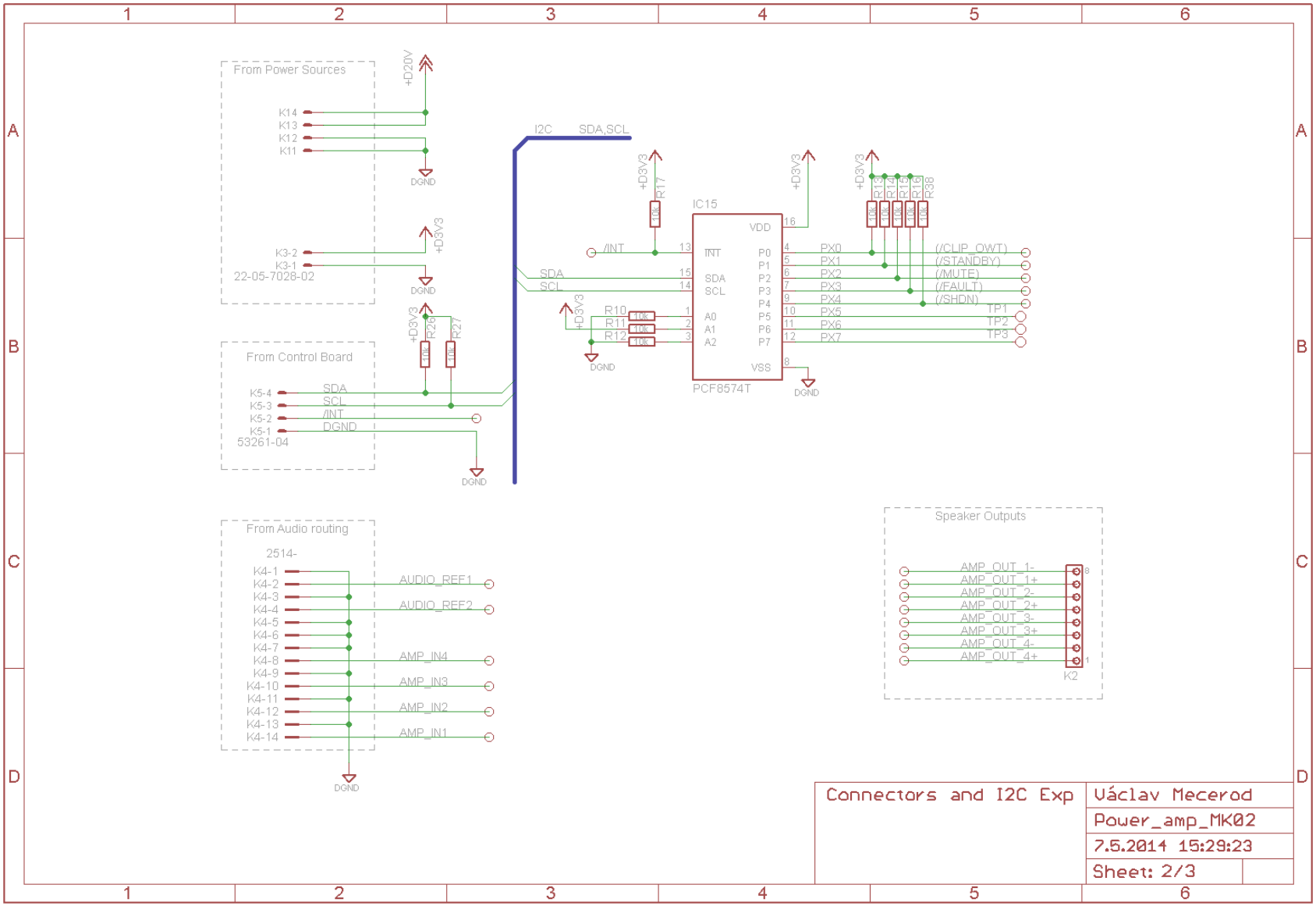

Fig. 90: Class D amplifier connectors

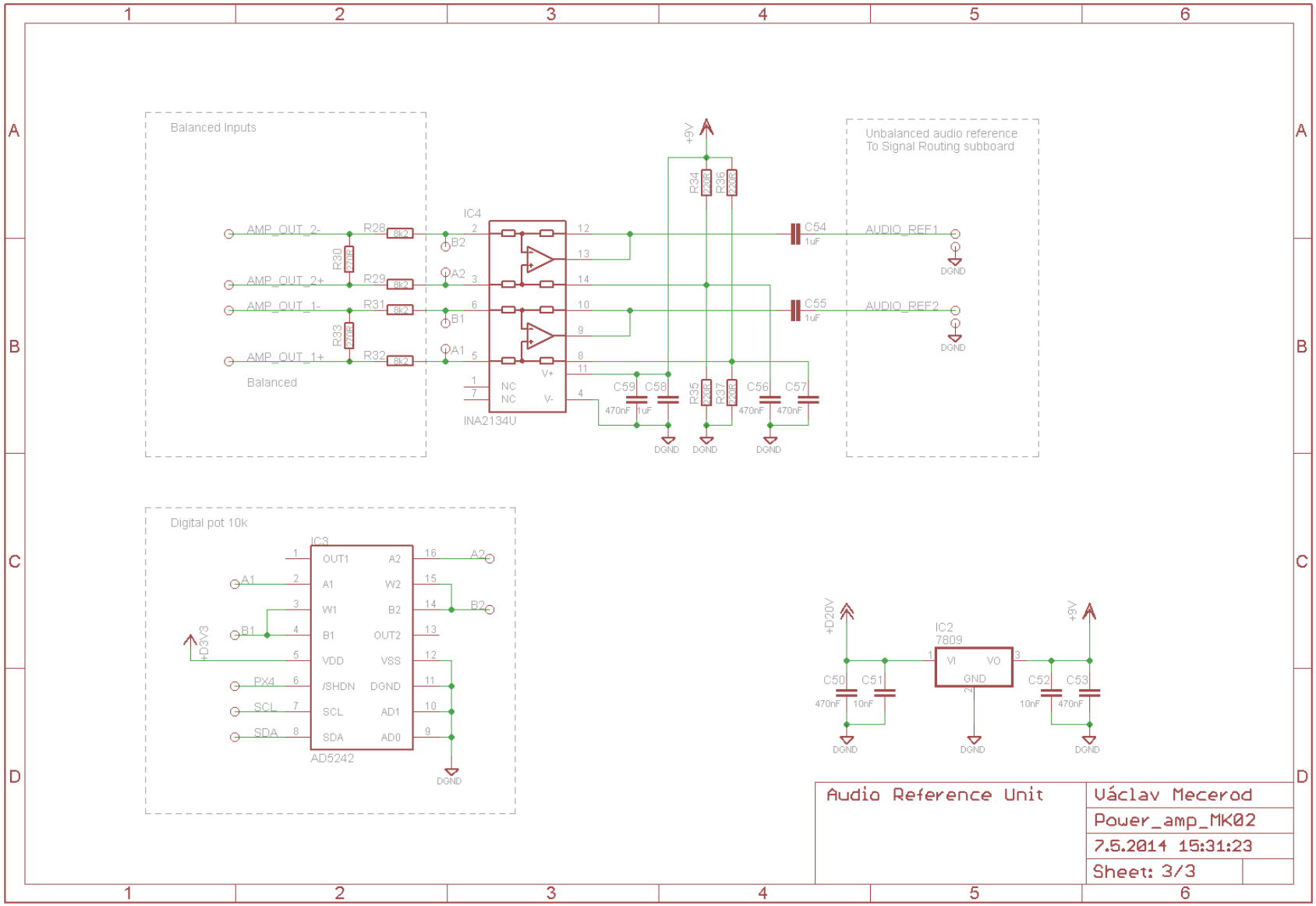

Fig. 91: Audio reference for the DUT

A.1.9 Class D Amplifier – PCB

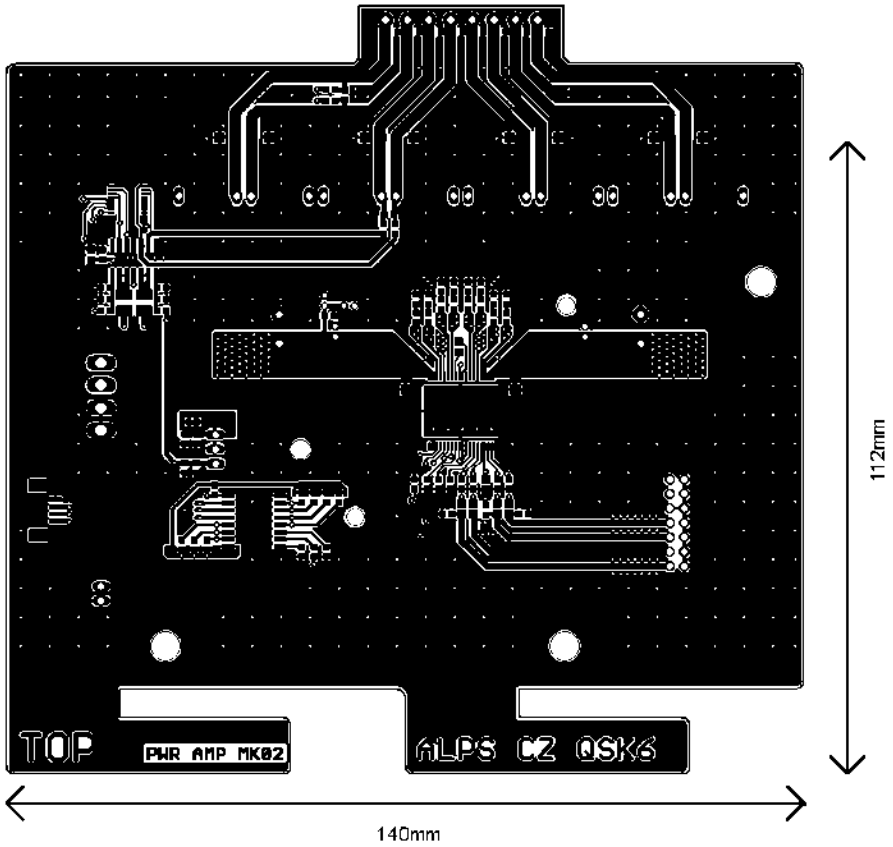

Fig. 92: Class D amplifier – top layer

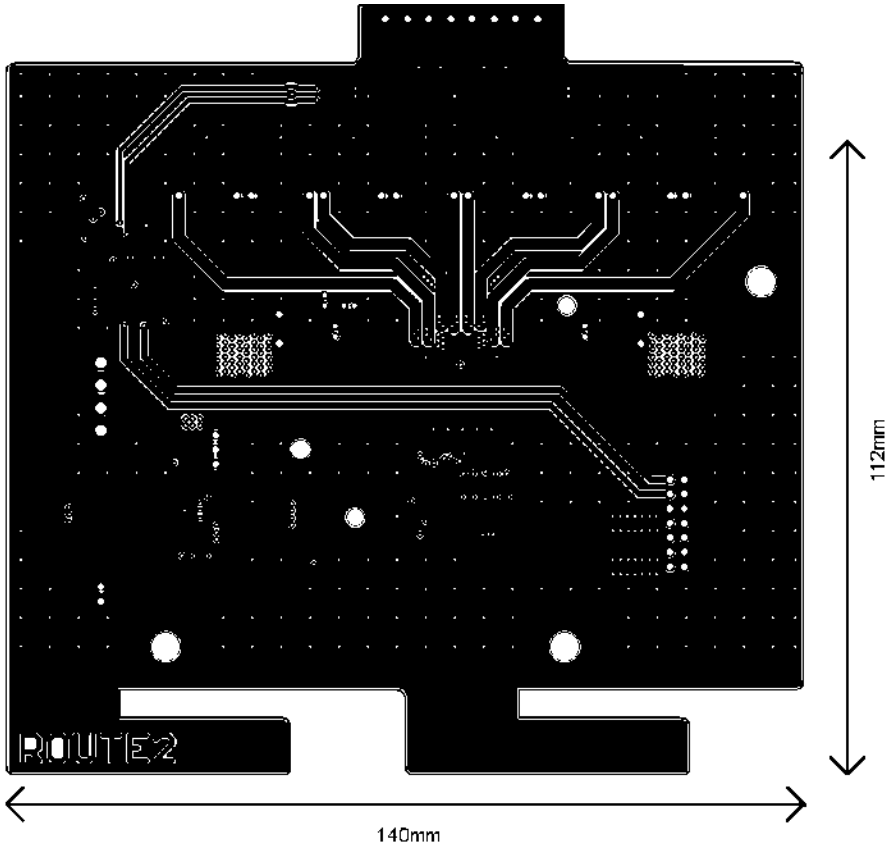

Fig. 93: Class D amplifier –second layer

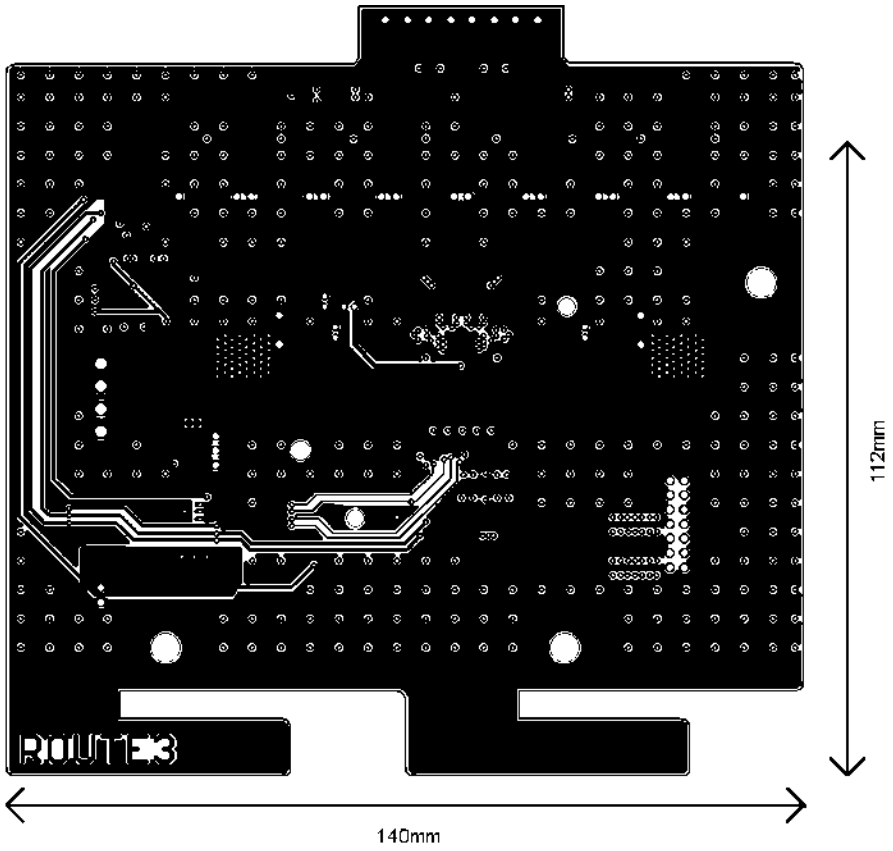

Fig. 94: Class D amplifier –third layer

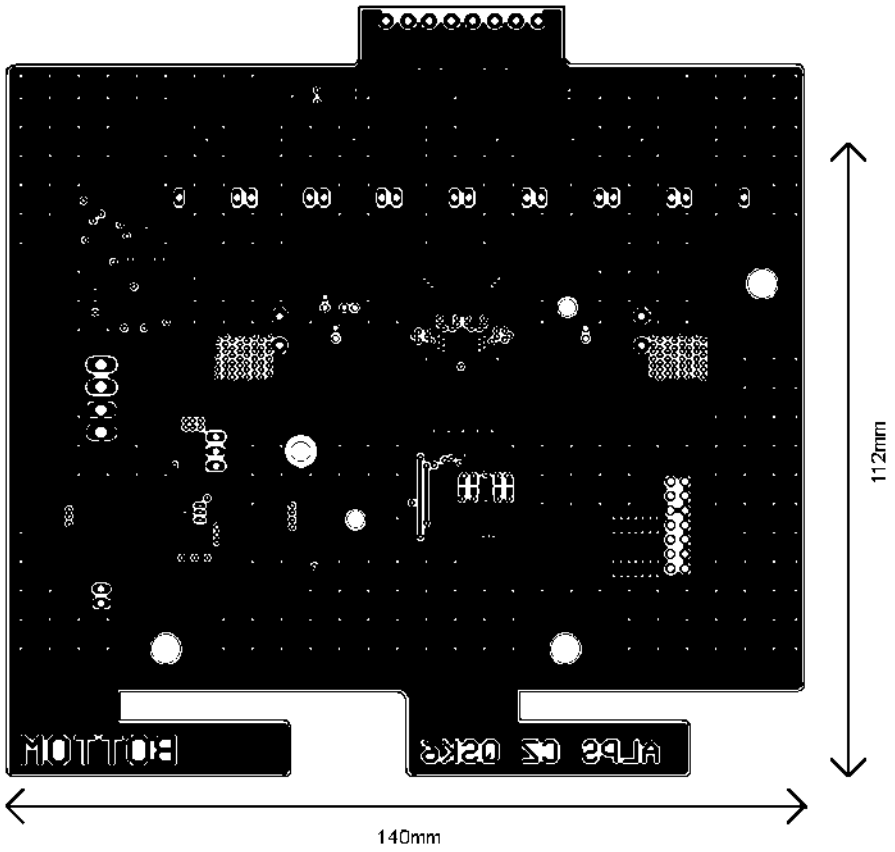

Fig. 95: Class D amplifier –bottom layer

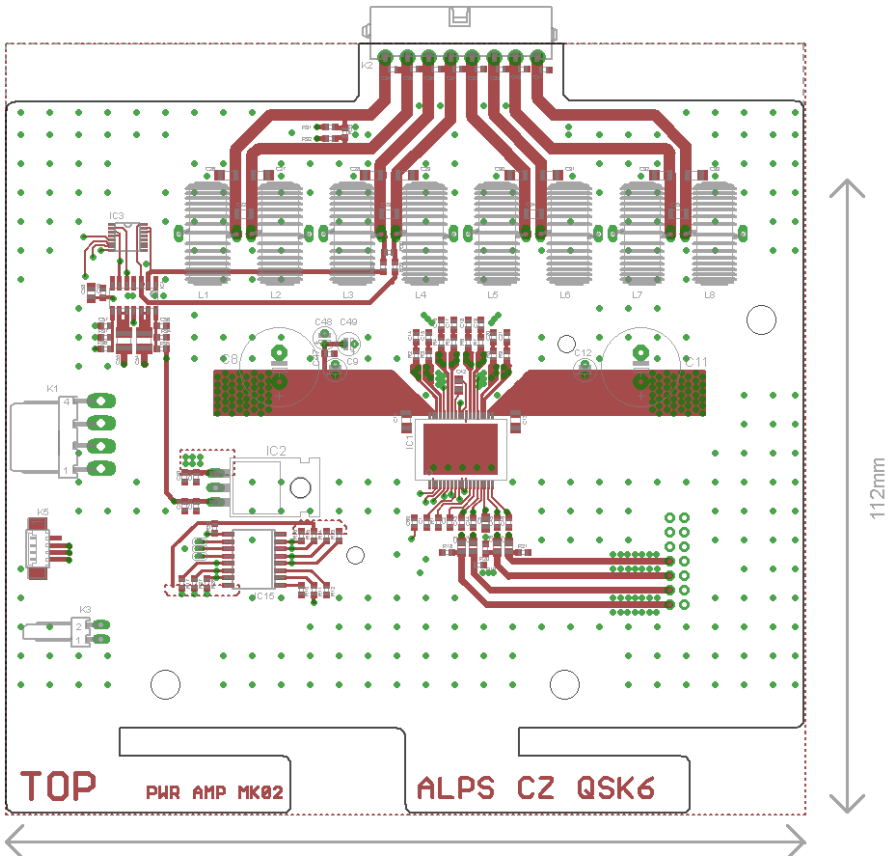

Fig. 96: Class D amplifier – layout of components – top

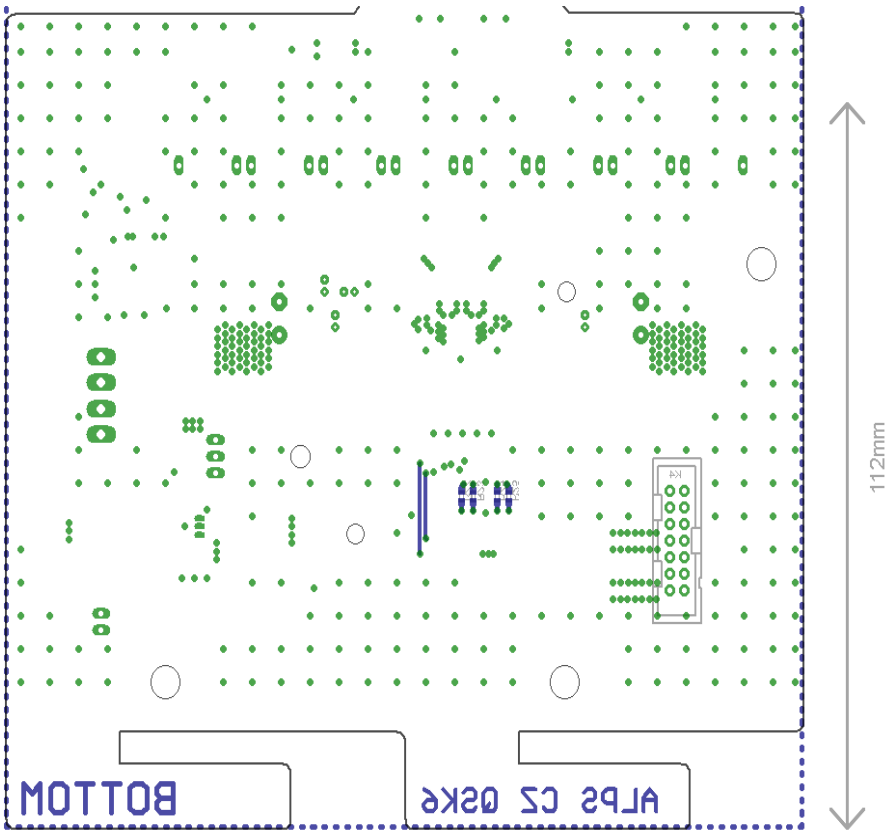

Fig. 97: Class D amplifier – layout of components – bottom

A.1.10 Control board – schematic

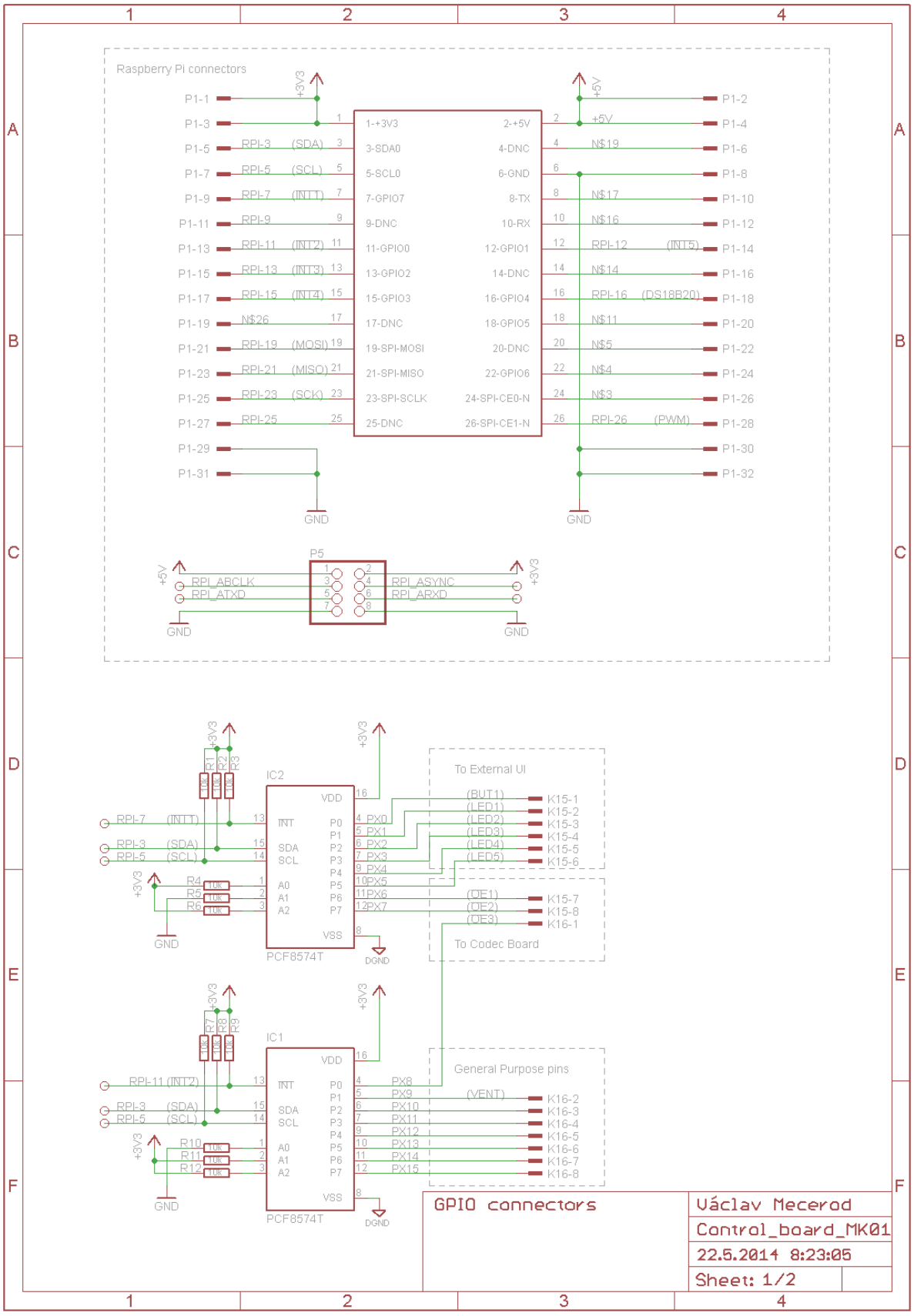

Fig. 98: GPIO connectors

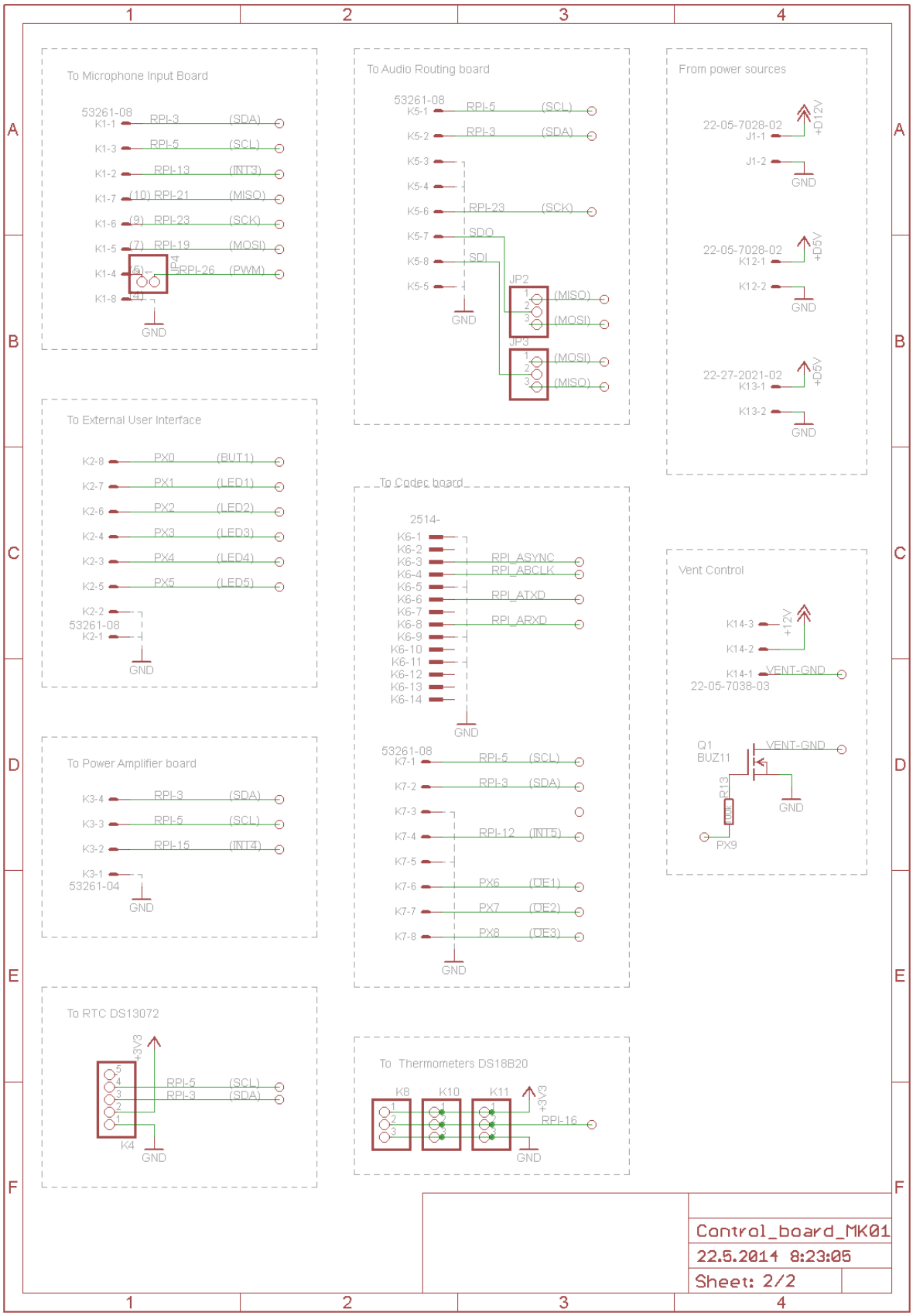

Fig. 99: Control board connectors

A.1.11 Control board – PCB

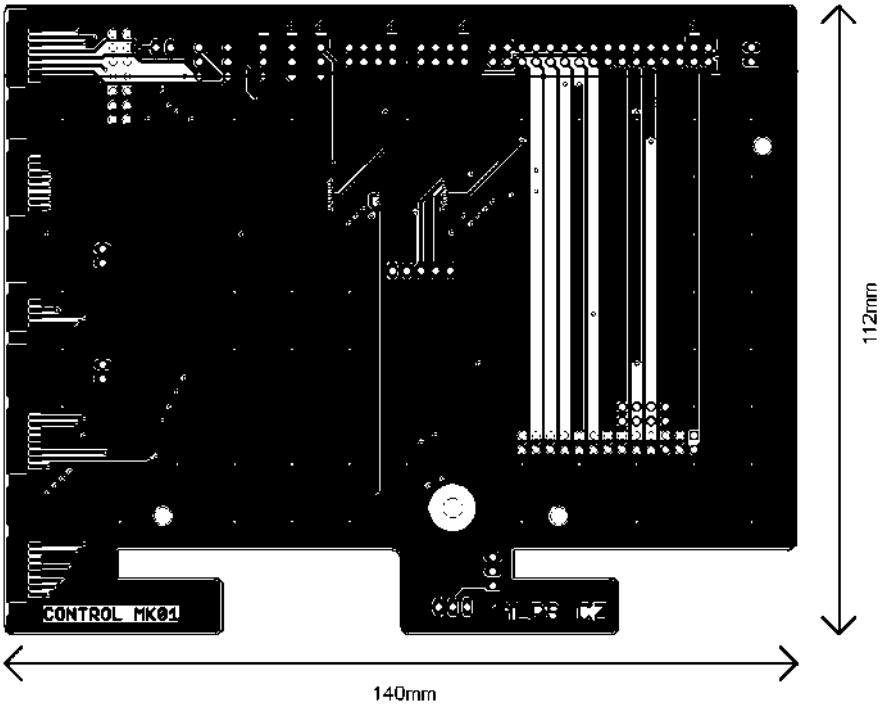

Fig. 100: Control board – top layer

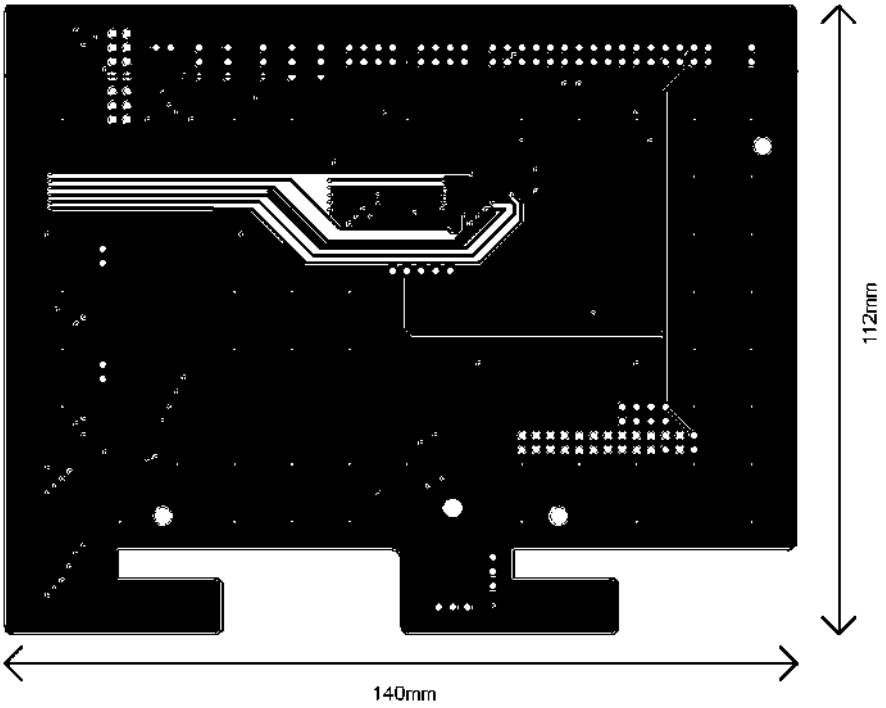

Fig. 101: Control board – second layer

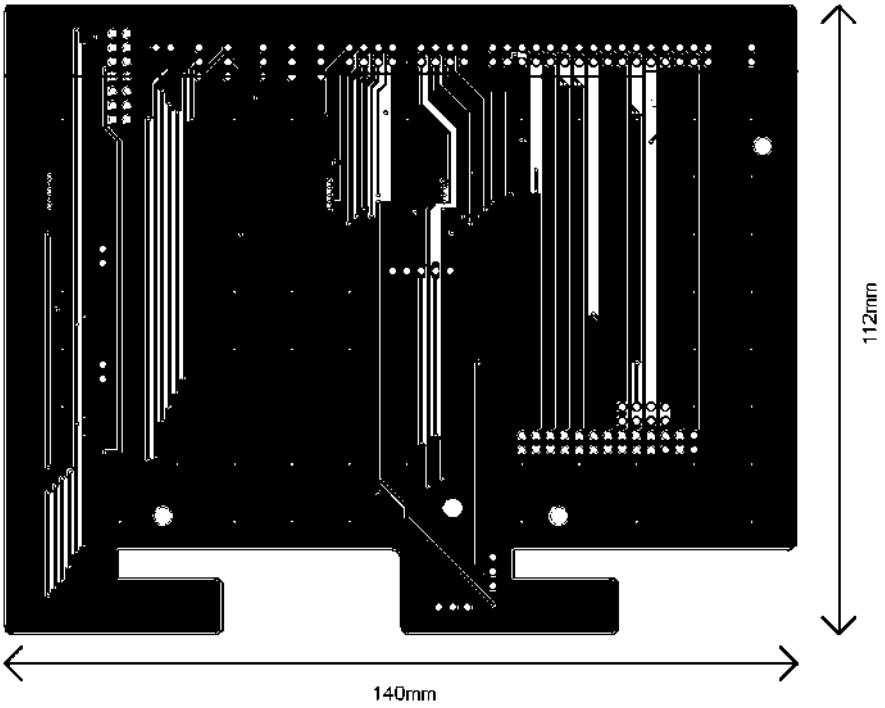

Fig. 102: Control board – third layer

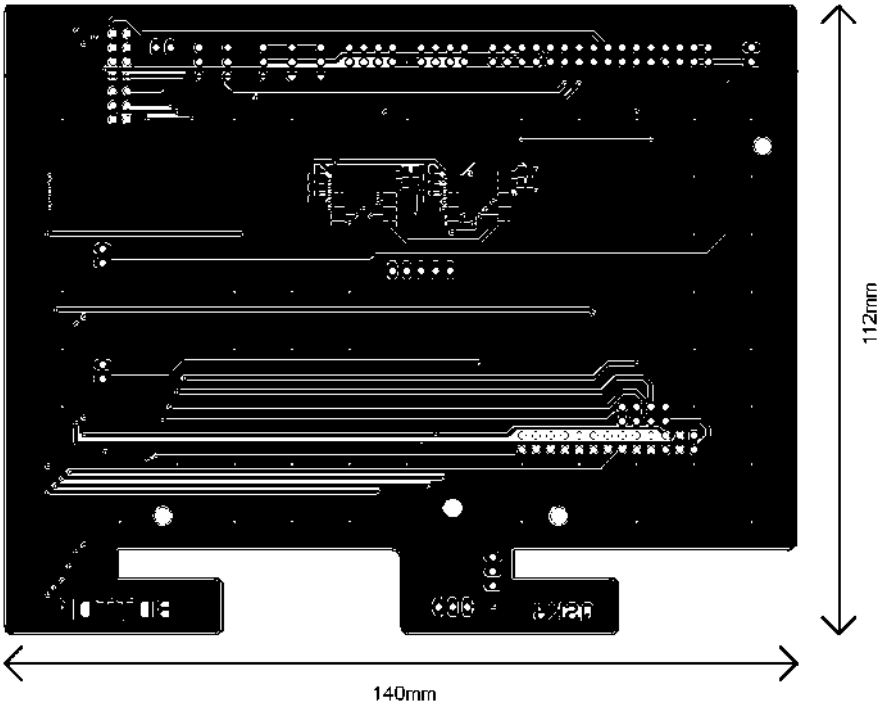

Fig. 103: Control board – bottom layer

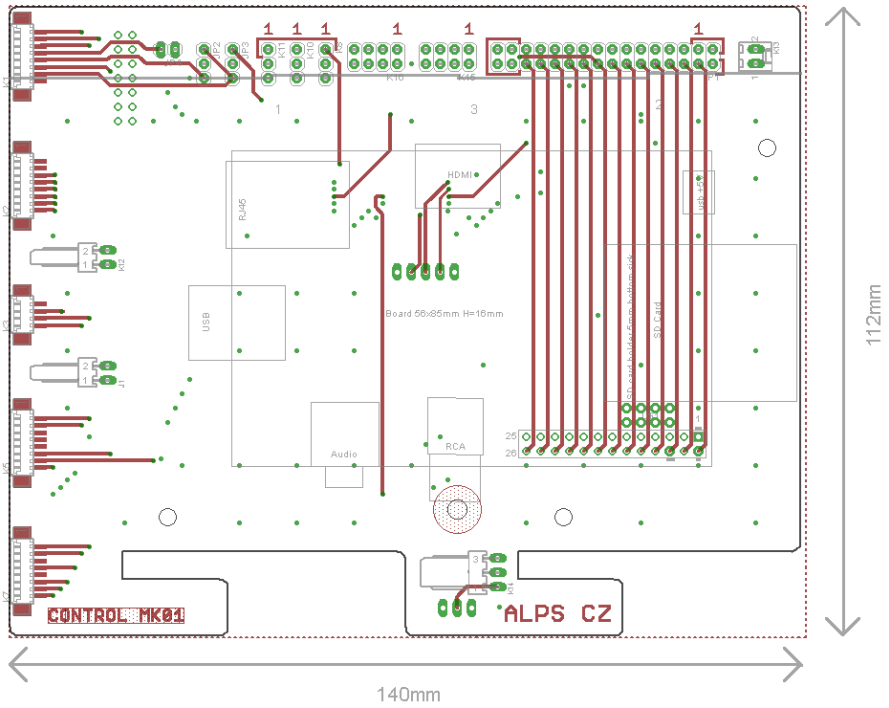

Fig. 104: Control board – layout of components – top

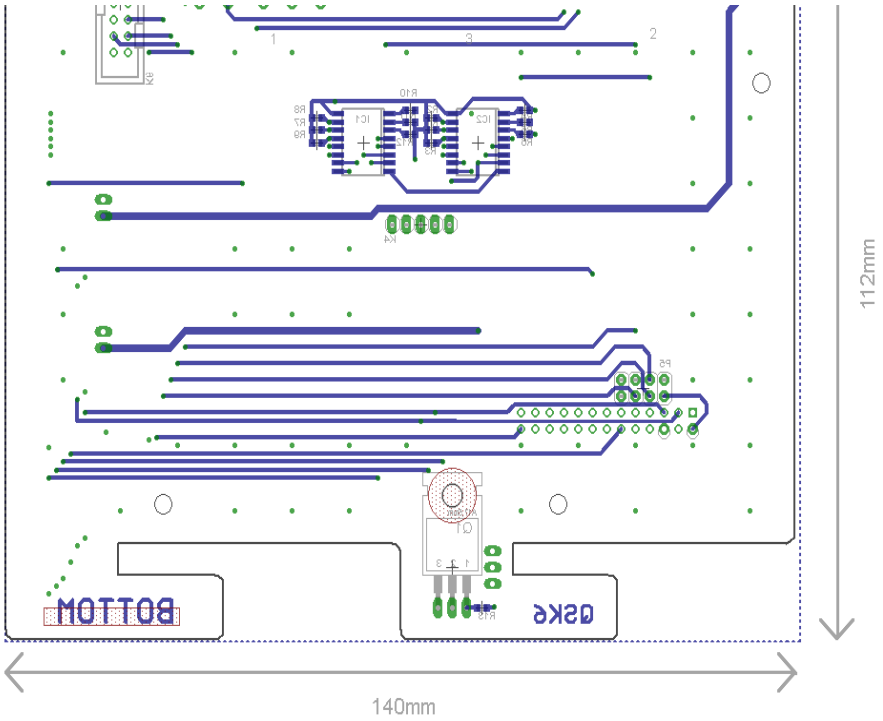

Fig. 105: Control board – layout of components – bottom

A.1.12 Power sources – schematic

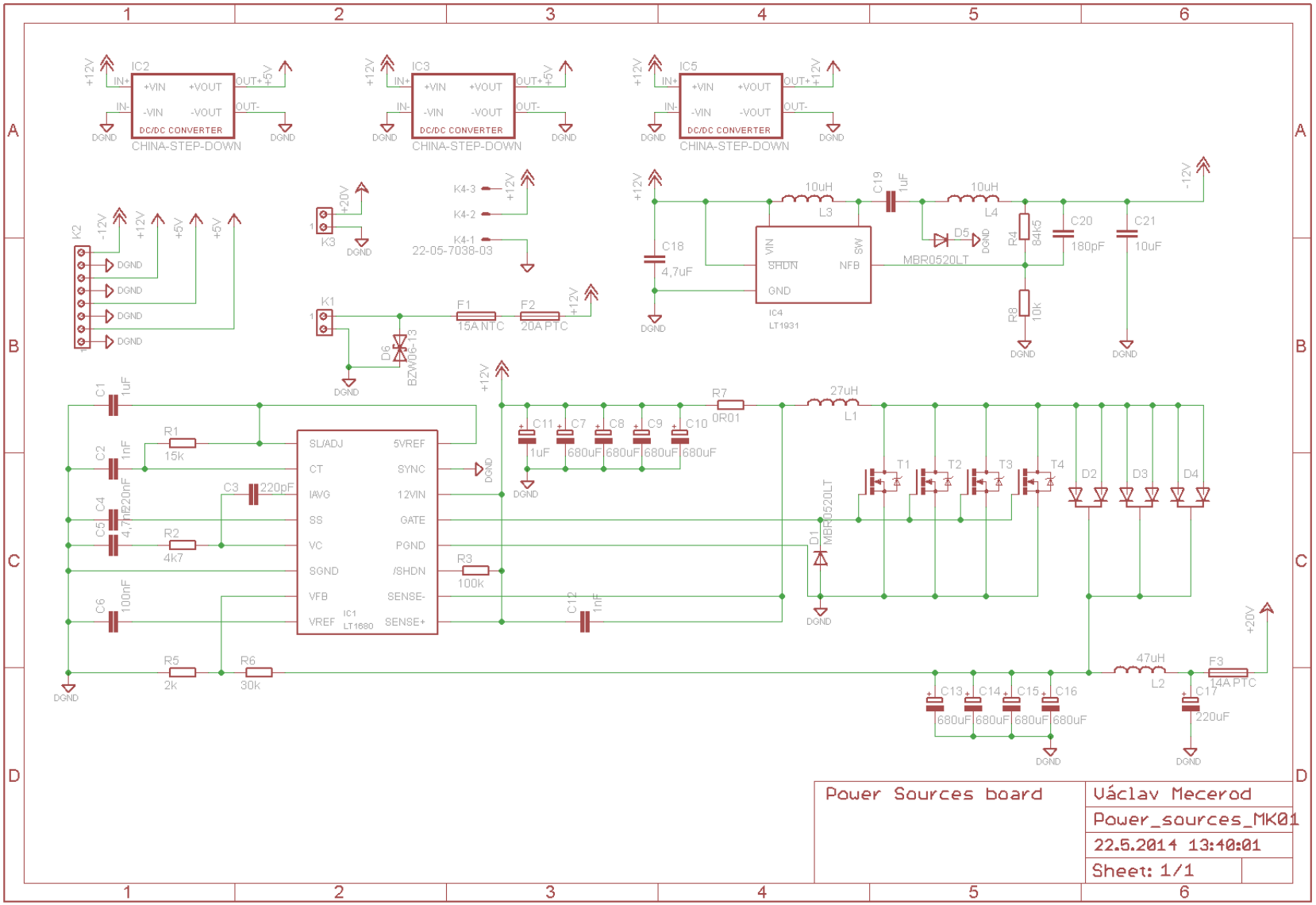

Fig. 106: Power sources

A.1.13 Power sources – PCB

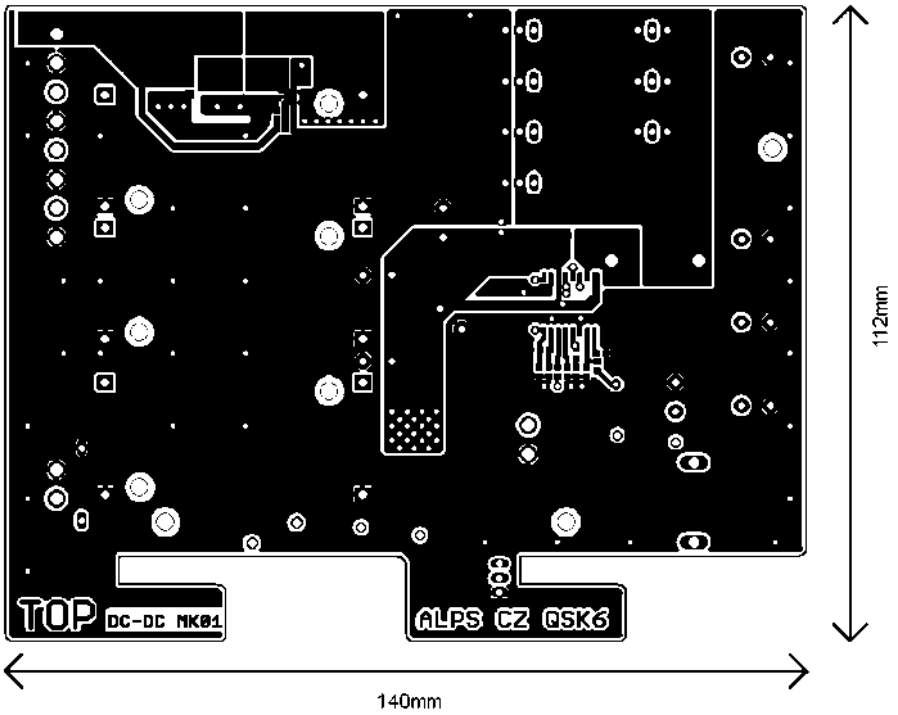

Fig. 107: Power sources – top layer

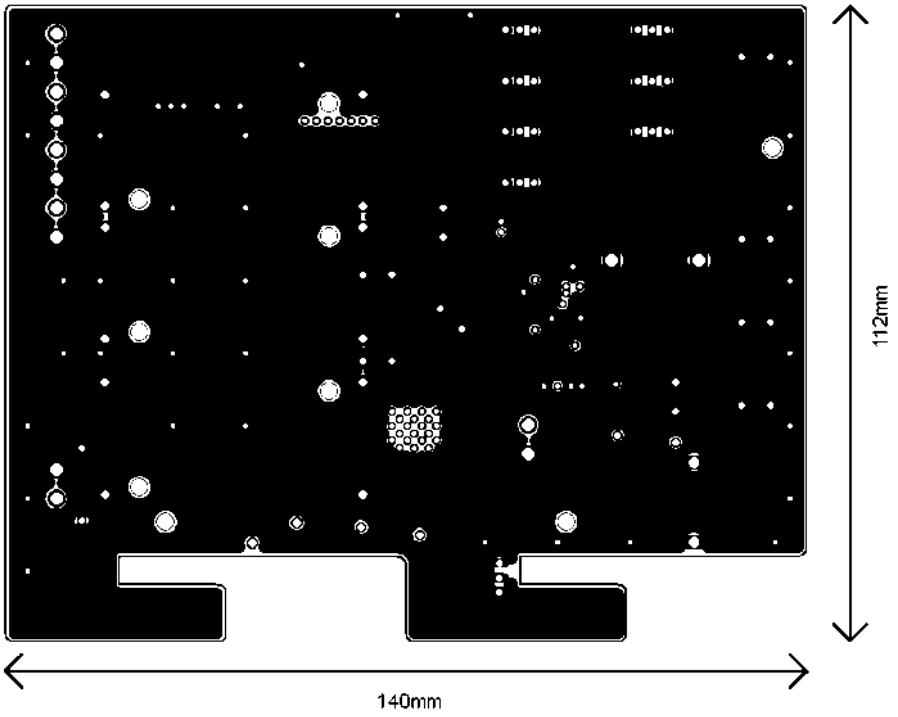

Fig. 108: Power sources – second layer

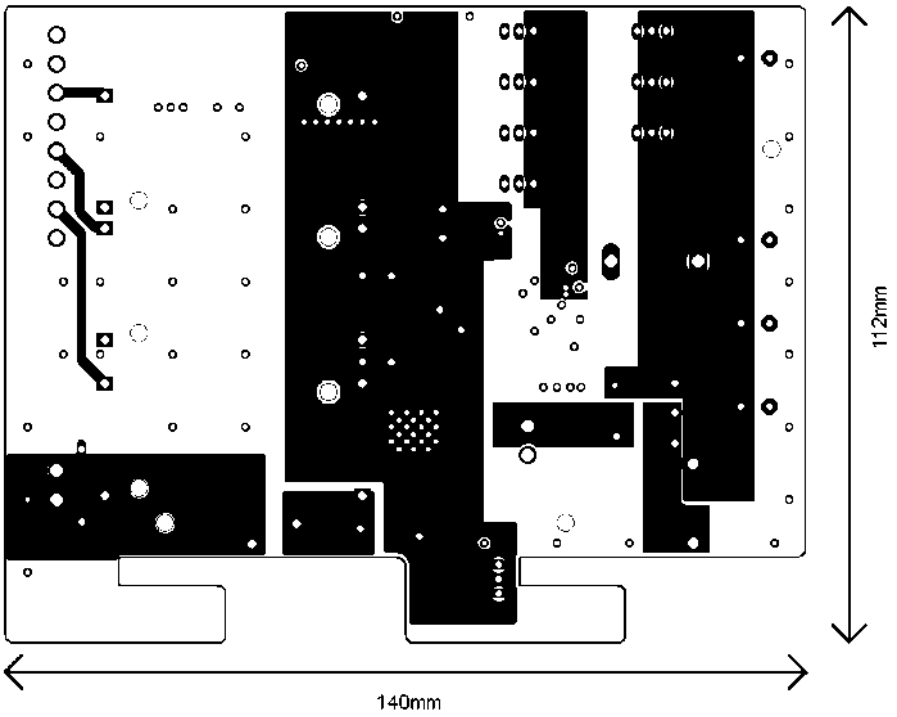

Fig. 109: Power sources – third layer

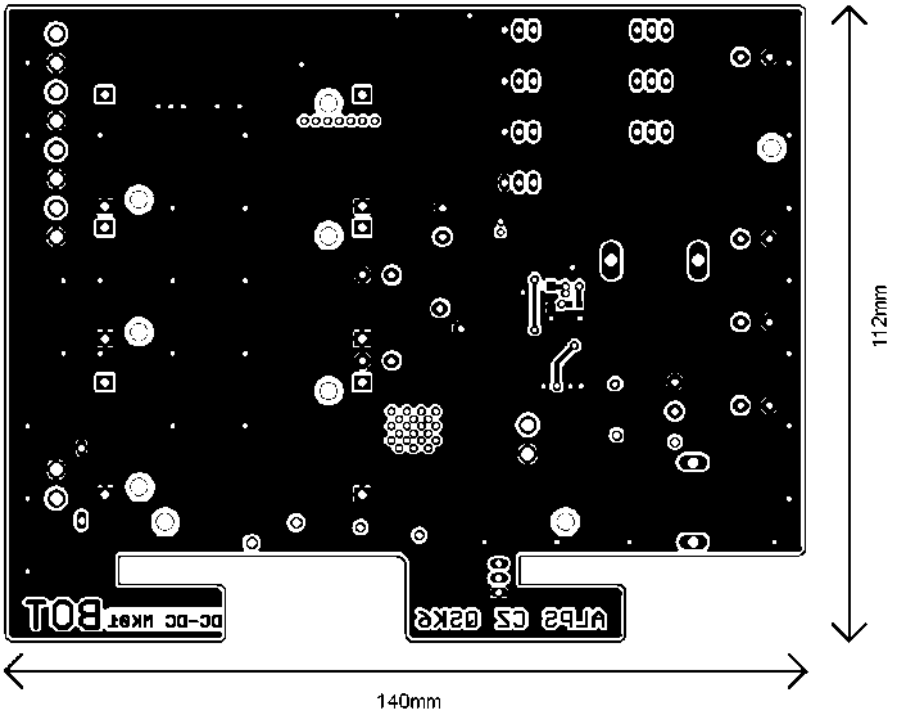

Fig. 110: Power sources - bottom layer

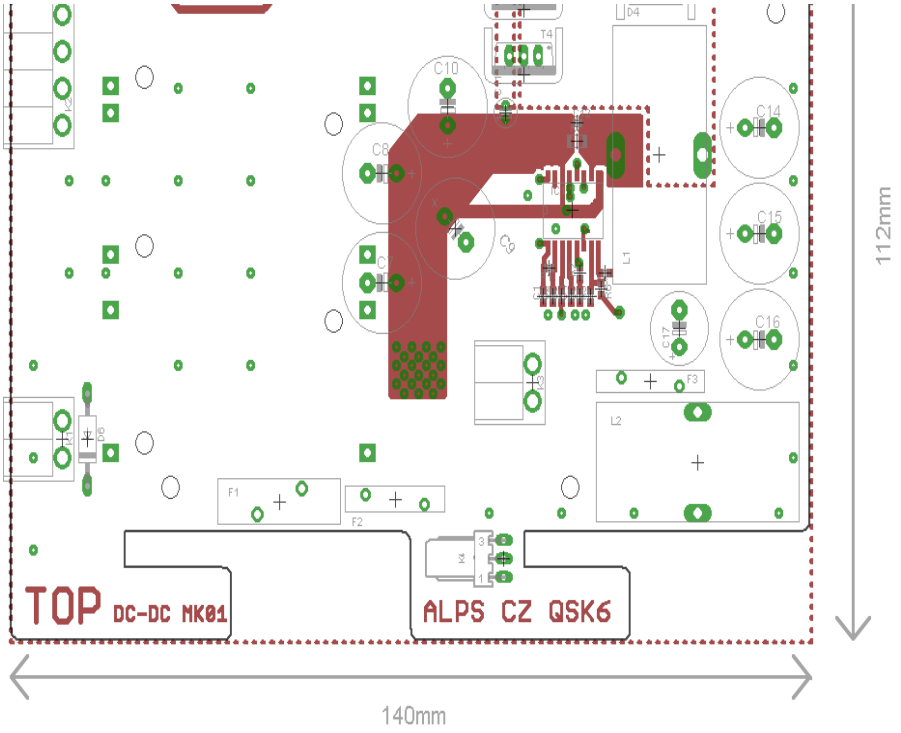

Fig. 111: Power sources – layout of components – top

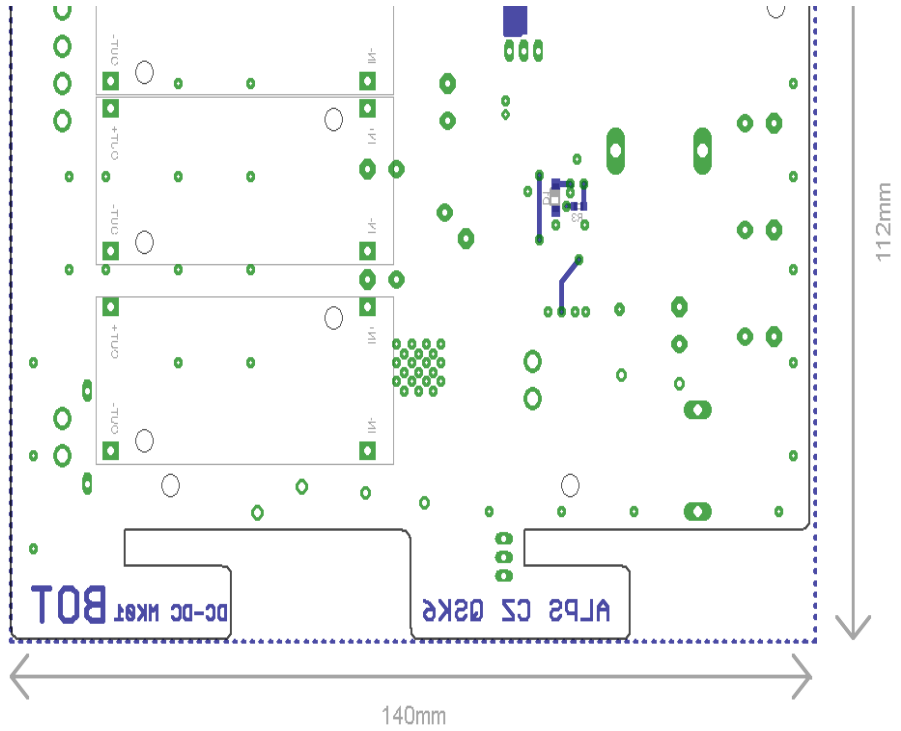

Fig. 112: Power sources – layout of components – bottom

A.2 Measured results

A.2.1 Microphone input

Tab. 3: Used apparatus for microphone input measurement

Used apparatus:	
Power sources:	Manson SDP2405: 1x (0-40) V / (0-5) A
	Diametral P230R51D: 2x (0-30) V / (0-4) A + 5 V / 3 A
Multimetr:	
Oscilloscope:	Agilent Technologies DSO7014B 100MHz, 2GS/s, 4 CH
Audio analyzer:	Kenwood VA-2230A

Tab. 4: Frequency response of PGA112 (IC4)

G	[-]	1
Vin	[dBV]	-0,5
f [Hz]	Vout [dBV]	Ku rev.2 [dB]
50	-0,6	-0,1
75	-0,6	-0,1
100	-0,6	0,0
250	-0,5	0,0
500	-0,5	0,0
1000	-0,5	0,0
5000	-0,5	0,0
10000	-0,5	0,0
15000	-0,4	-0,1
20000	-0,7	-0,2

Tab. 5: Frequency response and THD of whole audio path (microphone input)

Vin	[dBV]	-13	
THD+N	[%]	0,0763(A)	@ 1 kHz
THD	[%]	0,0036(A)	@ 1 kHz
f_{PWM}	[kHz]	740	

f [Hz]	Vout [dBV]	Ku [dB]	f [Hz]	Vout [dBV]	Ku [dB]
25	-28,3	-15,3	500	-13,3	-0,3
50	-20,1	-7,1	1000	-13,1	-0,1
60	-18,5	-5,5	2500	-13,1	-0,1
65	-18,1	-5,1	5000	-13,8	-0,8
70	-17,4	-4,4	7000	-14,3	-1,3
75	-16,9	-3,9	7500	-14,6	-1,6
80	-16,4	-3,4	7700	-16,0	-3,0
90	-15,8	-2,8	8000	-22,8	-9,8
100	-15,3	-2,3	8500	-34,4	-21,4
150	-14,1	-1,1	10000	-60,6	-47,6
250	-13,5	-0,5	20000	-62,5	-49,5

Tab. 6: THD of PGA112 (IC4) depending on gain

Vin	[dBV]	-30
f	[Hz]	1000
G [-]	THD+N(A) [%]	THD(A) [%]
1	0,0054	0,0041
2	0,0177	0,0045
4	0,0570	0,0069
8	0,1265	0,0156
16	0,2508	0,0320
32	0,5320	0,0520
64	1,2000	0,1360

Tab. 7: THD of PGA112 (IC4) depending on frequency

G	[-]	1
Vin	[dBV]	-0,5
f [Hz]	THD+N(A) [%]	THD(A) [%]
25	0,0052	0,0036
50	0,0056	0,0042
75	0,0053	0,0012
100	0,0045	0,0056
250	0,0064	0,0031
500	0,0056	0,0037
1000	0,0049	0,0041
2500	0,0048	0,0042
5000	0,0045	0,0041
10000	0,0034	0,0026

Tab. 8: Measurement of the test-signal generator

N	[dBV]	-61
Vout	[dBV]	-14,8
THD+N	[%]	0,106(A)
THD	[%]	0,055(A)

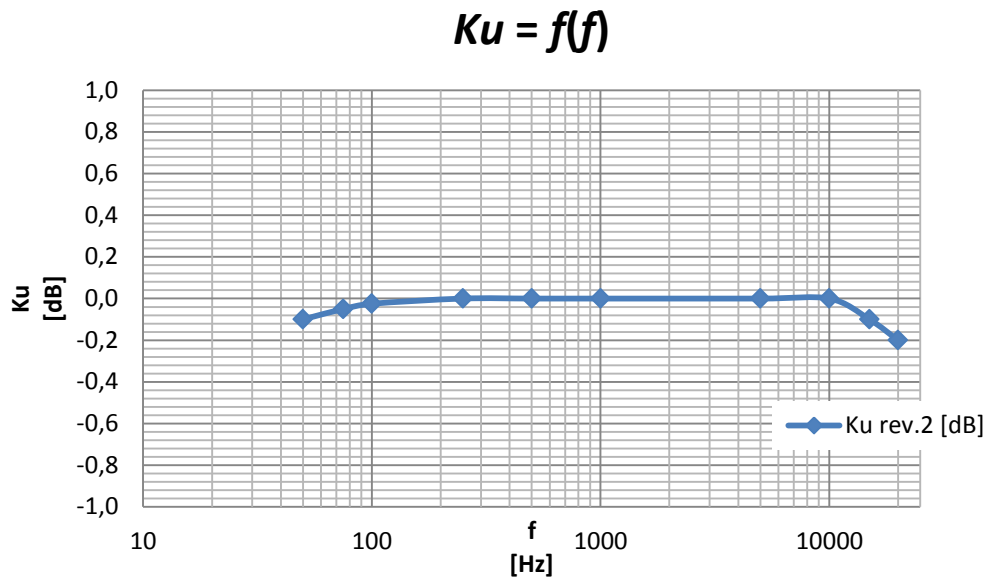

Fig. 113: Frequency response of preamplifier (PGA112)

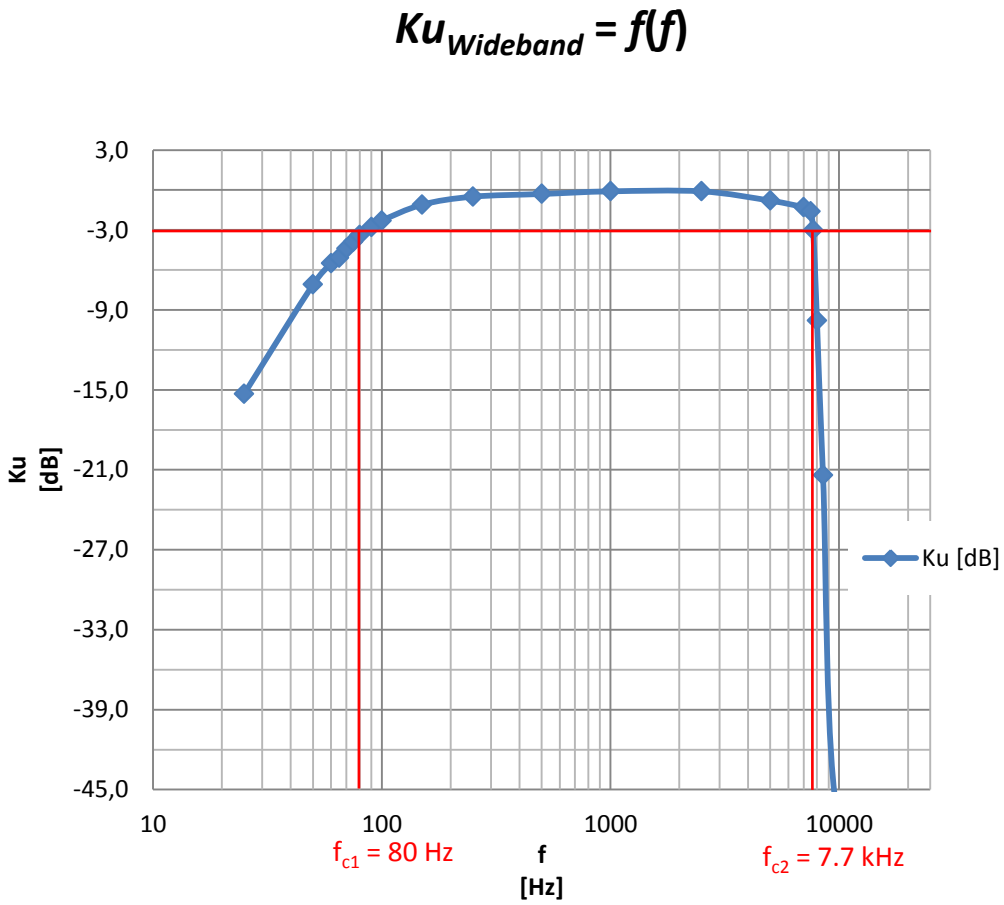

Fig. 114: Frequency response of whole audio path (microphone input)

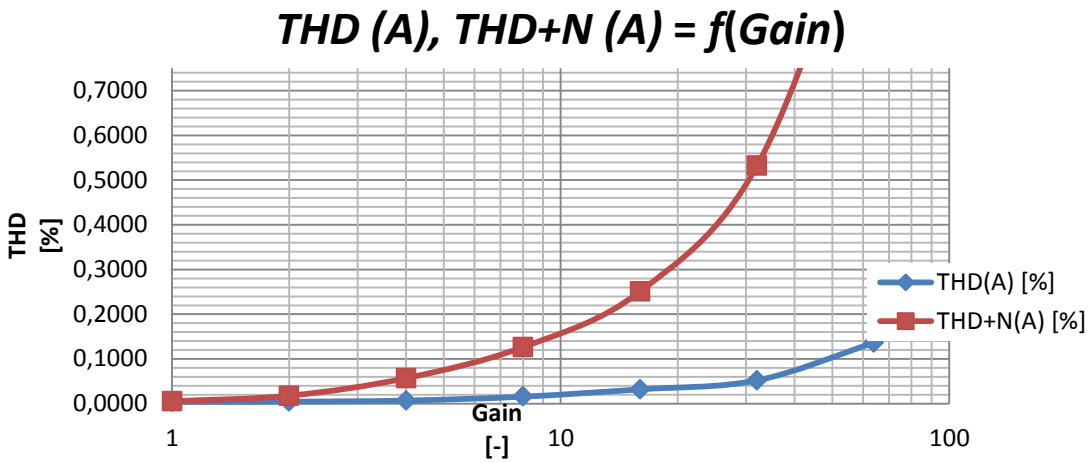

Fig. 115: *THD*, *THD+N* depending on gain of the preamplifier (PGA112)

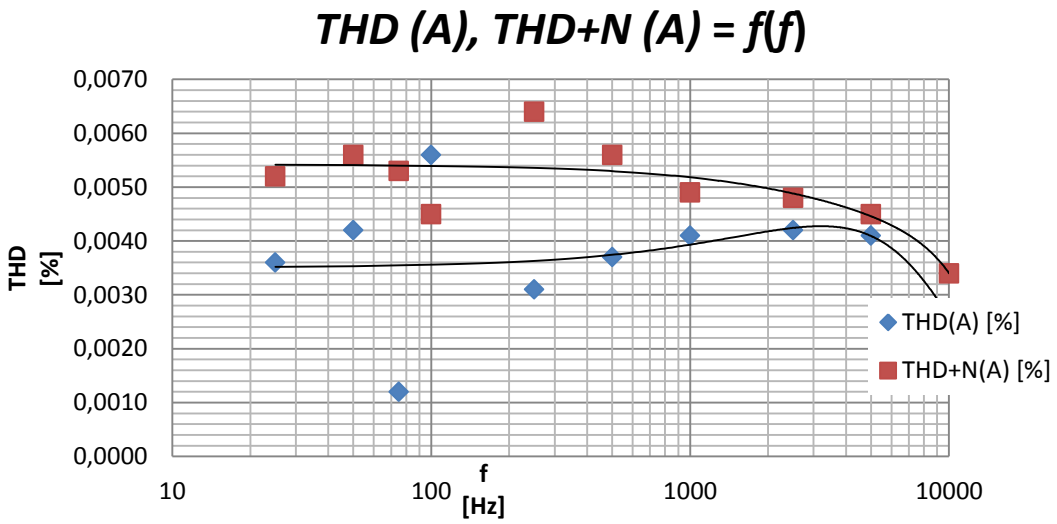

Fig. 116: *THD*, *THD+N* of preamplifier (PGA112) depending on frequency

A.2.2 Audio routing

Tab. 9: Used apparatus for audio routing measurement

Used apparatus:	
Power sources:	Manson SDP2405: 1x (0-40) V / (0-5) A
	Diametral P230R51D: 2x (0-30) V / (0-4) A + 5 V / 3 A
Multimetr:	
Oscilloscope:	Agilent Technologies DSO7014B 100MHz, 2GS/s, 4 CH
Audio analyzer:	Kenwood VA-2230A

Tab. 10 Frequency response of audio routing

Vin	[dBV]	0
f [Hz]	Vout [dBV]	Ku [dB]
80	5,7	5,7
100	5,7	5,7
200	5,8	5,8
400	5,8	5,8
600	5,8	5,8
800	5,8	5,8
1000	5,8	5,8
2000	5,8	5,8
4000	5,8	5,8
6000	5,8	5,8
8000	5,8	5,8
10000	5,8	5,8
20000	5,5	5,5

Tab. 11: Crosstalk of audio routing

f	[kHz]	1
Vin	[dBV]	0
Channel	[-]	5->4
Vout-4 [dBV]	Crosstalk [dB]	
-60,7	-60,7	

Tab. 12:THD of audio routing

Vin	[dBV]	1,5,2014
THD+N (A)	[%]	0,017
THD (A)	[%]	0,0025

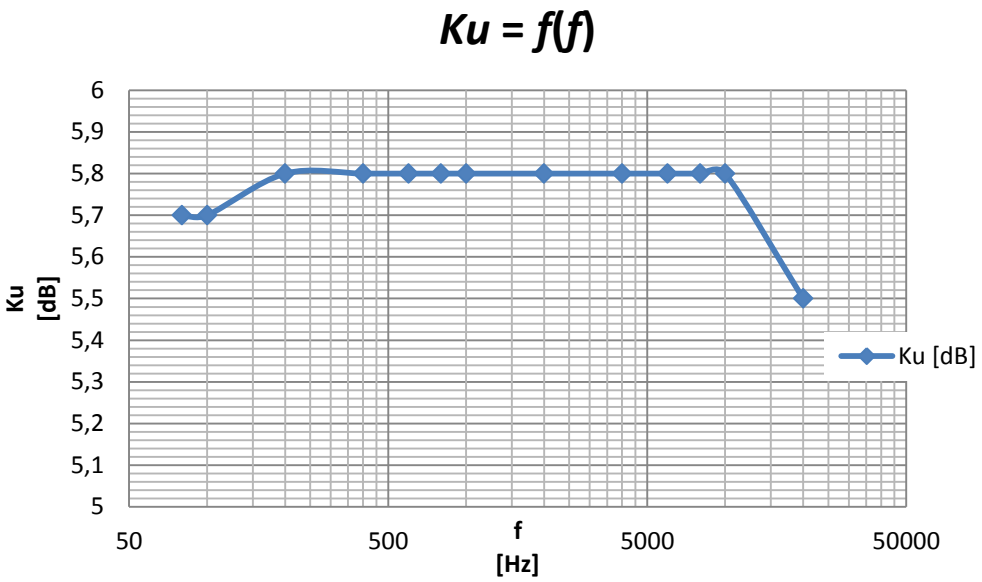

Fig. 117: Frequency response of audio routing

A.2.3 Class D amplifier

Tab. 13: Used apparatus for class D amplifier measurement

Used apparatus:	
Power sources:	Manson SDP2405: 1x (0-40) V / (0-5) A
	DC-DC Sep-Up Uin=12V, Uout=20V
	Diametral P230R51D: 2x (0-30) V / (0-4) A + 5 V / 3 A
Multimetr:	
Oscilloscope:	Agilent Technologies DSO7014B 100MHz, 2GS/s, 4 CH
Audio analyzer:	Kenwood VA-2230A

Tab. 14: Frequency response of class D amplifier (G = 12, G = 20)

Gain	[-]	12	Gain	[-]	20
Vin	[dBV]	-7,5	Vin	[dBV]	-7,5
f [Hz]	Vout [dBV]	Ku [dB]	f [Hz]	Vout [dBV]	Ku [dB]
25	5,0	12,5	25	12,5	20,0
50	4,7	12,2	50	12,8	20,3
75	4,7	12,2	75	12,8	20,3
100	4,8	12,3	100	12,9	20,4
250	4,7	12,2	250	12,8	20,3
500	4,7	12,2	500	12,8	20,3
1000	4,7	12,2	1000	12,8	20,3
5000	5,1	12,6	5000	13,1	20,6
10000	5,1	12,6	10000	12,9	20,4
15000	4,9	12,4	15000	12,7	20,2
20000	5,1	12,6	20000	12,6	20,1

Tab. 15: Frequency response of power amplifier (G = 26, G = 32)

Gain	[-]	26
Vin	[dBV]	-10
f [Hz]	Vout [dBV]	Ku [dB]
25	15,5	25,5
50	16,0	26,0
75	16,0	26,0
100	16,1	26,1
250	16,0	26,0
500	16,0	26,0
1000	16,0	26,0
5000	16,2	26,2
10000	16,0	26,0
15000	15,8	25,8
20000	15,7	25,7

Gain	[-]	32
Vin	[dBV]	-16
f [Hz]	Vout [dBV]	Ku [dB]
25	15,1	31,1
50	16,3	32,3
75	16,3	32,3
100	16,4	32,4
250	16,3	32,3
500	16,3	32,3
1000	16,3	32,3
5000	16,6	32,6
10000	16,3	32,3
15000	16,1	32,1
20000	16,1	32,1

Tab. 16: THD of power amplifier depending on frequency and gain

Gain	[dB]	12
f	[Hz]	1000
Vin [dBV]	THD+N(A) [%]	THD(A) [%]
-20,0	0,036	0,025
-17,5	0,039	0,027
-15,0	0,034	0,031
-12,5	0,035	0,032
-10,0	0,041	0,040
-7,5	0,043	0,044
-5,0	0,053	0,051
-2,5	0,084	0,083
0,0	0,298	0,297
2,5	1,107	1,104
5,0	3,390	3,395

f	[Hz]	1000
Gain [dB]	THD+N(A) [%]	THD(A) [%]
12	0,052	0,048
20	0,097	0,096
26	0,145	0,141
32	0,240	0,213

Tab. 17: Crosstalk of power amplifier depending on frequency and gain

G	[dB]	26
Vin	[dBV]	-10
Pout	[W]	10
Channel	[-]	3->4

f [Hz]	Vout-3 [dBV]	Crosstalk [dB]
75	-46,9	36,9
100	-45,2	35,2
250	-45,5	35,5
500	-44,3	34,3
1000	-46,6	36,6
5000	-46,2	36,2
10000	-45,3	35,3
15000	-45,8	35,8
20000	-46	36

f	[kHz]	1
Vin	[dBV]	-10
Channel	[-]	4->3

G [dB]	Pout [W]	Vout-3 [dBV]	Crosstalk [dB]
12	0,4	-60,2	60,2
20	2,5	-52	52
26	10,0	-44,9	44,9
32	39,6	-40,3	40,3

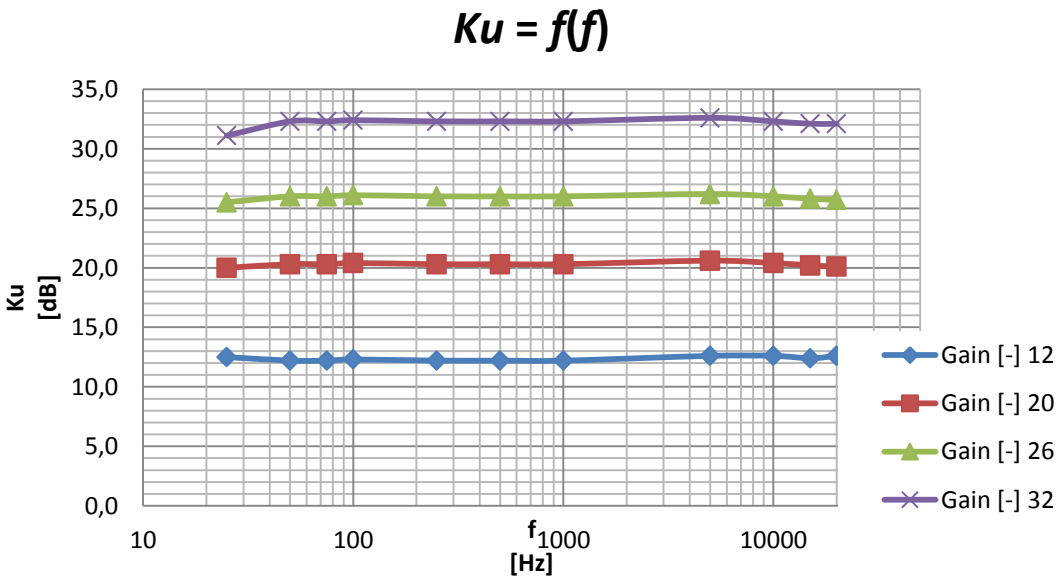

Fig. 118: Frequency response of power amplifier

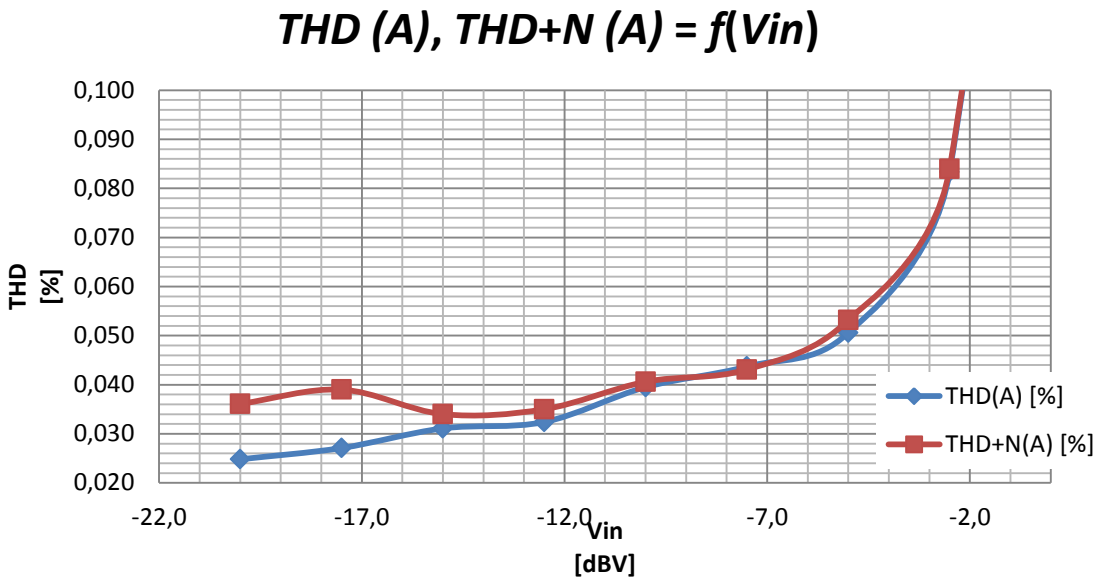

Fig. 119: *THD*, *THD+N* of power amplifier depending on input signal level

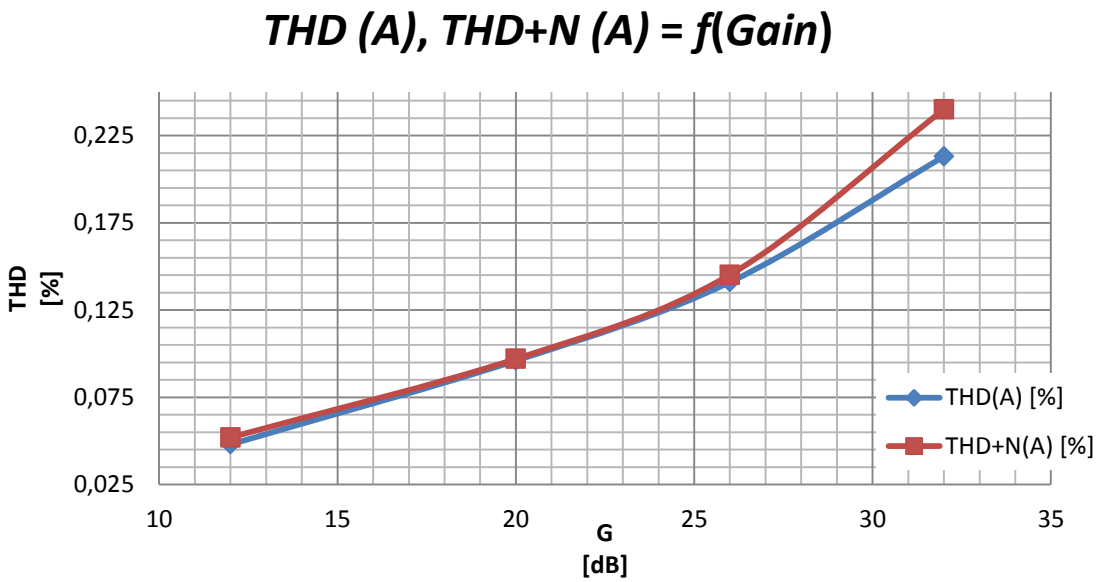

Fig. 120: *THD*, *THD+N* of power amplifier depending on gain

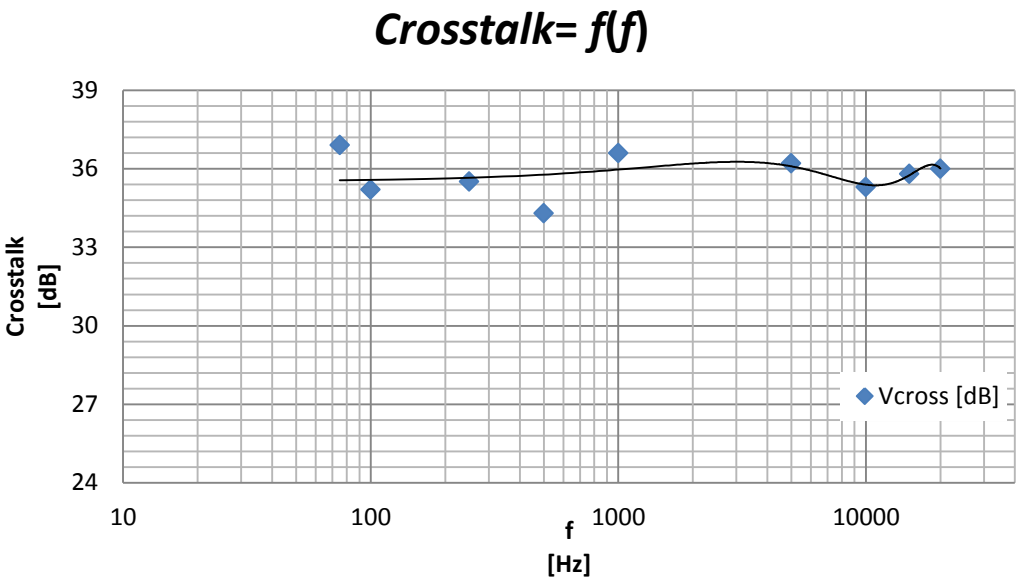

Fig. 121: Crosstalk of power amplifier depending on frequency

A.2.4 DC-DC modules

Tab. 18: Used apparatus for DC-DC modules measurement

Used apparatus:	
Power sources:	Diametral P230R51D: 2x (0-30) V / (0-4) A + 5 V / 3 A
	LIPO battery pack 1000mAh 40C
Multimetr:	Iskra MI7045
Osciloskop:	Tektronix TDS2014 100MHz, 1GS/s, 4 CH
Programable load:	GW Instek PEL-300

Tab. 19: Measured data of DC-DC module No. 1 (BACK-BOOST) V_{out} = 5 V

Iout-set [mA]	Vin [V]	Iin [A]	Vpp-in [mV]	Pin [W]	Vout [V]	Iout [A]	Vpp-out [mV]	Pout [W]	η [%]
0	12	0,03	40	0,31	5,00	0,00	45	0,00	0,00
10	12	0,03	50	0,38	5,00	0,01	50	0,05	12,76
110	12	0,09	100	1,08	5,00	0,11	155	0,55	50,93
210	12	0,15	125	1,80	4,98	0,21	220	1,05	58,16
310	12	0,21	140	2,52	4,98	0,31	260	1,55	61,34
410	12	0,27	155	3,24	4,96	0,41	284	2,04	62,86
510	12	0,34	210	4,08	4,96	0,51	305	2,53	62,07
610	12	0,40	225	4,80	4,96	0,60	335	2,99	62,21
710	12	0,45	240	5,40	4,94	0,70	355	3,47	64,22
810	12	0,50	250	6,00	4,94	0,80	345	3,96	66,03
910	12	0,56	255	6,72	4,92	0,90	352	4,45	66,19
1010	12	0,63	260	7,56	4,92	1,00	345	4,94	65,34
1500	12	0,94	300	11,37	4,88	1,49	345	7,28	64,01

Tab. 20: Measured data of DC-DC module No. 1 (BACK-BOOST) V_{out} = 3.3 V

Iout-set [mA]	Vin [V]	Iin [A]	Vpp-in [mV]	Pin [W]	Vout [V]	Iout [A]	Vpp-out [mV]	Pout [W]	η [%]
0	12	0,03	36	0,30	3,30	0,00	40	0,00	0,00
10	12	0,03	35	0,36	3,30	0,01	50	0,03	8,98
110	12	0,07	90	0,84	3,30	0,11	130	0,36	43,21
210	12	0,11	105	1,32	3,30	0,21	185	0,69	52,55
310	12	0,16	115	1,86	3,28	0,31	220	1,02	54,74
410	12	0,20	125	2,34	3,30	0,41	250	1,35	57,91
510	12	0,25	140	2,94	3,26	0,51	270	1,66	56,62
610	12	0,27	145	3,24	3,26	0,60	275	1,96	60,57
710	12	0,32	215	3,84	3,24	0,70	280	2,27	59,23
810	12	0,36	220	4,32	3,24	0,80	280	2,60	60,15
910	12	0,40	220	4,80	3,24	0,90	280	2,93	61,02
1010	12	0,44	225	5,28	3,22	1,00	275	3,23	61,23
1500	12	0,64	265	7,68	3,18	1,49	305	4,74	61,78

Tab. 21: Measured data of DC-DC module No. 3 (BACK) V_{out} = 5 V

Iout-set [mA]	Vin [V]	Iin [A]	Vpp-in [mV]	Pin [W]	Vout [V]	Iout [A]	Vpp-out [mV]	Pout [W]	η [%]
10	12	0,01	50	0,12	5,00	0,01	53	0,05	40,83
110	12	0,06	80	0,72	5,00	0,11	45	0,55	76,39
210	12	0,12	105	1,38	5,00	0,21	55	1,05	76,09
310	12	0,17	120	2,04	4,98	0,31	75	1,54	75,73
410	12	0,22	135	2,64	4,98	0,41	85	2,04	77,45
510	12	0,27	145	3,24	4,96	0,51	90	2,53	78,14
610	12	0,32	210	3,84	4,96	0,60	92	2,99	77,89
710	12	0,38	215	4,56	4,94	0,70	100	3,47	76,05
810	12	0,43	235	5,10	4,94	0,80	105	3,96	77,68
910	12	0,48	250	5,76	4,92	0,90	105	4,45	77,22
1010	12	0,53	245	6,30	4,92	1,00	105	4,94	78,41
1500	12	0,79	330	9,48	4,88	1,49	100	7,28	76,80

Tab. 22: Measured data of DC-DC module No. 3 (BACK) V_{out} = 3.3 V

Iout-set [mA]	Vin [V]	Iin [A]	Vpp-in [mV]	Pin [W]	Vout [V]	Iout [A]	Vpp-out [mV]	Pout [W]	η [%]
10	12	0,01	35	0,10	3,30	0,01	13	0,03	33,69
110	12	0,04	80	0,53	3,30	0,11	40	0,36	68,75
210	12	0,08	100	0,96	3,30	0,21	55	0,69	72,26
310	12	0,12	120	1,44	3,30	0,31	65	1,02	71,13
410	12	0,16	125	1,86	3,30	0,41	75	1,35	72,81
510	12	0,19	130	2,28	3,28	0,51	80	1,67	73,45
610	12	0,23	155	2,70	3,28	0,60	85	1,97	73,13
710	12	0,26	165	3,12	3,26	0,70	90	2,29	73,35
810	12	0,30	155	3,54	3,26	0,80	95	2,61	73,86
910	12	0,32	240	3,84	3,24	0,90	95	2,93	76,28
1010	12	0,39	240	4,68	3,24	1,00	90	3,25	69,51
1500	12	0,56	300	6,72	3,20	1,49	90	4,77	71,05

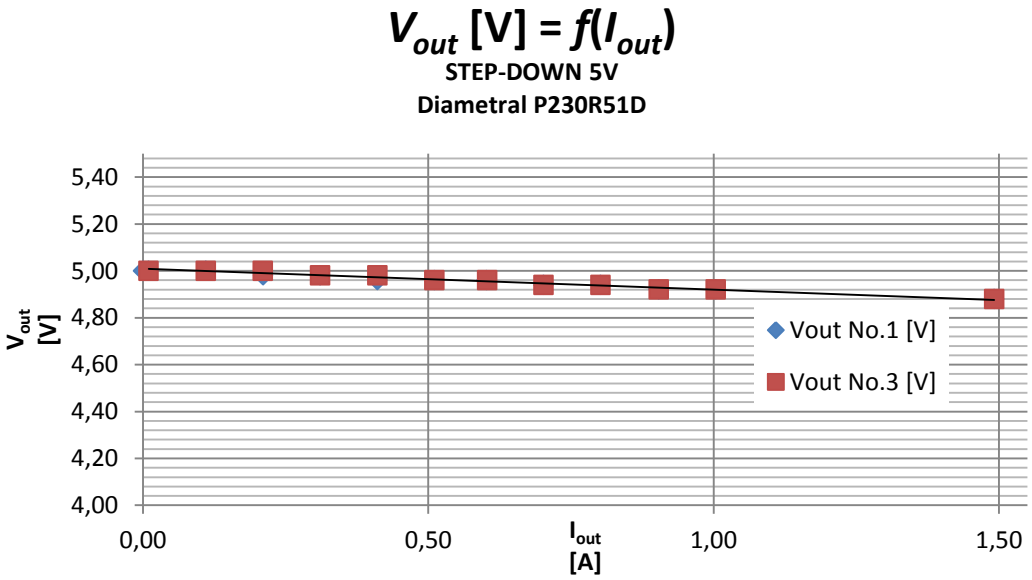

Fig. 122: DC-DC modules measured load characteristic, V_{out} = 5 V

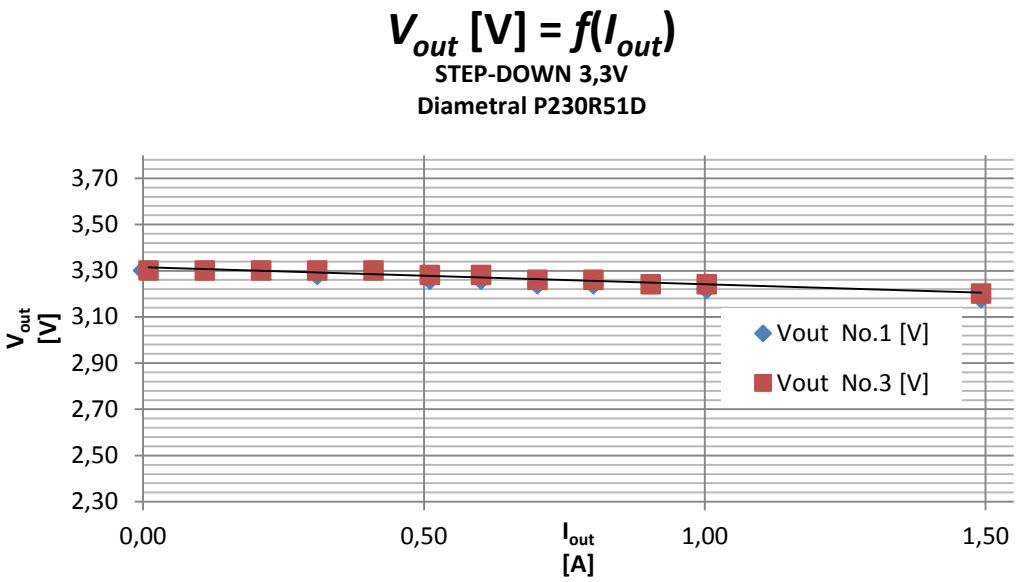

Fig. 123: DC-DC modules measured load characteristic, V_{out} = 3.3 V

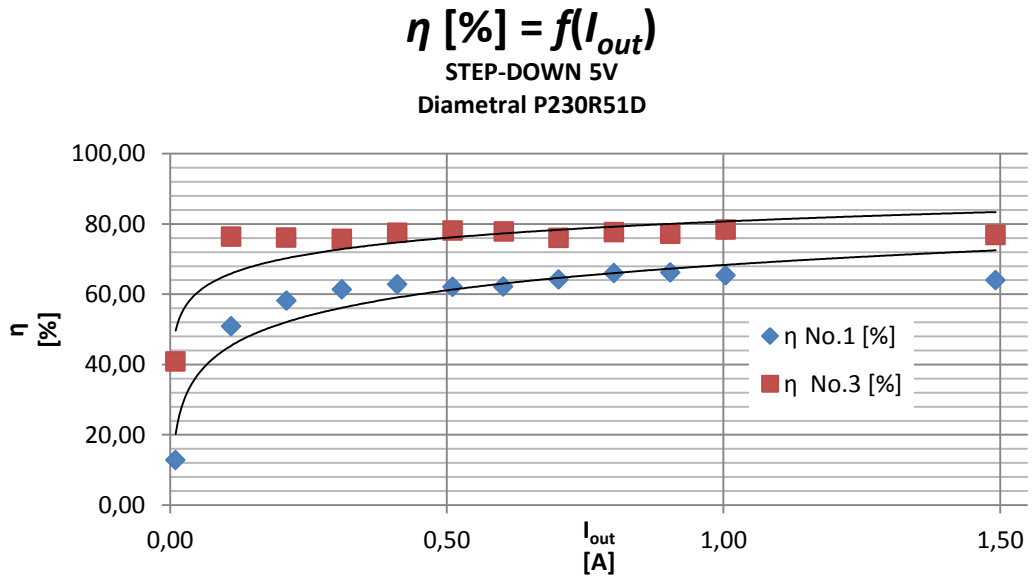

Fig. 124: DC-DC modules measured efficiency, V_{out} = 5 V

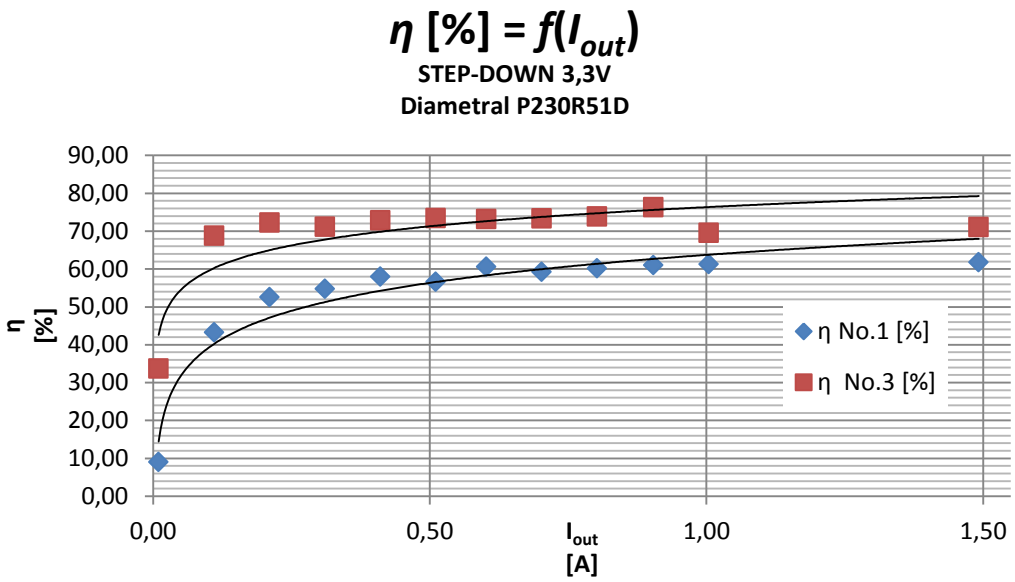

Fig. 125: DC-DC modules measured efficiency, V_{out} = 3.3 V

Tab. 23: Measured data of DC-DC module No. 4 (BOOST) V_{in} LIPO battery pack

Iout-set [mA]	Vin [V]	Iin [A]	Vpp-in [mV]	Pin [W]	Vout [V]	Iout [A]	Vpp-out [mV]	Pout [W]	η [%]
0	12	0,02	65	0,21	20,02	0,00	40	0,00	0,00
10	12	0,04	115	0,43	20,02	0,01	90	0,20	45,21
110	12	0,21	150	2,63	20,00	0,11	300	2,20	83,69
210	12	0,40	225	4,96	20,00	0,21	380	4,20	84,68
310	12	0,56	295	6,89	20,00	0,31	430	6,20	90,01
410	12	0,72	350	8,86	19,98	0,41	480	8,17	92,27
510	12	0,90	408	11,07	19,98	0,51	712	10,17	91,87
750	12	1,30	560	15,73	19,96	0,74	960	14,81	94,15
1000	12	1,80	695	21,78	19,94	0,99	1250	19,78	90,82
1500	12	2,70	1000	32,40	19,90	1,49	1700	29,69	91,64
2000	12	3,60	1000	42,48	19,84	1,99	1900	39,56	93,13
2500	12	5,50	2000	64,35	19,76	2,99	2880	59,12	91,88
3000	12	7,70	2000	88,55	19,60	3,99	3850	78,24	88,36
4000	11	10,00	2000	114,00	19,60	4,99	4550	97,84	85,83
6000	11	12,00	3000	133,20	19,52	5,99	5150	116,96	87,81
7000	12	14,50	3000	171,10	19,40	7,00	5700	135,80	79,37
8000	11	15,00	2500	160,50	18,66	7,98	5600	148,91	92,78

Tab. 24: Measured data of DC-DC module No. 5 (BOOST) V_{in} LIPO battery pack

Iout-set [mA]	Vin [V]	Iin [A]	Vpp-in [mV]	Pin [W]	Vpp [V]	Iout [A]	Vpp-out [mV]	Pout [W]	η [%]
0	12	0,02		0,29	20,00	0,00	135	0,00	0,00
10	12	0,04	225	0,53	20,00	0,01	135	0,22	40,51
110	12	0,22	225	2,67	20,02	0,11	150	2,22	83,20
210	12	0,40	230	4,96	20,00	0,21	180	4,22	85,00
310	12	0,56	250	6,94	20,00	0,31	250	6,22	89,52
410	12	0,74	270	9,10	19,98	0,41	288	8,11	89,12
510	12	0,90	320	11,07	19,98	0,51	350	10,20	92,16
750	12	1,30	490	15,86	19,96	0,75	400	14,93	94,14
1000	12	1,80	440	21,78	19,96	1,00	520	19,96	91,64
1500	12	2,70	560	32,40	19,90	1,50	720	29,89	92,25
2000	12	3,60	680	43,20	19,86	2,00	850	39,76	92,04
2500	12	4,60	760	54,74	19,82	2,50	1100	49,55	90,52
3000	12	5,60	850	64,96	19,78	3,00	1150	59,38	91,41
4000	13	7,50	1060	93,75	19,70	4,00	1250	78,80	84,05
5000	11	10,00	970	113,00	19,62	5,00	1700	98,10	86,81
6000	11	12,00	1200	133,20	19,54	6,00	2000	117,28	88,05
7000	11	15,00	1300	162,00	19,46	7,00	2300	136,22	84,09

Tab. 25: Measured data of DC-DC module No. 6 (BOOST) V_{in} LIPO battery pack

Iout-set [mA]	Vin [V]	Iin [A]	Vpp-in [mV]	Pin [W]	Vout [V]	Iout [A]	Vpp-out [mV]	Pout [W]	η [%]
0	13	0,02	1	0,21	20,01	0,00	3	0,00	0,00
10	13	0,05	2	0,63	20,08	0,01	8	0,21	34,06
110	12	0,25	2	3,10	20,06	0,11	2	2,22	71,70
210	12	0,46	2	5,70	20,06	0,21	2	4,23	74,13
310	12	0,70	4	8,68	20,04	0,31	4	6,23	71,76
410	12	0,88	4	10,91	20,02	0,41	4	8,22	75,33
510	12	1,00	4	12,30	20,02	0,51	19	10,22	83,07
750	12	1,50	5	18,30	19,98	0,75	20	14,99	81,89
1000	12	2,10	6	25,62	19,96	1,00	25	20,00	78,06
1500	12	3,00	7	36,00	19,90	1,50	26	29,85	82,92
2000	12	3,60	25	43,20	19,84	2,00	28	39,72	91,94
2500	13	5,00	31	62,50	19,78	2,50	26	49,41	79,06
3000	12	6,00	37	70,20	19,72	3,00	80	59,16	84,27
4000	12	8,50	42	98,60	19,60	4,00	35	78,40	79,51
5000	11	11,00	41	122,10	19,46	5,00	35	97,30	79,69
6000	11	11,50	40	125,35	16,40	6,00	30	98,43	78,53
8000	11	11,50	40	124,20	13,76	7,00	35	96,32	77,55

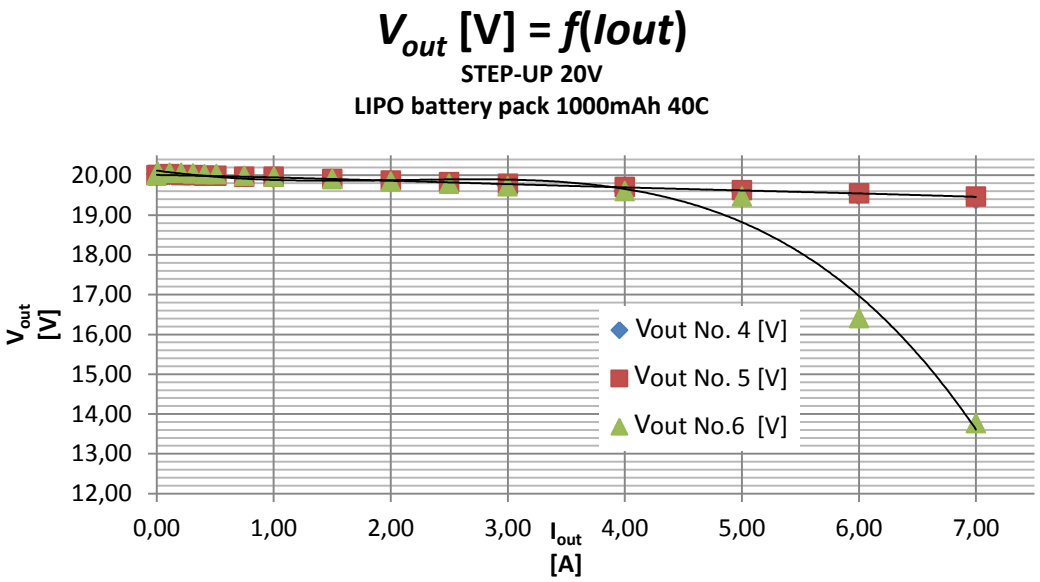

Fig. 126: Amplifier power sources measured load characteristic

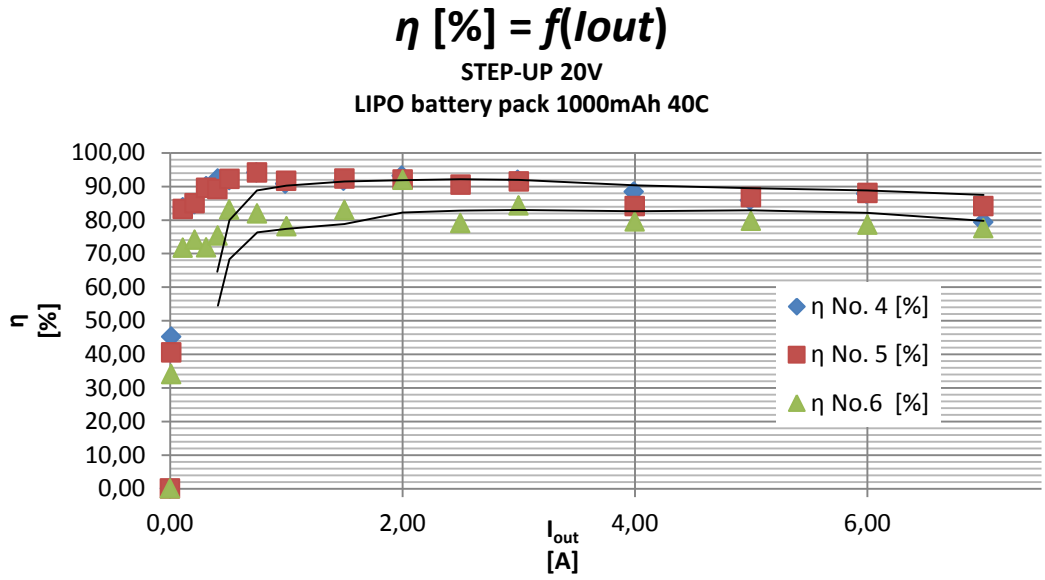

Fig. 127: Amplifier power sources measured efficiency

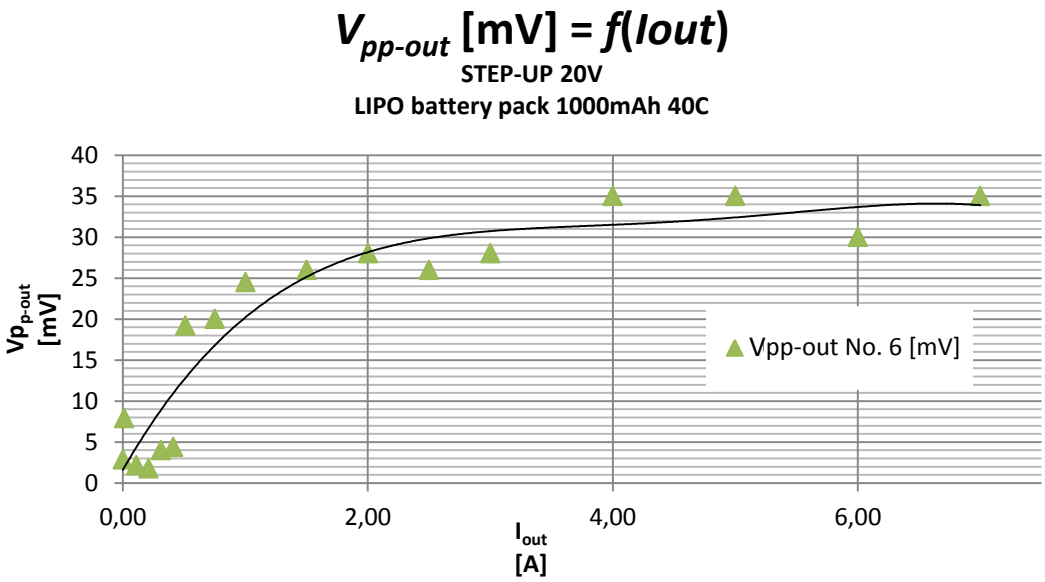

Fig. 128: Amplifier power source No. 6 measured output noise

A.3 Photo documentation

Fig. 129: Case of the testing tool and example of the main rails

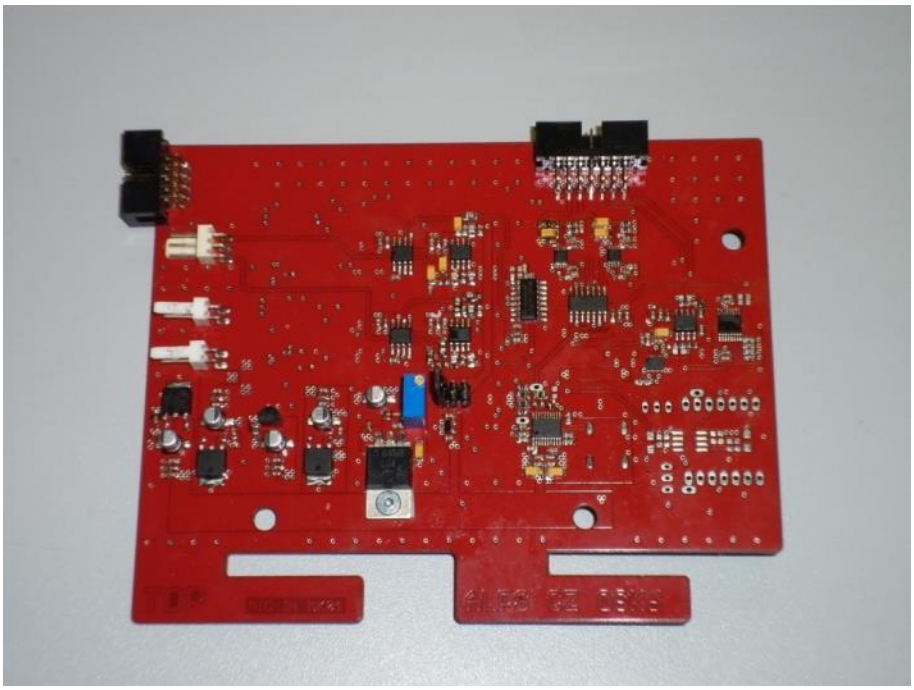

Fig. 130: Microphone input board - top

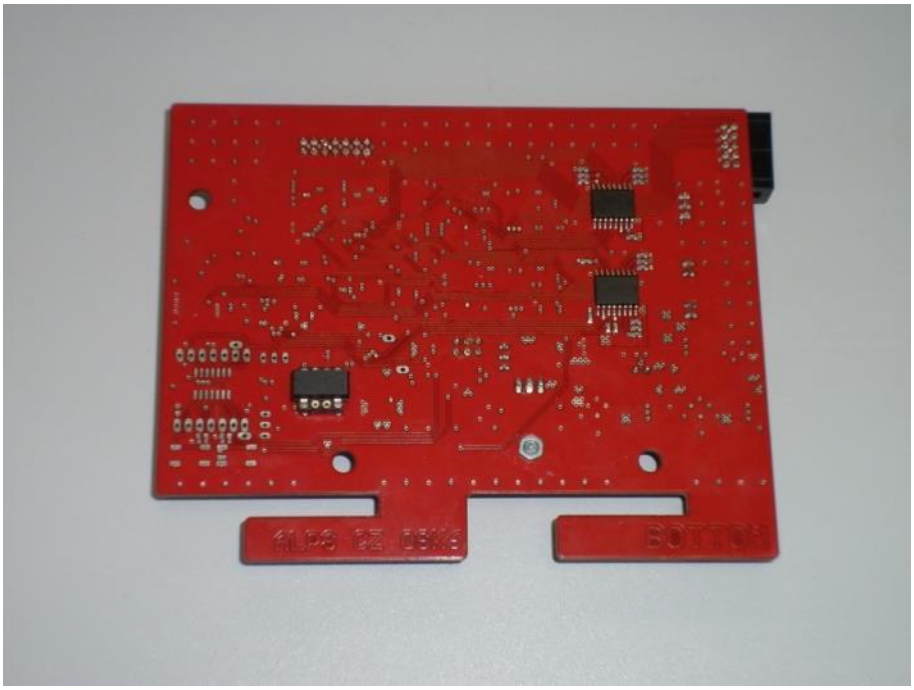

Fig. 131: Microphone input board - bottom

Fig. 132:External user interface sub-board

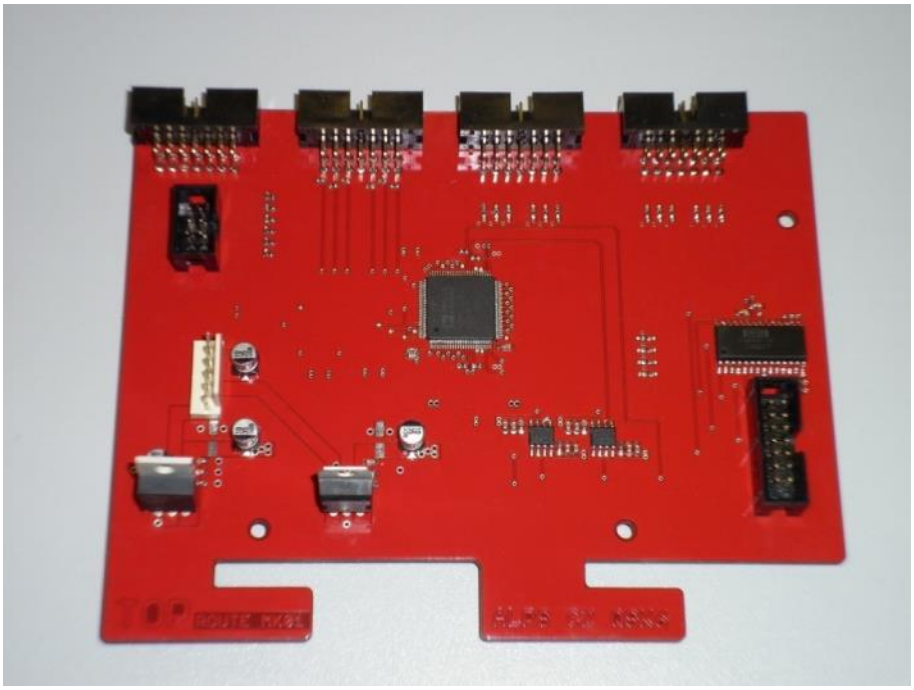

Fig. 133: Audio routing board – top

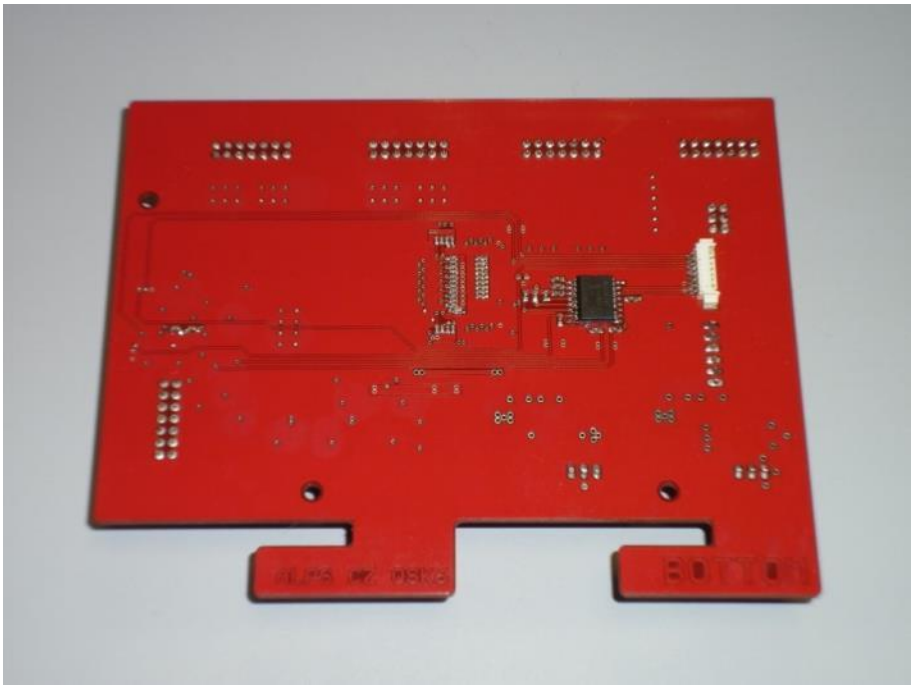

Fig. 134: Audio routing board – bottom

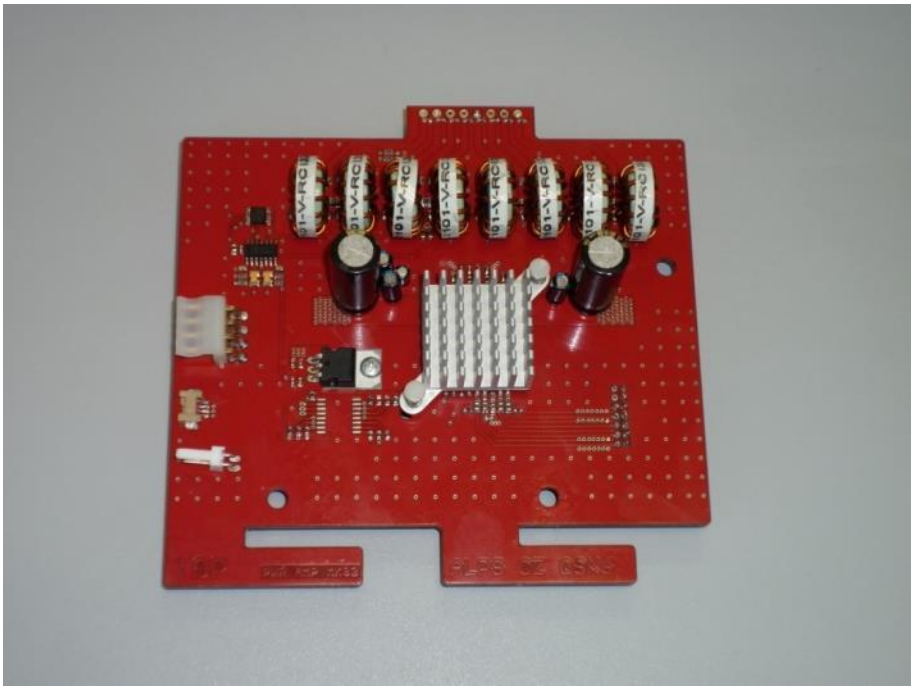

Fig. 135: Class D amplifier board - top

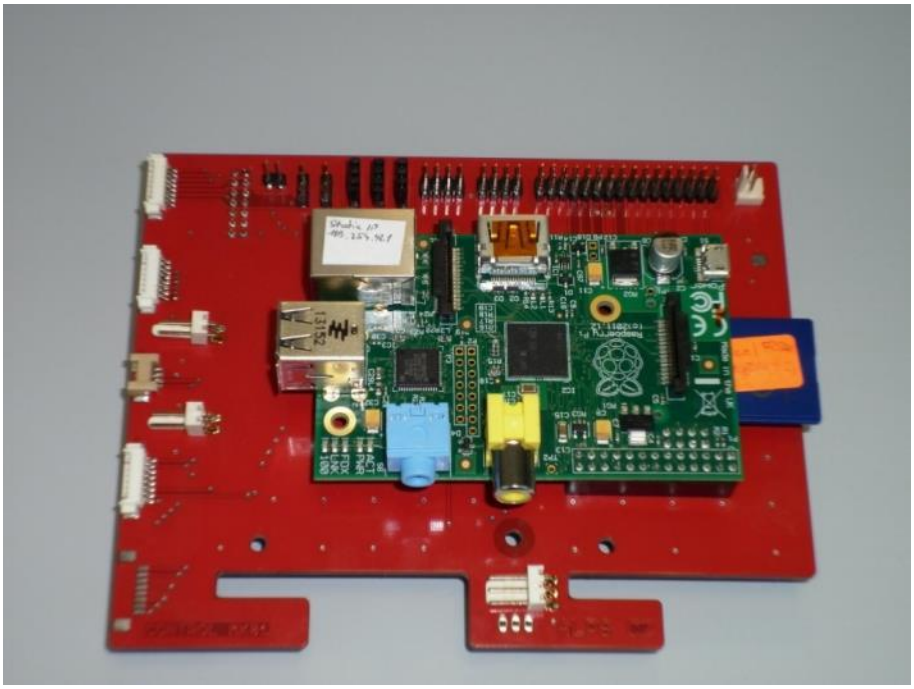

Fig. 136: Control board - top

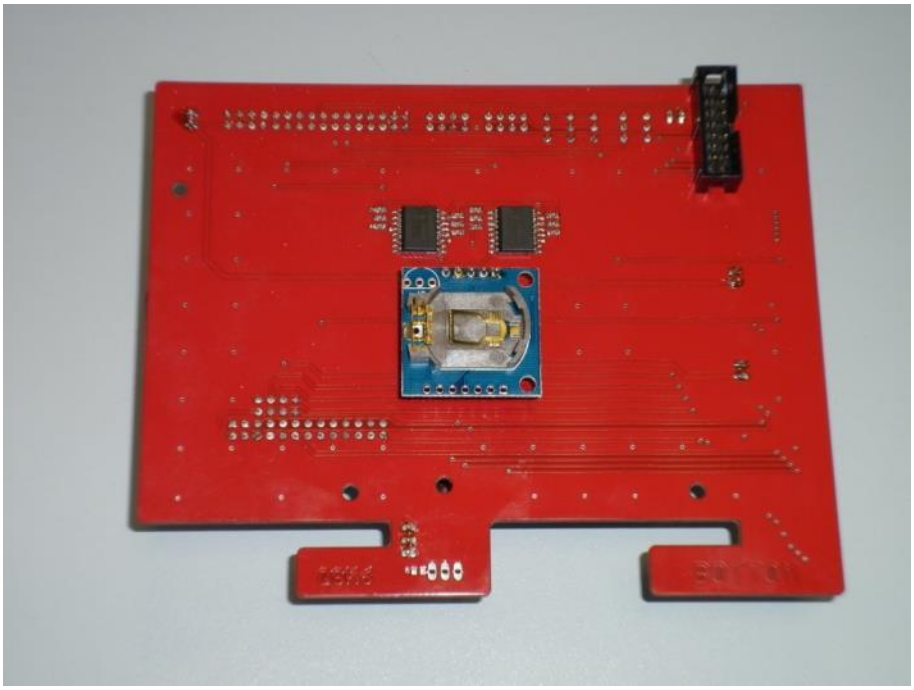

Fig. 137: Control board – bottom

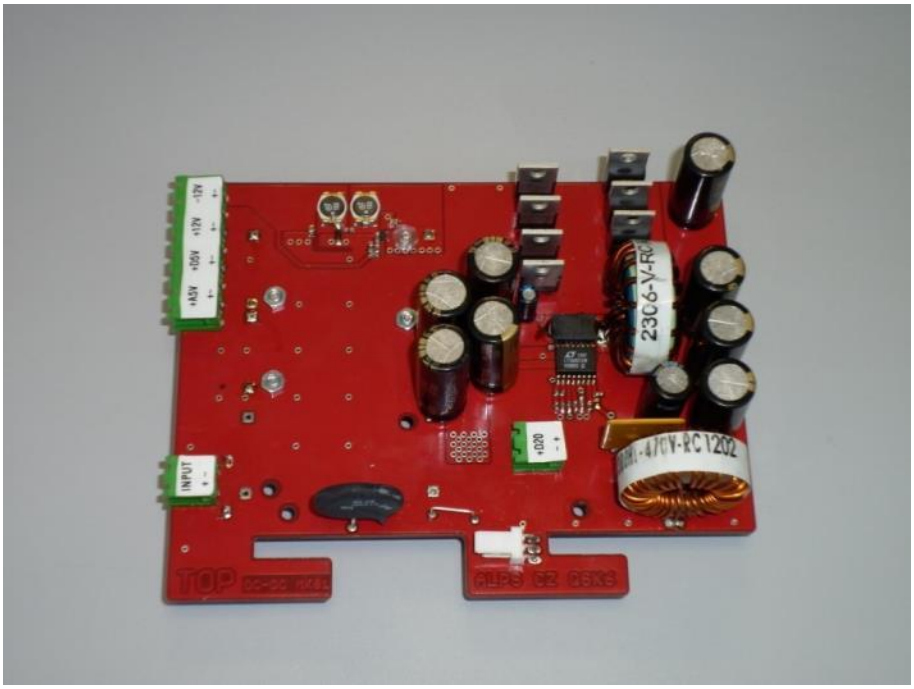

Fig. 138:Power sources board - top

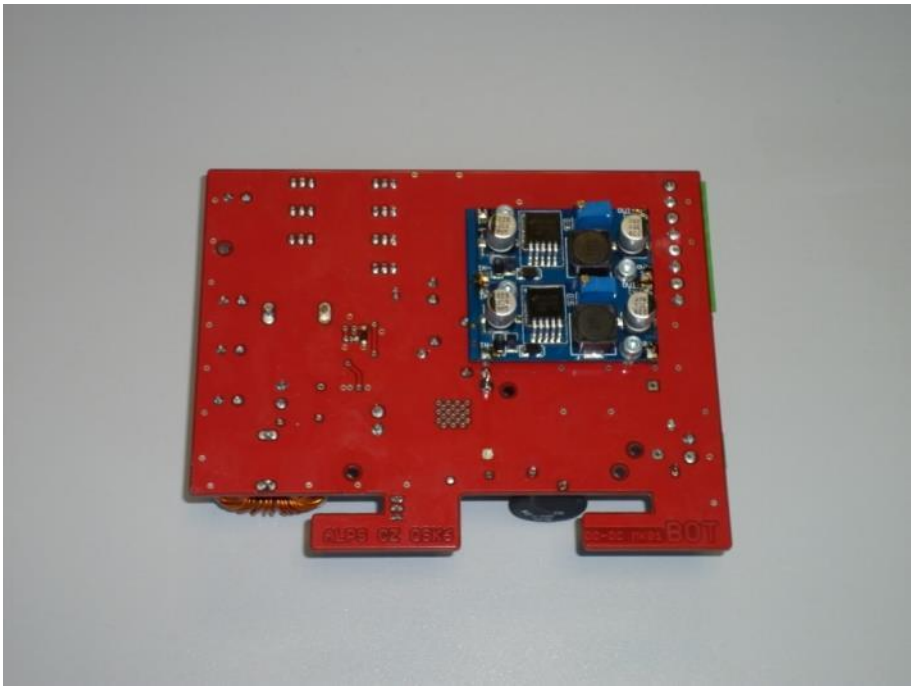

Fig. 139: Power sources – bottom

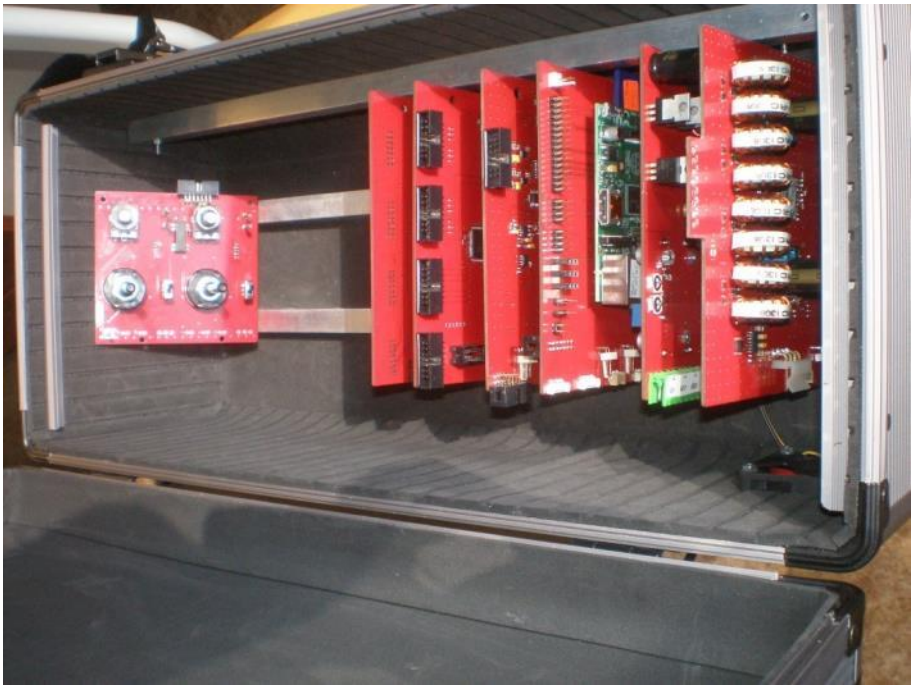

Fig. 140: All boards in the tool case